Dissertation

Characterization of Pozzolan-lime Mortar

On the utility of comprehensive image-based analysis and experimental archeology for understanding historical mortar

Charakterisierung von Puzzolan-Kalk-Mörtel

Über den Nutzen von umfassenden bildbasierten Analysen und experimenteller Archäologie zum Verständnis historischer Mörtel

Carried out for the purpose of obtaining the academic degree of Doctor of Natural Sciences.

Dissertation zur Erlangung des akademischen Grades
Doktor der Naturwissenschaften (Dr.rer.nat.)

eingereicht an der Universität für angewandte Kunst Wien

bei Hon.-Prof. Dr. phil. Johannes Weber
Fach: Naturwissenschaften in der Konservierung und Archäometrie
1. Beurteiler: Hon.-Prof. Dr. phil. Johannes Weber (Universität für angewandte Kunst Wien, Institut für Konservierung und Restaurierung/University of Applied Arts Vienna, Institute of Conservation)
2. Beurteiler: Prof. Norman Weiss (Graduate School of Architecture, Preservation and Planning, Columbia University in the City of New York)

vorgelegt von Anthony John Baragona, MSc.

Matrikelnummer 01274224

Ich erkläre hiermit,
dass ich die Dissertation selbständig verfasst, keine andere als die angegebenen Quellen und Hilfsmittel benutzt und mich auch sonst keiner unerlaubten Hilfen bedient habe,
dass diese Dissertation bisher weder im In- noch im Ausland (einer Beurteilerin / einem Beurteiler
zur Beurteilung) in irgendeiner Form als Prüfungsarbeit vorgelegt wurde, dass dieses Exemplar mit der beurteilten Arbeit übereinstimmt.



8/7/2021 _____

Datum Unterschrift

Vindobona, Ab urbe condita MMDCCLXXIV

Fortis fortuna adiuvat
-Pliny the Elder, 79 A.D.

Abstract

Historical mortar, concrete and other cementitious systems attracts the interest of researchers from a wide range of disciplines whose focus is understanding the past by analyzing and interpreting the built environment. As such, a large body of work exists that analyzes mortar produced over the centuries by various cultures, exploration utilizing every type of scientific method known by researchers in the fields of archeology and conservation science. Additionally, this interest has led to the innovative application of methods not typically used in materials science as well as the development of entirely new techniques specifically to analyze mortar. This work focuses on one type of mortar binder system – Roman-era pozzolanic mortar, which was produced by mixing either volcanic ash/sand or crushed ceramic as a reactive aggregate with lime and water to produce a strong, dense, and water-resistant mortar or concrete material. This mortar type was used profusely in structural applications and is widely found in archeological areas of the former Roman Empire. Both ceramic and volcanic pozzolanic mortars are studied herein.

During the course of studying this material two separate, but linked, processes were used. The first, detailed in the first half the experimental set-up, concerned itself with the production of pozzolanic mortar through experimental archeological methods in order to produce a material that shared the same qualities as "fresh" Roman-era mortar (Chapter 3). These samples would then serve the twofold purpose of allowing the study of the hypothetical initial qualities of Roman mortar, as well as control specimens that could then be compared to a wide variety of archeological samples, comparing the fresh mortar with those from archeological sites.

The second process, detailed in the second half of the experimental set-up (Chapter 5) and forming the core of the results of this study, involved a comprehensive, image-based analytical protocol used to study polished petrographic thin sections made of both the experimental and archeological mortars. This involved studying the thin sections sequentially by optical microscopy (OM – SM and PLM), scanning electron microscopy coupled with energy-dispersive X-ray spectroscopy (SEM-EDX) and Fourier transform infrared spectroscopy mapping (FTIR-m); results were then combined through image analysis. Both the application of the FTIR-mapping itself and this sequential image-based protocol represent a novel approach to studying petrographic thin sections of mortar.

The efficacy of this protocol was evaluated by comparing its results with those obtained by more traditional means allowing for an assessment of the current state of the art of mortar analysis.

Zusammenfassung

Historische Mörtel, Beton und andere zementartige Baustoffe sind für mehrere Wissenschaftsdisziplinen von Interesse, die sich dem vertieften Verständnis vergangener Epochen auf der Basis von Architekturanalysen und -interpretationen widmen. Demzufolge liegen auch zahlreiche Studien zur Mörteltechnologie über die Jahrhunderte in verschiedenen Kulturen vor, welche sich aller möglichen Analyseverfahren bedienen, die üblicherweise im Rahmen archäologischer und konservierungswissenschaftlicher Forschung zur Anwendung kommen. Darüber hinaus hat das rege Interesse an den verschiedenen Fragestellungen sowohl zur innovativen Anwendung solcher Analysenmethoden geführt, die typischerweise nicht den Materialwissenschaften entstammen, als auch zur Entwicklung gänzlich neuer Verfahren für die zielgerichtete Analyse von Mörteln.

Die gegenständliche Studie befasst sich mit einer bestimmten Gruppe von Mörtelbindemitteln, nämlich den römisch-antiken puzzolanischen Mörteln, die durch Zumischung von Vulkanasche oder –sand, oder aber von Keramikmehl oder –splitt als reaktive Zuschläge zu Kalk und Wasser zur Erzeugung fester, dichter und wasserbeständiger Mörtel oder Betone erzeugt wurden. Diese bautechnische Anwendung findet sich weit verbreitet im antiken Konstruktionsbau, jedenfalls was die Einflussgebiete des Römischen Imperiums betrifft. Die vorliegende Arbeit widmet sich sowohl den keramischen als auch den vulkanischen Puzzolanmörteln.

Im Zuge der Untersuchungen an Probenmaterial wurden zwei unterschiedliche, jedoch miteinander in Verbindung stehende methodische Ansätze verfolgt. Der erste, der im ersten Teil des Methodenkapitels beschrieben ist, richtet sich auf die Herstellung puzzolanischer Mörtel im Sinne experimenteller archäologischer Methoden, um über ein Material verfügen zu können, das gewissermaßen einem jungen römischen Mörtel entspricht. Diese Proben wurden dann mit einer Anzahl archaeologischer Originalproben verglichen.

Der zweite Ansatz dieser Studie, der im zweiten Teil des Methodenkapitels ausgeführt wird und die wichtigsten Resultate der Arbeit liefert, beinhaltet umfassende bildgebende Analysen an polierten petrografischen Dünnschliffen aus archäologischen sowie experimentell hergestellten Referenzmörteln. Diese Analysen umfassen – aufeinander aufbauend – die optische Mikroskopie im Auflicht bzw. Polarisations-Durchlichtmikroskop (OM – SM und PLM), die Rasterelektronenmikroskopie in Verbindung mit energiedispersiver Röntgenspektroskopie (SEM-EDX), sowie die Fourier-Transformations-Infrarotspektrometrie (FTIR-m); mittels Bildanalyse werden dann die Ergebnisse zusammengeführt, was gemeinsam mit der Verwendung der FTIR-Kartierung einen innovativen Methodenansatz im Studium petrografischer Mörtelschliffe darstellt.

Die Aussagekraft der skizzierten Vorgangsweise wird durch Ergebnisvergleiche mit herkömmlicheren Analyseverfahren beurteilt. Darauf aufbauend wird der heutige Stand der Mörtelanalyse einer grundsätzlichen Diskussion unterzogen.

Acknowledgements

The work of completing a dissertation from the initial concept to the last editing and formatting of the final tome can feel like a rather lonely process. The process is in fact a collaboration of the doctoral student with a huge support group of experts in any field even tangentially related to the theme of the dissertation. Of perhaps greater importance than the actual contents of the dissertation, is the creation of this network. Thus, the dissertation itself becomes of symbol of the acceptance of the student by these experts as a colleague. I am grateful to the people listed below, not just for their help in completing this work, but also for their time, patience and eventual acceptance of this American who turned up with some big ideas, but not much else!

None of this would have been possible without the help of my "doctoral father" **Johannes Weber**, not only did he guide the process from start to finish, but he also helped me navigate life at the University and in Austria in general. This thesis was conducted at his former department, the Department of Conservation Sciences (Abteilung für Naturwissenschaften in der Konservierung), which was closed in October 2020. Big thanks to advisor number two, **Norman Weiss**, who not only started me on this path, but helped across this finish line as well.

To my "Austrian" colleagues here in Vienna: Thank you to **Farkas Pintér** for making me a better microscopist and helping me out with the SEM; to **Matea Ban** for instructing me in using the ultrasonic pulse device, helping me secure pozzolans, and teaching me how to ask for a beer in Croatian; to **Marta Anghelone** and **Anja Diekamp** for tolerating the rather lengthy process it took for me to understand FTIR; and to **Tanja Bayerová** for all her help in the chemistry lab.

Thanks to the great crew up in Prague and Telč for the analytical help: to **Zuzana Slížková**, **Miloš Drdácký** and **Dita Frankeová** at the Institute of Theoretical and Applied Mechanics of the Academy of Sciences of the Czech Republic; special thanks to Dita for performing the TGA-DSC.

Thank you to the archeologists who provided me with Roman mortar fragments: **Paolo Tomassini** from Ostia Antica, **Martin Mosser** from Vindobona, **Katharina Zanier** from Školarice, once again to both **Farkas Pintér**, for helping me get some from his hometown of Aquincum and **Norman Weiss** for the "Caesarea connection".

It was a long time ago but thank you to **Astrid Huber-Reichl** for allowing me to use Bundesdenkmalamt-Mauerbach facility to make my experimental mortar – and to **Karl Stingl** for cooking me up some quicklime and traditional-style bricks. Thank you to **Walter Strasser** at Technische Prüfanstalt for helping me test my mortar beams, even if you said that they were "like marzipan". And finally, I am grateful for the big blocks of clay that **Wolfgang Gaggl** from Wienerberger AG provided for me to turn into ceramic pozzolan.

I apologize to anybody reading this whom I may have forgotten – it has been a rather long journey.

Grazie mille to my wife, the mother of our two children, and my number one supporter, **Valentina Pintus.**

TABLE OF CONTENTS

ABSTRACT 3
ZUSAMMENFASSUNG 4
ACKNOWLEDGEMENTS 5
LIST OF TABLES AND FIGURES 10
LIST OF ABBREVIATIONS 13

MAIN BODY

1.0 Introduction 14

2.0 On Pozzolanic Mortar – State of the Art 16

2.1 Pozzolans and Pozzolanicity – A Chemical Overview 16

2.1.1 Pozzolanic Mortar – Its Use Throughout History 20

2.2 Current Research into Pozzolans 21

2.2.1 As a Historical Building Material 22

2.2.2 As a Restoration Material 24

2.2.3 Methods of Study of Pozzolanicity and Pozzolanic Mortar 26

2.2.3.1 Chemical and Physical Testing 26

2.2.3.2 Microscopic, and Micro-analytical 28

2.2.3.3 Experimental Archeology 31

3.0 Production of Mortar Control Samples for Comparative Analysis 34

3.1 Producing Experimental Mortar in the Field 34

3.2 Producing Experimental Mortar in the Laboratory 37

3.3 Characterization of the Reactive Aggregates by Reactivity testing: pH change vs. Modified Chapelle Test: Methods 42

3.3.1 Reactivity testing, pH change vs. Modified Chappelle Test: Results 47

3.4 Additional Physical and Chemical Characterization of the pozzolans 50

3.5 Production of the Experimental Ceramic-Lime Mortar in the Laboratory 52

4.0 Physical and Chemical Analysis of the Experimental and Archeological Mortar 57

4.1 Strength Development as measured by resistance to ultrasonic pulse 57

4.2 Compressive Strength Testing 58

4.3 Chemical Dissolution Testing per RILEM TC-167 58

4.4 Thermogravimetric Analysis of Mortar 59

5.0 Comprehensive Image-Based Analytical Protocol 61

5.1 Historical Mortars Analyzed 62

5.2 Polished Thin Section Preparation 63

5.3 Mortar Petrography – Optical Microscopy 64

5.4 SEM-EDX – Images Combined with Chemical Analysis 66

5.5 FTIR Imaging – From Chemical Detection to Chemical Mapping 68

5.6 Composite Imaging, Digital Image Analysis, Pseudo-color Analysis 70

5.7 Summary of the Comprehensive Image-Based Protocol 72

6.0 Results: Physical and Chemical Characterization of the Mortars 74

6.1 Empirical Observations on the mortar making process applicable to archeological interpretation 75

6.2 Mortar Strength: Strength Development as measured by ultrasound resistance and Final Compressive Strength 77

6.3 Chemical Dissolution Test Results 81

6.4 Results of Thermogravimetric Analysis of Mortar Binder 85

7.0 Results: Mortar Characterization through Comprehensive Image-Based Analytical Protocol 90

7.1 Binder Characterization through lime lump Analysis 91

7.2 Detecting Pozzolanicity through Reaction Rim Characterization 94

7.2.1 Lime Reaction Rims 99

7.3 Binder Matrix Characterization – Overview 103

7.4 Binder Alteration Phenomena 103

7.5 Mortar Characterization by Image Analysis – pseudo-color analysis 109

7.6 Binder Matrix Hydraulicity Characterization by FTIR imaging 112

7.7 Summary 117

8.0 Conclusions and Outlook 118

8.1 Correlative Analysis of Image-Based Protocol 119

8.1.1 Direct Comparison of Binder to Aggregate Ratio Determination Methods 120

8.1.2 Direct Comparison of Methods for determining Mortar Binder Hydraulicity 123

8.1.3 Correlating Mortar Binder Hydraulicity with Compressive Strength 126

8.2 Outlook 129

8.2.1 Direct Comparison of Methods for determining mortar porosity 129

8.2.2 Application of Protocol to Quantification of Alteration Products 130

8.2.3 Value Assessment: Towards a Simplification of Historical Mortar Analysis 131

9.0 References 132

LIST OF TABLES AND FIGURES

Chapter 2

Figure 2.1: Idealized/ Simplified Chemistry of a Pozzolan-Lime Mortar 17
Figure 2.2: Basic Structure of C(A)SH 18
Figure 2.3: Simplified Schematic of a young pozzolan-lime mortar 19
Figure 2.4:C(A)SH by OM and SEM-BSE 20
Figure 2.5: Volcanic and Ceramic Pozzolan Structural Mortars 23
Figure 2.6: Practical Chemistry of an unaltered historical Pozzolan-Lime Mortar 33

Chapter 3

Figure 3.1: Traditional Lime Production 35
Table 3.2: Mortars Produced in the Field 36
Figure 3.3: Polished cross section images of experimental archeological mortars 37
Figure 3.4: Heating curves for the "750 degree" and "950 degree" ceramics 39
Figure 3.5: Visual appearance of the clays as greenware and fired at different temperatures. 40
Figure 3.6: Polished thin sections of the four types of ceramic used to make mortar, with archeological comparisons. 41
Figure 3.7: Polished thin sections of the four types of ceramic used to make mortar, with archeological comparisons. 41
Table 3.8: Baseline alkalinity of pozzolanic materials 44
Figure 3.9: Chart and Table Describing the Results of the pH test 46
Figure 3.10: Daily Rate of pH change 47
Figure 3.11: Results of the Chapelle Test for pozzolanicity 48
Figure 3.12: Sieve Fraction of Experimental Aggregates before incorporation into Mortar 50
Table 3.13: Water absorption characteristics of the lab-produced aggregates 51
Table 3.14: Oxide content of the lab-produced aggregates 52
Table 3.15: Mortars Produced in the Laboratory 53
Figure 3.16: Model of the Experimental Mortar formwork 54
Figure 3.17: Photos illustrating the laboratory mortar making process 55
Figure 3.18 Polished cross-section images of experimental laboratory mortars 55

Chapter 4

Figure 4.1: Set up for measuring the ultrasonic resistance on cured mortar beams 58

Chapter 5

Table 5.1: A quick guide to the appearance of antique mortar constituents by PLM 65
Table 5.2: Suitability of OM for the study of pozzolan-lime mortar 66
Table 5.3: Suitability of different image-based techniques for the study of mortar thin sections 73

Chapter 6

Table 6.1: Types of Result by Technique 74
Table 6.2: Observations on the mortar making process 75
Figure 6.3: An Archeological Mortar visually compared to an Experimental Archeological Mortar 77
Figure 6.4: Ultrasound Pulse Velocity During Mortar Curing for the laboratory mortars 78
Figure 6.5: Rate of Strength Development as a percentage of final ultrasound velocity during mortar curing for the laboratory mortars 79
Figure 6.6: Compressive Strength of Mortars from both Experimental Mortar Programs 80
Table 6.7: Comparison of ultrasound velocity to compressive strength at 42 days 81
Table 6.8: Binder to aggregate ratio and weight percentage for both Experimental and Archeological Mortar per RILEM TC-167 82
Figure 6.9: Scatter Chart of Binder to aggregate ratio (mean values), expressed as a weight percentage, for Experimental and Archeological Mortar per RILEM TC-167. 83
Table 6.10: Soluble Silica proportion by weight for both Experimental and Archeological Mortar per RILEM TC-167 84
Figure 6.11: Scatter Chart of Soluble Silica in Experimental and Archeological Mortar per RILEM TC-167 85
Figure 6.12: Example thermographs of experimental and archeological mortar binder types 87
Figure and Table 6.13: Percentage weight loss in bound water in the binder of a selection of experimental and archeological mortars 88

Chapter 7

Table 7.1: Mortar Analysis Goals and those achieved by Comprehensive Image Analysis 90
Figure 7.2: Two lime lumps in experimental mortar 91
Figure 7.3: Two lime lumps in experimental mortar, detection, and imaging by wavenumber shift 93
Figure 7.4 Using FTIR to correctly identify an object previously characterized as a lime lump 94
Figure 7.5: Reaction Rims in experimental mortar 96
Figure 7.6: Reaction Rims in ancient mortar 98
Figure 7.7: Reaction Rims near lime lumps in experimental mortar 99
Figure 7.8: Reaction Rims preferentially near lime lumps relative to ceramic grains in experimental mortar 101
Figure 7.9: Reaction Rims on large calcite grain 102
Figure 7.10: Binder Alteration on a ceramic lime mortar, superficial gypsum formation 105
Figure 7.11: Binder Alteration on a pozzolana - lime mortar, ettringite and secondary calcite 106
Figure 7.12: Binder Alteration on a ceramic lime mortar, binder separation in to silica gel and Mg, Ca – CO_3 108
Figure 7.13: Pseudo-Color Analysis of Experimental and Historical Mortar 110
Table 7.14: Binder to aggregate ratios of Experimental and Historical Mortar 111

as determined by pseudo-color analysis
Figure 7.15: Binder to aggregate ratios of Experimental and Historical Mortar 111
as determined by pseudo-color analysis, rendered as a percentage
and overlaying the same samples as analyzed by chemical dissolution
Figure 7.16: Comparison of the reactive products of two experimental mortars 113
Figure 7.17: Comparison of the reactive products of an archeological mortar 114
and a restoration mortar
Figure 7.18: Comparison of the reactive products of two archeological mortars 115
Figure 7.19 Surface Area Percentage determinations by FTIR-imaging 116
for some common mortar contents
Table 7.20: Pozzolanic Reaction Products detected in both Experimental and 117
Archeological Mortar per image analysis

Chapter 8

Figure 8.1: Venn diagram illustrating the methods used during the course of this work 118
Figure 8.2: Scatter Plot showing the correlation between the chemical dissolution and 121
pseudo-color editing techniques for determining binder to aggregate ratio
Figure 8.3: Grouping Tables of showing the correlation between the chemical 122
dissolution and pseudo-color editing techniques for determining binder to
aggregate ratio or experimental and archeological mortars
Figure 8.4: Comparative Values of the Index of Hydraulicity for the experimental and 123
archeological mortars
Figure 8.5: Scatter Plots of the chemical dissolution and image analysis techniques for 124
determining the C(A)SH content in mortar
Figure 8.6 Correlation Percentages by mortar type for the methods used to determine 124
their binder hydraulicity
Figure 8.7: Comparison between methods of binder hydraulicity detection as 127
compared to tested mortar compressive strength
Figure 8.8: Mortar Strength Adjusted by detected binder C(A)SH % per sample 128

List of Abbreviations

ASTM/ EN	American Society for Testing of Materials/ European Norm
B:A	Binder-to-Aggregate Ratio
C-(A)-S-H, C(A)SH	Calcium (Alumino-)Silicate Hydrate
FTIR(-m)	Fourier transform infrared spectroscopy (-mapping)
OM/SM/PLM	Optical Microscopy/ Stereomicroscope (with polarizer)/ Polarizing Light Microscope

OM Abbreviations:

PPL	Plane Polarized (transmitted) Light
XPL	Cross Polarized (transmitted) Light
PPLD	Plane Polarized (transmitted) Light, Dark Field Mode
IL	Incident (reflected) Light (plane polarized)
ILW	Incident (reflected) Light, white background
ILXP	Incident (reflected) Light, Cross Polarized

SEM-BSE	Scanning Electron Microscope – Back-scattered Electron Mode
SEM-EDX	Scanning Electron Microscope – Energy Dispersive X-Ray Spectroscope (also as adv. "Microscopy"/ "Spectroscopy")
TGA-DSC	Thermo-gravimetric analysis- Differential Scanning Calorimetry
XRD	X-ray diffraction

1.0 Introduction

Mortars, renders and plasters are some of the most widely studied materials when examining an archaeological or historical building. Not only are they durable and ubiquitous, but they also encapsulate many aspects of a society's material culture and technological development, such as access to certain materials and relative proficiency of technique. In many ways, the ability to both execute a sophisticated architectural design, and have it survive far into the future is dependent on the level of mortar technology employed [1]. Professionals with backgrounds in archeology, architecture and construction, geology, history and art history, material science, and conservation science and restoration have all shaped the methods by which this research is undertaken. The result is that even a cursory search for academic articles online will result in thousands of publications resulting from collaborations between these researchers, each of whom bring their own perspective and "toolbox" when analyzing any of the cementitious systems that have been produced and used over the past three millennia at myriad building sites. A large amount of work has been done on understanding the systems of wall painting and render mortars, with the clear goal of prescribing an appropriate treatment to conserve the appearance of an archaeological site in an appropriate way [2,3]. This work focuses on the less-seen structural mortars, specifically on those made from combining lime binder with a reactive aggregate known as a pozzolan, detailed below. While bedding mortar, fill mortar (such as Roman-era opus caementicium), and water-proofing mortars are perhaps less important from an art-historical perspective, studying them does shed light on the durability of these ancient structures as well as provide perspectives on how similar materials could be used in current construction practice [4,5].

A number of previous studies have emphasized experimental archaeology - an approach based on the laboratory analysis of mortar produced in a manner similar to how it would have been produced historically [6-8]. Likewise, this work starts with observations of archeological mortar followed by the production of similar mortars produced "in the field" with the methods available in the past. Following this, a series of comparison mortars of similar composition were manufactured in a controlled laboratory setting. These "field" and "laboratory" samples were made to serve as control specimens to help evaluate the efficacy of the analytical methods employed, as well as to emulate the (presumed) starting conditions of archeological mortar. A novel protocol consisting of comprehensive, image-based analytical methods was then performed on high quality, polished (uncovered) petrographic thin sections of these mortars. This allowed for the same preparation of a sample to be examined successively by optical

microscopy (OM), scanning electron microscopy combined with energy-dispersive X-ray spectroscopy (SEM-EDX) and Fourier transform infrared spectroscopy imaging, here used in reflection mode. These results were complimented by and compared to more traditional mortar analytical methods. It is this protocol that should be considered the most important feature of the following work.

While every method has its advantages and disadvantages, imaging-based analytical techniques performed on polished thin sections are the best methods for examining the compositional and micro-structural inhomogeneity frequently encountered in the layered structure of a mortar sample. The thin sections preserve the spatial relationships and context between a mortar's micro-features. Studying them through the proposed protocol is the key to understanding the methods, materials and techniques employed by an artisan in producing the mortar, as well as the alteration phenomena that have taken place since [9]. In this manner a wide variety of correlative analyses can be performed on the same sample preparation.

This work applies this protocol to two series of experimental pozzolan-lime mortars, and in parallel, a wide variety of mortars from Roman antiquity. All of mortars studied were made from an air-lime (non-hydraulic) binder mixed with a reactive aggregate, either ceramic or volcanic pozzolan. The results of the analytical protocol were compared between experimental and archaeological mortars, and to data produced by more traditional types of laboratory testing, both physical and chemical. In addition to demonstrating the efficacy of this analytical protocol, the usefulness of both producing and testing experimental mortar as a means of understanding historical and archeological mortar, as well as traditional mortar analytical methods are explored. The latter is particularly important when assessing methods that result in the destruction of the sample. The emphasis is thus placed on gaining the largest amount of information from a single sample preparation, economizing in time, money and required number of samples.

2.0 On Pozzolanic Mortar and its Study – State of the Art

The firing of clay to form ceramics and the burning of limestone to create quicklime, likely first employed as a floor covering whitewash, are technologies that have been employed by human beings for thousands of years, stretching into prehistoric times [10-14]. At some point during this period, it was noticed that combining these two materials in powder form with water created a strong, waterproof mortar. Archeologists have discovered remnants of ceramic pozzolan – lime mortar dating as far back as at least the Minoan period, over 3500 years ago [15]. This technology has been in use to a greater or lesser extent since then. Volcanic pozzolan, while formed by a different process than ceramic, reacts in with quicklime and water in a similar fashion and has been in use since at least "a few hundred years" before it was written about by Vitrivius and Pliny [16-17]. Although the chemical process that creates this versatile building material was unknown at the time (and indeed remains the subject of study) the ingredients of ceramic pozzolan-lime mortar are ubiquitous, and thus have been used over a wide range of time and across regions, leading to it being studied and analyzed by a similarly wide range of scientists. The study of pozzolanic mortar involves the study of both the structures built with it, as well as the chemistry behind pozzolanicity. This work attempts to build upon this tradition by studying both the process behind and material of, pozzolanic mortar.

2.1 Pozzolanic Mortar - A Chemical Overview

This work is predominately concerned with the analysis of pozzolanic mortar, which is made by mixing a pozzolan - any finely graded siliceous or alumina-siliceous material, that has no cementitious properties of its own – with hydrated lime, either quicklime and water or lime putty (See Figure 2.1) [18]. This is a hydration reaction known as the pozzolanic reaction. Both volcanic ash/ sand and ceramic powder are considered pozzolans. Reactive volcanic ash is composed of acidic siliceous and aluminous material that has condensed from clouds of pyroclastic flow, stone that was melted within a volcano then ejected and aerosolized during an eruption. Both loose ash deposits and finely ground tuff, a highly porous, amorphous stone formed by these deposits, can be used as a pozzolan [19-21]. Ceramic is made from the firing of clay, a material also mostly made of alumina and silica. At around 500 ºC the process known as dehydroxylation (the driving off of bound water) occurs leaving these clay minerals in a semi-crystalline state. When finely ground, the resulting powder, composed of poorly

crystalline and amorphous alumina-silicates, is reactive pozzolanically. It has been established that the low-temperatures used historically to fire clay into common ceramics, such as amphorae, result in an ideal material that can be used to make a pozzolanic mortar [22-23]. With both volcanic and ceramic pozzolans, the poorly crystalline to amorphous state of the alumina and silicates, as well as their high specific surface, is essential to their ability to react in the short term [18-23].

When either pozzolan is in a highly alkaline, aqueous environment, the reactive, acidic silicate material dissolves and combines with calcium and hydroxide to form a molecule known as **c**alcium **s**ilicate **h**ydrate, abbreviated as C-S-H (or C-A-S-H as it may also include **a**lumina); hereafter generically referred to as C(A)SH [22-23]. This binder is the distinguishing characteristic of pozzolanic mortar, thus the study of pozzolanic mortar is in a large part the study of the pozzolanic reaction and C(A)SH.

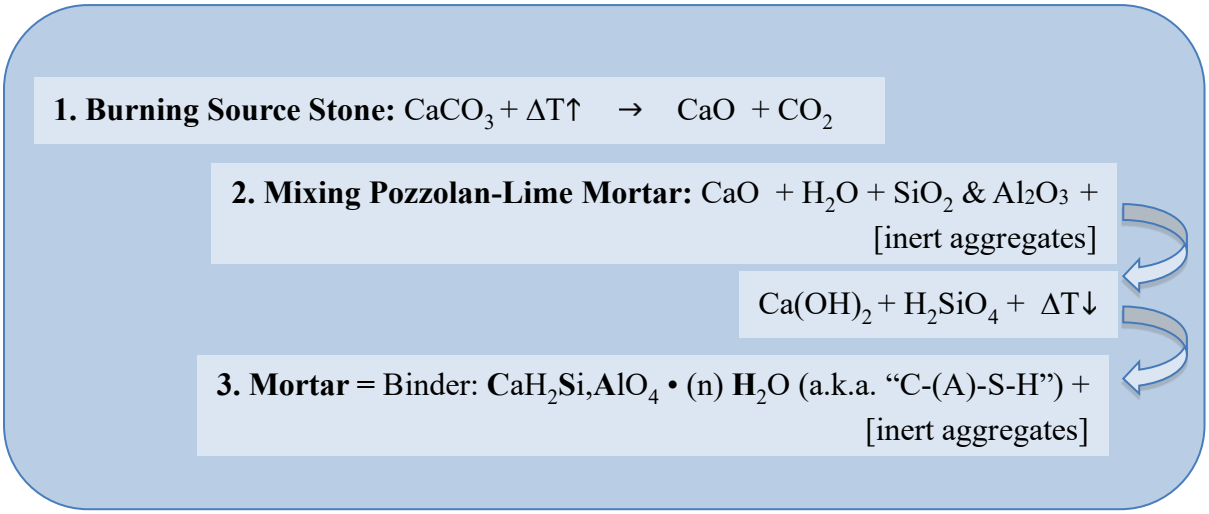


Figure 2.1: Idealized/Simplified Chemistry of a Pozzolan-Lime Mortar

Calcium (alumina-) silicate hydrates are made up of long chains of silicate (SiO_4)[1] bound to a core of calcium oxide (CaO). The fundamental unit of the silicate chain is a three-molecule unit known as a dreierkette. All three tetrahedrons are bound together, but while two of them are bound to the central Ca-O core, a third one is free to bind in a different direction. During the pozzolanic reaction, these silicate units link to each other, but also are able to bind with free Ca^{2+} and free water in the reactive environment because this third silicate tetrahedron has a net

[1] In C(A)SH Al serves as a replacement for Si in some instances, depending on the mineral species. In general, when discussing C(A)SH, when "silicate" is mentioned, it can in fact be replaced in this manner (Si,Al).

negative charge and is thus drawn to both the positive calcium ions and the positive poles of the free water. This is known as bridging; these silicate units form a bond between silicate-calcium oxide chains through an interlayer of Ca^{2+} and water [24-25]. This process is illustrated in a simplified form in Figure 2.2 below. As this occurs, chains become longer and more cross-linked, a process sometimes described as "geo-polymerization" [26,49].

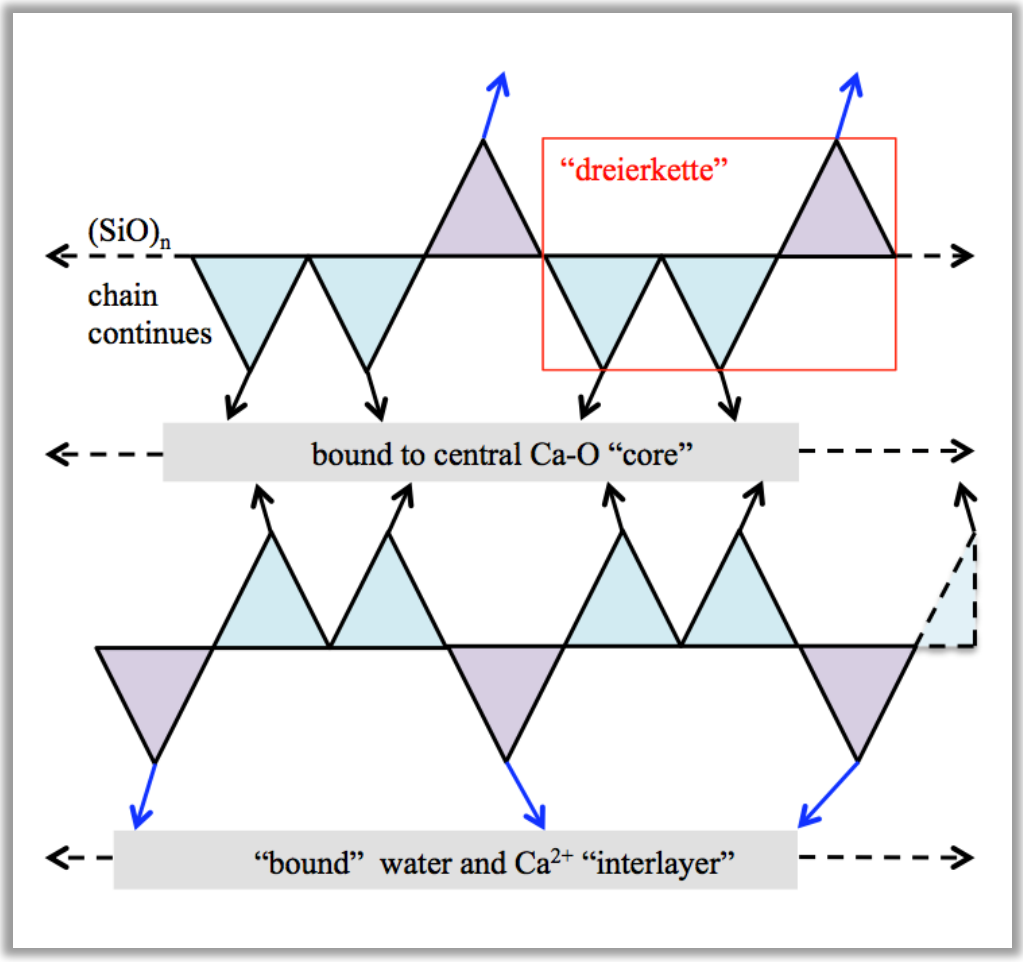


Figure 2.2: Basic Structure of C(A)SH - image after [22-24]

C(A)SH has been described as being both gel-like and poorly crystalline [27-28]. The difficulty in describing the structure of C(A)SH is partly responsible for its nomenclature (usually written C-A-S-H), which describes the variable structure as well as the variable stoichiometry of calcium-alumina-silica and – hydroxyl [29-32]. This range of stoichiometry is generally described by the similarity of the C-S-H phases to two naturally occurring minerals, jennite and tobermorite, which are close to the theoretical maximal or minimal proportion of CaO/SiO_2, found in artificially produced C-S-H of 1.5 to 0.83, respectively [30, 31]. Adding to the variety of minerals formed is the presence of reactive alumina, which is prevalent in both volcanic and ceramic pozzolans (see, for example Table 3.14 describing the oxide content of the pozzolans

used to create mortar for this work). Because of alumina's ability to substitute silica in forming the "dreierkette" chain, a variety of calcium alumina-silicate hydrates are formed during the pozzolanic reaction, such as strätlingite, hydrogarnet and aluminum-substituted tobermorite [4, 5, 20-22, 28, 30, 32]. If sulfate minerals are present in the pozzolan, lime binder, or even water used for mixing the mortar, there exists the possibility of sulfate for hydroxide (from the interlayer water) substitution forming the mineral ettringite [4,5].

Regardless of composition, C(A)SH forms a complex lattice within a mortar, binding it together, as illustrated in Figure 2.3 below. As alkaline calcium hydroxide (the blue octagonal lozenges) reacts with the particles of pozzolan (brown-yellow objects), either acidic or made acid by the interaction, the constituent ions of both recombine in an acid-base reaction to form C(A)SH. The C(A)SH fills the interstitial spaces between un-dissolved pozzolan, unreactive aggregate and unreacted calcium hydroxide which may remain in the system as crystalline portlandite. Although this process is a slow-speed reaction, it was found in practice within the scope of this work that the resulting mortar composed of pozzolan and lime had undergone an initial set within 4-24 hours after which they could be de-molded (see Section 3.5).

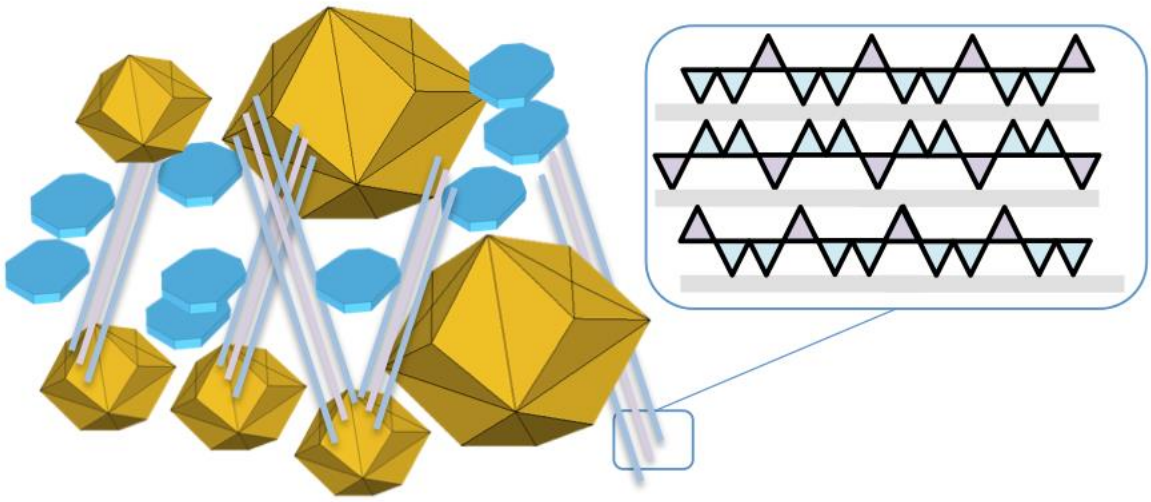


Figure 2.3: Simplified Schematic of a young pozzolan-lime mortar, blow-up refers to Figure 2.2 above.

Ultimately, detection of either C(A)SH or one of its alteration products is one of the main goals in describing an historical mortar, thus proving its either intentional or incidental pozzolanicity [33]. A wide variety of methods used by researchers to detect C(A)SH are described in the following sections: this work focuses on its visualization and localization, but not identification of specific phases. C(A)SH is often described as having a needle-like

crystalline structure, which can be seen in the examples given in Figure 2.4 below, which show this by both light microscopy and scanning electron microscopy. Later, it will be shown how it is detectable and even (semi-) quantifiable by FTIR-Imaging combined with digital image analysis, which was used to detect C(A)SH by the distinctive spectra of the interlayer water and silicate chains.

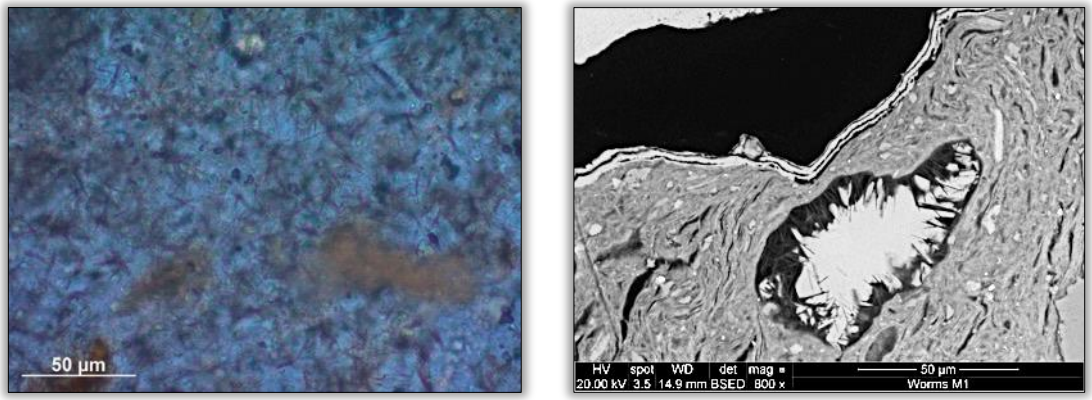


Figure 2.4: C(A)SH by PLM (plane polars) (L) and SEM-BSE (R). Both examples are ancient ceramic-lime mortar, (L) from a Roman bath at Aquincum, Hungary and (R) from a baptistery in Worms, Germany (C(A)SH are the dark needles surrounding the central bright lime inside of the ceramic body).

2.1.1 Pozzolanic Mortar – Its Use Throughout History

While archeologists are continually discovering the use of pozzolanic mortar from different regions and eras, the oldest historical references to its use are found in the works of Vitruvius' 10 Books on Architecture and Pliny's Natural History, both written during the early Roman Empire (1st Century CE). In their works, they refer to the use of both crushed ceramic (as *opus signinum*) and volcanic pit sand (as *harena foscia*) for their use in making a strong, water-resistant mortar, and how this practice was already in use throughout the Empire "for quite some time" [16-17]. They give systematic instructions for which applications this special mortar should be used in, as well as recommended ratios of lime to aggregate (assumed to be by volume) for each application. The virtues of the sand from the region near Pozzuoli which allow for building "even under water", are given high praise; Vitruvius even attempts to give a scientific explanation, based on the ancient, empirical understanding of the natural world, of how the pozzolanic reaction (named after *pulvis puteolanis* "dust of Pozzuoli") works [16-17]. These works are important for two reasons. Firstly, because they set an absolute latest time for

when pozzolanic mortar was being intentionally produced, which coupled with the knowledge gained through modern archeology gives us a greater understanding on how the wonders of Roman-era construction worked [34-36]. Secondly, by writing about these materials, they ensured that their knowledge would survive the collapse of the Roman Empire, at least on a local level. This knowledge was brought back into the mainstream of materials science by the work of John Smeaton, who sought a mortar that would set under water, and thus could be used in a lighthouse he was engineering. As described in his work regarding this construction, he experimented with and eventually used a variety of pozzolana-lime (from Italian volcanic ash) and pozzolan (ground Rhenish trass) – hydraulic lime mortars to build the Eddystone Lighthouse [37]. During the industrial revolution of the 19th century, there was intense interest in developing hydraulic binders from the burning of clay-rich limestone (that Smeaton was in fact attempting to "improve" by adding pozzolans) to produce what is now known as hydraulic lime. One of the preeminent scientists in this field was Louis Vicat, who published his treatise on making concrete structures using hydraulic lime and pozzolanic materials, such as metallic and coal slags, in 1818 [37A]. Concurrently, the mid-19th century also saw the development of a higher temperature version the process of making hydraulic lime that used marlstone to produce a fast-setting cement known as Roman cement, which was produced in the United Kingdom, France, Austria-Hungary, Germany and the United States [37B]. This line of rigorous experimentation with hydraulic binders quickly led to the invention of Portland cement (in which the clay and limestone are sources separately, burned together) by Joseph Aspdin in 1824 [38-40]. Portland cement, like pozzolan-lime cement, uses a hydration reaction to form a C(A)SH binder in concrete, and additionally produces a large amount of calcium hydroxide (portlandite). Modern concrete now often incorporates pozzolan to react with this calcium hydroxide creating a denser C(A)SH fabric, thus, pozzolans can in fact be found in a very wide variety of binders throughout history [18,21,41]. While this work deals with material from antiquity, many of its findings could be applied to any cementitious system that incorporates pozzolanic material.

2.2 Current Research into Pozzolans and Pozzolanic Mortar

Due to its long history of use, its durability, and potential for applications in modern construction materials, research into pozzolanic mortar has been robust since Smeaton's time, increasing since the professionalization of materials science in the 19th century. The relevance

of this research to the discipline of conservation science can be described as falling into three broad categories. The first is the study on a case-by-case basis of archeological and historical structures that use volcanic or ceramic pozzolan with lime as a binder. The second examines and recreates the same types of binders as a restoration material of these same cultural resources. The third more specifically focuses on methods and techniques of studying these types of materials, both historical and modern. This work has applicability to all three of these categories but is focused mostly on the third.

There exists a broad movement of research into materials sciences that targets the identification and qualification of new sources of pozzolan, from natural ones [18,42-44] to industrially produced products or by-products[46-48], often focusing on how they can be used as an environmentally friendly concrete additive [50-53]. Developments in this area can advance those in the field of historical building materials research and vice versa; the ability to apply the lessons learned from studying of historical building material is often cited as justification for their study in the first place [54-56], a methodology that can indeed be traced back to Smeaton's study of Roman concrete during his quest to find a strong hydraulic binder. Although this study is not intended to have direct application to the production of new materials, it shares a common background.

2.2.1 Ceramic and Volcanic Pozzolan – Lime Mortar as a Historical Building Material

Conservation scientists and archeologists have studied pozzolan (both volcanic and ceramic) -lime mortar construction in historic structures intensively, often with the goal of understanding which mortars were used in particular parts of a building. Additionally, changes in the materials used and technique of application are cited as evidence used to establish building chronology, often with the subtext of understanding increasing (or decreasing) levels of technological sophistication and/or importance of that building type.

The use of crushed ceramic has been demonstrated from times as far back as the Mycenean [55] and Hellenistic times [56], but it is thanks to both the writings of Vitruvius and Pliny, as well as the large number of remaining Roman-era sites and structures, we know that both ceramic and volcanic pozzolans were used profusely by the Roman civilization. Volcanic pozzolana was used for a number of high-value projects, especially on the Italian peninsula and Anatolia [57-60], sometimes even in combination with ceramic aggregate [61], most famously for the Pantheon in Rome which uses volcanic ash as the pozzolan in the dome with aggregates

that decrease in density as the oculus is approached [36, 38] Additionally, volcanic pozzolana was so valuable for use in the construction of underwater piers of Roman concrete that it was shipped as the ballast in ships for use in harbor construction around the Mediterranean; pozzolana from Pozzuoli had been found in Roman piers in Brindisi, Alexandria (Egypt) and Caesarea Maritima [62]. Samples from this last site have been analyzed by this author, showing that volcanic pozzolana was used for a number of structural applications such as a pool, a breakwater and the foundations of a residential structure; analytical results for these mortars are discussed in the Results chapter (mortars labeled "CAE" or Caesarea). More prosaically, volcanic pozzolana was used in *opus caementitium* cavity wall construction and as a bedding mortar for both stone and brick masonry [34-36], generally based on local availability of volcanic pozzolana; examples of this application are shown in Figure 2.5 below.



Volcanic Pozzolanic Mortar as fill and bedding mortar, Pompeii, Italy

Volcanic Pozzolanic Mortar as fill and bedding mortar, Ostia Antica, Italy

Ceramic Pozzolanic bedding mortar. San Vitale, Ravenna, Italy

Ceramic Pozzolanic bedding mortar. Ottoman Fortress, Istanbul, Turkey

Figure 2.5. Volcanic and Ceramic Pozzolan Structural Mortars, as described. *Photos Author's own Work*

The bulk of Roman pozzolan-lime mortar used ceramic as its reactive aggregate, especially in buildings from the provinces [63-64]; many examples presented herein are of this type, for example the mortars presented from Vindobona (Vienna), Aquincum (Budapest), Augusta Vangionum (Worms) and Školarice (Ancient name unknown). In these examples, as well as many other in the Roman world [60-65], ceramic pozzolan is used in many of the same applications as volcanic pozzolan would have been used, if it were available. For example, the walls of cisterns and baths and the lining of aqueduct channels were often made of thick cocciopesto layers. It is evident that where Roman building tradition continued following the decline of the Western Empire, i.e., in the Byzantine and subsequent Ottoman Empire and Venice, there was a transition from volcanic to ceramic pozzolan for use in bedding mortar, illustrated in Figure 2.5 above. Following the disintegration of the Roman Empire the use of

volcanic pozzolana was generally abandoned, as evidenced by its disappearance from the archeological record. Ceramic-lime mortar, however, was used continuously in the Medieval, Renaissance and early Modern period, often as a flooring material, in prestigious buildings such as The Cathedral of Pisa, the Doge's Palace in Venice, and Westminster Abbey in London [65-67].

Several studies use this fact coupled with the observation that mortar compositions and techniques changed over time, to trace the history of successive occupations of a site [15, 68-70] or the building chronology of repairs or additions to a building [71-72]. Similarly revealing is studying which specific formulae of pozzolan-lime were used, depending on structural requirements, e.g how did the binder to aggregate ratio, aggregate grading, and/or artisanship differ between a cocciopesto floor and the lining of a water channel [73]. Provenance studies of pozzolans (in particular, those of volcanic origin) reveal to which lengths ancient builders went to gain these prized building materials [74].

While studying specific buildings and mortar applications, the nature of pozzolans and pozzolanic mortar is studied from a physical-chemical standpoint. Of particular interest is how pozzolans interact with lime [75-76] and if certain preparations are more effective at making a strong binder material than others. Due to the continued existence of a many from antique times built using pozzolan-lime mortar and concrete, the high strength and durability of this material is the subject of many studies [5, 77-81]. Techniques of studying pozzolanicity are further elaborated in Section 2.2.3 below and many of them form the theoretical background for the experiments and analysis (Chapters 3 and 4) performed within this work. Further, the protocol developed herein is in effect a method of studying pozzolanicity, as well as structures made possible by pozzolanic mortar.

2.2.2 As a Restoration Material

Modern cements, especially Portland cement, has been well established to be inappropriate as a repair material for many types of historical buildings, there has been quite a bit of research into the use of pozzolan-lime mortar as a "like for like" replacement or repair mortar [7, 82-83]. A wide variety of laboratory experiments have been conducted into the formation and nature of artificial pozzolans, such as the effect of firing clay at different temperatures and how this affects the reactivity of the resulting powders [84]. Other experiments focus on the use of industrial waste as a pozzolans [85]. The material that is often the focus of this type of research

is metakaolin, a pozzolan formed from the firing of very pure kaolin clay [86-88]. Regardless of the source of the metakaolin used as pozzolan, it was found to be a better replacement for historical lime mortar, especially in humid conditions, than those made with Portland cement [85, 86]. Lime mortars produced with either metakaolin (or any other pozzolan) need to be kept in a humid curing environment for optimal strength development [87], something that is either achieved by covering during restoration application, or by nature of the fact that these mortars are used in closed systems (as opposed to wall covering). In fact, pozzolan-lime mortar formulae can be adjusted by the introduction of more water or plasticizing agents in order to inject a repair mortar into closed systems that will then hydrate and gain strength in this environment [88]. Since metakaolin is white, it is suitable to a number of applications that are color-sensitive, in that the resulting mortar can either be pigmented to any color or is a suitable for over-painting [89]. Ceramic pozzolan, while only moderately reactive, can be combined in special cases with natural hydraulic lime, boosting the hydraulic properties of a mortar [90-91]. Both air lime and naturally hydraulic lime – pozzolan mortars perform well for restoration purposes when they have similar performance characteristics, such as compressive and tensile strength, water vapor permeability, porosity and modulus of elasticity, as those used in historical structures [91]. Care must be taken when combing pozzolan with naturally hydraulic lime, as the strength of these mortars can approach that of the Portland cement repair mortar that was being avoided in the first place [90]. Similar to the results shown in this work, there has been research that compares the characteristics, advantages and drawbacks volcanic pozzolan mortars to those of ceramic pozzolan mortars, in many cases assessing their suitability as restoration mortar [92]. When not applied to a specific problem, research of this nature blends into the realm of basic research discussed below (Section 2.2.3), albeit one that emphasizes cultural heritage applications.

Outside of a purely laboratory setting, practical aspects of restoration mortars can be assessed on a problem- or site-specific basis. These “boutique” solutions are calibrated on a case-by case basis, for example the creation of a porous pozzolanic “sacrificial layer” to protect masonry or render layers from frost or salt attack [93]. Finding the compatible repair mortar for a building or archeological site often requires the boutique approach as well, balancing historical and physical compatibility, aesthetics, and environmental concerns. For the protection of an archeological resource, often pozzolan-lime mortar is the ideal solution as is described in a number of publications [85-89, 91,94].

2.2.3 Methods of Study of Pozzolanicity and Pozzolanic Mortar

As a type of basic research, the continual development of techniques for detecting, qualifying and quantifying pozzolanic activity both in historical and new materials is strong, with applications outside the realm of conservation science, most especially in relation to modern building materials. A wide variety of methods are used to understand pozzolanic mortar, which can be roughly divided into physical and chemical techniques (which generally destroy a sample), microscopic and micro-analytical techniques (which generally preserve the sample). These can be complemented by using experimental archeology, in which a new material is produced according to techniques available historically. In practice, there is quite a bit of overlap between these categories, and they are used in conjunction in individual case studies. Generally speaking, a combination of techniques is used to complete a study. The state-of-the-art methods that informed test protocols used herein are summarized in the following sections.

2.2.3.1 Chemical and Physical Testing

Although not the main methods prescribed by this work, many of the standard techniques for analyzing mortar are based on physical and chemical testing - test methods that destroy the sample. Through the destruction of the sample, chemical and or thermal dissolution provides highly accurate quantitative analysis of a mortar's contents. Thermo-gravimetric analysis (TGA, with its rate being expressed as DSC) is the thermal breakdown of a mortar, especially its binder. The corresponding weight loss at different temperatures correlates with different parts of the binder, free water, bound water (in hydraulic mortar), organic and carbonate, and is widely used to understand historic pozzolan-lime mortar [7,95-96]. Many TGA-DSC devices also have the option of performing mass spectrometry (MS) for increased confirmation of the results. In the case of ceramic-lime mortar, this is often compared with XRD analysis on the remaining ceramic aggregate [81], which reveals the chemical phases of the ceramic, as well as information regarding its potential reactivity based on its crystallinity [6]. Both the bound water content of the binder (identified by TGA) and the amorphous proportion of an aggregate (found by XRD) are related to the (potential) pozzolanicity or hydraulicity of a mortar. Portions of both binder and aggregate can be powdered and tested through FTIR or Inductively Coupled Plasma - Mass Spectroscopy (ICP-MS) for the highest level of chemical detail [96-97].

Chemical dissolution of a mortar represents an older, more accessible technique, as it does not require the use of sophisticated devices. RILEM codified these techniques in 2005, with an exhaustive publication on the subject [99]. Like TGA, chemical methods provide results expressed gravimetrically (i.e., weight loss of the sample when treated with acid). It is used in this work (Sections 4.4 and 6.4) to help interpret results found by microscopy, predominately related to the detection of soluble silica found in the binder. All of these techniques rely upon correlation between methods, which can be variously effective [99].

While the above methods are used to understand the contents of a mortar, physical testing is often used to understand the performance of a mortar. This approach has been mostly standardized through test procedures codified by research and governmental agencies such as the European Committee for Standardization (EU-Norm, EN) and the roughly equivalent American Society for Testing of Materials (ASTM) with the tests of compressive strength (ASTM C109/ EN 196) and flexural strength (ASTM C349/ EN 13286) being used most typically. The experimental mortar produced in this work was likewise subjected to these tests (Sections 4.2 and 6.2)[2]. These techniques require a standardized sample size and mortar curing environment (ASTM C192 in the laboratory, C31 in the field) and are therefore not directly compatible for analyzing historical samples. Although physical testing of non-standardized pieces of historical mortar can be performed [101], this was not attempted, as there would be little correspondence between the experimental and historical mortars examined herein. However, strength development during the curing period of the experimental mortar was evaluated by means of an ultrasonic pulse device [102] (per EN-12504/ ASTM C 597; See Sections 4.1, 6.2) similar to the technique as employed in the laboratory [103]. Not addressed in this work, but a recommended path of investigation for a similar study would involve nano-indentation of mortar as a measure of its strength [104-105]. The method of nano-indentation, which can also be performed on a polished thin section, use a diamond needle to test the hardness of different parts of a mortar, moving, for example, from the binder matrix through a. reaction rim into an aggregate. This information can reveal the strength of the bond between binder and aggregate and the density and hardness of each part of the mortar giving a good indication of its overall strength [ibid], but because this leaves microscopic scratches on the thin section, this method was not pursued.

When working with historical mortar, a correlation is often made between physical characteristics (such as compressive strength or water vapor permeability) and the mortar's

[2] Only compressive strengths are reported herein; since the tensile strength values of many experimental mortars were too low to be measured with confidence.

performance as part of a building system (such as how well it binds bricks or protects a surface). One key area of research focuses on the comparison of mortars with different formulae, adjusting the water/ binder (w/b) binder ratio, the aggregate type or grading or binder to aggregate ratios (b/a) [106-107]. As discussed below, and in Chapter 3.0, only the aggregate type was adjusted in this work. Other key factors affecting a mortar's performance are its porosity and water permeability [108-109]. While porosity is described within the context of this work, experiments testing water permeability, salt transport and other physical issues related to porosity are not explored.

While the above methods describe chemical and physical testing methods of mortar (pozzolanic or otherwise), the pozzolanic ingredient itself it the focus of a wide variety of research, which has applications beyond the practice of conservation science. This is because pozzolans can be valuable for modern building materials as a cement replacement for concrete. ASTM D5370 and EN 197-1 have codified their incorporation into concrete when used in contemporary buildings. Often research into both volcanic and ceramic pozzolans in the conservation sciences field acts a bridge between ancient and modern applications of pozzolana [4, 43-44,110]. The reactivity of heat-treated clays, kaolin-like or otherwise, is of great interest to materials scientists of all sorts; of particular interest is which clays are most reactive [111], the level of reactivity of different clays achievable at different firing temperatures [84], how reactive they become [112], and finally which properties they exhibit when combined into a mortar [113]. Within the context of this work, the reactivity of the pozzolans was gauged both by physical and chemical means. Firstly the theoretical reactivity of pozzolanic powders was tested in a laboratory setting by their ability to alter the pH of a $Ca(OH)_2$ solution [114] and by their ability to bind a set amount of lime [115] (Sections 3.3-3.3.1). Finally, the mortar strength testing mentioned previously (Sections 4.1,4.2) can also be considered a method by which to assess the reactivity of the pozzolan - higher strength implies greater reactivity.

2.2.3.2 Microscopic, and Micro-analytical Techniques

In the methods listed above, it is generally the case that there is sufficient sample material to dissolve one part of a sample thermally or chemically, while leaving a portion from which a petrographic thin section can be produced. This is an important step to not only characterizing the aggregate and binder used, but also how the mortar's constituent parts relate to one another, giving a greater understanding to the mortar's performance. This

microstructural data includes quantity and shape of macro-porosity and cracking of the mortar (generally the porosity that can be directly seen by SM and counted in imaging software), the morphology and density of relic lime clasts (lime lumps), alteration of aggregate as both a sign of pozzolanicity or degradation, and evidence of binder alteration, such as the dissolution and re-precipitation of calcium carbonate within the mortar [1, 9, 128-130]. Studying these phenomena is the key to understanding the "life story" of the mortar: the production of the binder material, the selection of aggregate, the production and application of mortar and subsequent physical and chemical changes that occur both during its service life and as an archaeological remnant [1, 9, 128]. Mechanical, chemical, and thermal dissolution of the sample deletes this sort of information. Furthermore, when studying ancient, highly altered pozzolanic mortar, mechanical and chemical separation of a mortar's binder and aggregate is often difficult to impossible to perform [129]. Therefore, the main analytical tools used in this work, detailed in Chapter 5, are microscopic and micro-analytical. Moving in a comprehensive way from optical microscopy through SEM-EDX and finishing with a novel application of FTIR and digital image analysis, the protocol described herein aims to gain both the information described above, as well as that typically provided by thermal and chemical dissolution techniques, from single sample preparation that is left intact.

A standard method of mortar analysis, partially because the equipment is so accessible, but also because it gives such good results without a huge expense of time and resources, is optical microscopy on petrographic thin sections. Mortar morphology displayed through optical microscopy, both stereo- and polarizing light microscopy, gives information about the skill level of its artisans [1, 71, 123] and can additionally establish a building chronology [131]. Analysis of the binder material source, and the binder itself, is a typical method for accomplishing this task, as these retain characteristic features of the resources and technology available to the builders [132-133]. In the case of ancient pozzolanic mortars this takes the form of the study of relic lime clasts, also known as lime lumps, traces of unburned or un-dispersed quicklime as a main indicator of binder technology [1,121,122]. In the case of decorative plasters, ideally the thin section contains all layers of a painted surface, from the scratch/brown coat to the arrici and intonaci including the paint(s) used, so that the different stratigraphic layers can be studied all at once and in relation to each other [1, 134]. Studying the reactive aggregate, either intentionally used as a pozzolan or otherwise, gives information on the long-term stability of the mortar, and additionally is applicable for understanding the behavior of modern materials [135-137].

After analysis by optical microscopy, a common next step is the examination in high detail of particularly interesting areas by scanning electron microscope. The process of performing examination by PLM and SEM has to some extent become a standardized method of examination [138]. Generally, the SEM is coupled with an energy dispersive x-ray spectroscope (EDX), which allows for the elemental analysis (often presented in terms of balance oxide percentages) of the binder, aggregates, and alteration products. SEM-EDX can be used in combination with XRD to provide in-depth data regarding the aggregates, which can then be used to determine the provenance of materials [120,139]. SEM is a powerful tool for visualizing many phenomena that are associated with the pozzolanic reaction, such as the primary cementing phase C(A)SH [140], reaction rims on aggregates [141], the interface between the binder and relic lime clasts [142], and alteration products of C(A)SH, such as ettringite [143] or silica gel [144]. It is the second step in the comprehensive image-based protocol used here and espoused in earlier works with which it is associated [9, 128, 144].

The final steps in the protocol used herein rely on the application of both FTIR-imaging and digital image analysis to the study of mortar thin sections. Since mortar is both durable and a good indicator of the level of building technology employed a historical site, a wide variety of spectroscopic and micro-analytical techniques have been applied to analyzing historical mortar, generally reflective of the time and resources available to an analyst, and often reflecting their personal proficiency in the technique. One of the most common is the application of Raman spectroscopy to cement or mortar, either in powdered form or prepared as cross or thin sections. Raman spectroscopy utilizes a laser to induce a virtual energy state in the target molecule, which responds by scattering the laser light inelastically in a distinctive manner allowing for its identification [145]. Applied to mortar, it can be used to study mineral aggregates [146], fuel residue and pigment [147] and indeed both remnant cement clinker phases as well as different types of cement hydrates [148-150] including those found in Roman-era mortar. However, the ceramic fines found in both the archeological and experimental mortar discussed herein were found to create significant fluorescence problems when analyzed by Raman. Since main foci of this work include both the reaction rims at the ceramic-binder interface as well as the binder matrix, which is typically filled with ceramic fines, this technique was not pursued further.

FTIR was selected for the final analytical step in this protocol, building upon its application to identify inorganic materials in general [151] and its use to study cement minerals [152-157] and petrographic thin sections [158] specifically. It has previously been applied with success to ceramic materials [159]. The underlying techniques used by these authors, as well as the "library" of known spectra within their works provided was used to identify the minerals found

within both the experimental and archeological pozzolan-lime mortar which had previously been studied by OM and SEM-EDX. Once reaction product spectra were identified, they were then mapped throughout a sample, allowing for their further analysis by image-processing software, both integral to the FTIR device and externally. As will be shown, FTIR was the important final step in confirming the occurrence of the pozzolanic reaction, as it can be used to indicate co-molecularity of the constituent parts of both C(A)SH and its degradation products.

The novelty of this work is its application in sequence of this combination of techniques on polished petrographic thin sections of both experimental and historical mortars, as discussed in the following sections in detail. These were done to understand more fully the processes that go into the creation of pozzolan-lime mortar, its behavior, and the alteration processes that it undergoes. The application of this comprehensive, image-based analytical protocol produced the core results presented herein in Chapter 7; how they were produced is detailed in Chapter 5.

2.2.3.3 Experimental Archeology

Experimental archeology is a mixture of science and the historical reenactment of some traditional technology in order to understand both the production and performance of an artifact. If successful, the resulting product can give a good idea of how the historical item would have performed when new, additionally providing, by comparison, how the historical item has changed over time. As applied to the study of historical pozzolan-lime mortar, this means slaking (mixing with water) quicklime produced in a traditional manner and mixing it in the required proportion with a pozzolan acquired or produced in a traditional manner. Many studies of this sort use the writings of Vitruvius and Pliny as a starting point [16-17], much as actual artisans did throughout history, as they would have also been following these texts. This work is no different and the process by which experimental mortar was produced is described in detail in Chapter 3.

The technique of slaking and mixing the mortar is also important to its performance and appearance. Longer lime slaking times have been associated with higher eventual strength development, both for “hot-slaked” sand-quicklime mixtures [123A] and for lime putty without aggregates. Recently a number of small experimental limekilns have been built to further explore this topic, to study the effect of firing temperatures and times on the resultant lime [116-

119]. Rather than produce a homogenous quicklime powder, these kilns leave traces of under- or over-burned limestone, residual fuel and other products that are also discoverable in historical mortars. Vitruvius recommended using lime putty (fully slaked lime) for ornamental plaster (intonaco layer of a wall painting), but left no particular recommendation for structural mortars, just that they be well mixed and in the case of *opus signinum* pointed out that the ceramic be well crushed in the mixing process [16]. For Roman structural mortars, such as the ones both emulated and studied in this work, both art historical depictions (such as on Hadrian's column, Rome) and surviving texts, such as Josephus's account of the building of Caesarea Maritima describe a method known as "basket slaking" in which baskets of pozzolana and lime are mixed with water (with excess water draining out) shortly before the placing of this mixture in formworks or cavity walls [119a]. Experimental re-creation of this technique has shown that the mixture can retain heat for a protracted period [62, 77]. Regardless of structural application, if quicklime and pozzolan were mixed with water, the pozzolanic reaction would start immediately[3]; this led to the application of mortar while it was still warm and while the lime was still slaking, which is detectable by microscopy (in the form of both under-slaked remnant "lime lumps" and underburned pieces of lime source stone "relicts") [76, 120-124]. Because it was decided that "basket -slaking" was the likely method used to produce the archeological mortar studied in this work, this was the technique used to produce the experimental mortars studied in parallel.

The production of historically accurate mortar for understanding the past, as well as to formulate repair materials, is of great importance to this work. Two sets of experimental mortar were produced, one in the laboratory and one in the field. Production of historically accurate pozzolan-lime mortar in the lab (Section 3.2) has a long history, with its usefulness as a repair mortar often being emphasized [82,92,107,123, 123A]. The idea that ceramic pozzolan represented a type of ancient (and future) recycling has been explored [124-125]. As in this work, the idea of producing basket-slaked lime mortar under laboratory conditions has been attempted, with an emphasis on the physical and chemical properties induced by this method [76].

Field production of experimental mortar represents a closer approximation to what would have occurred traditionally. Unlike lab-produced mortars that more closely emulate an ideal

[3] Although the reaction indeed takes time, the author has direct personal experience (including results of Vicat time of initial set testing, performed in the context of his master's thesis) that indicates that any mixture of a highly reactive pozzolan with calcium hydroxide putty or quicklime and water would have set strongly enough to be unworkable in the space of a few hours, certainly long enough for heat of slaking to dissipate and long before the formation of a "well cured lime" that can be achieved by storing calcium hydroxide in anaerobic conditions (with or without the inclusion of non-reactive aggregate ("sand slaking") for long periods of time.

mortar as shown in Figure 2.1 above, field mortars often reproduce all the "impurities" that researchers see in actual historical mortar, such as lime lumps, fuel residues and a wide variety of unreactive or semi-reactive aggregates. This creates the more realistic environment shown schematically in Figure 2.6 below. Ceramic-lime mortar has been replicated as Roman flooring [126] or Byzantine brick and mortar beds [127] to demonstrate its utility and explore its potential from the decorative to the practical. Volcanic pozzolan - lime concrete has been replicated for underwater constructions, emulating the high point of Roman engineering [8, 62]. In the course of this work, standard test prisms were created from both pozzolans, but under field slaking, mixing, casting, and curing conditions (Section 3.1).

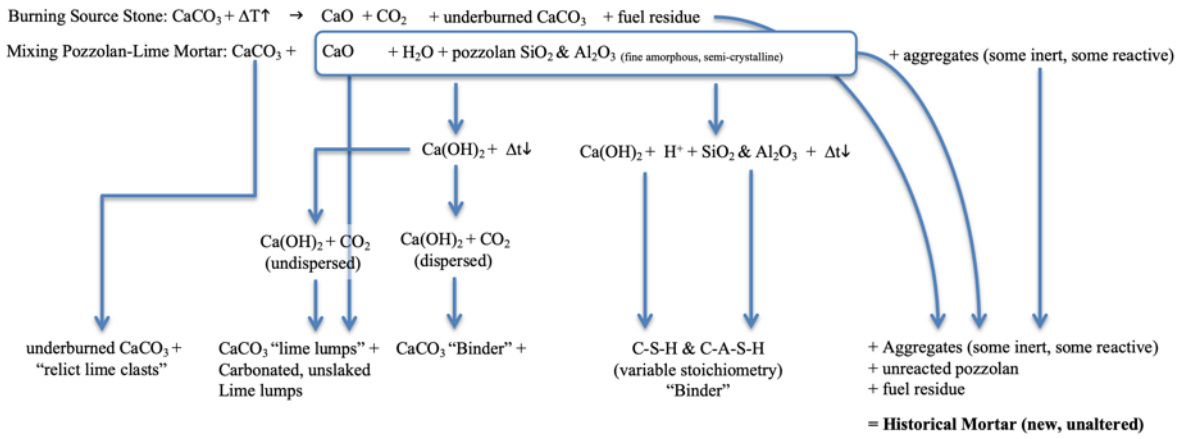


Figure 2.6: Practical Chemistry of an unaltered historical Pozzolan-Lime Mortar

3.0 Production of Mortar Control Samples for Comparative Analysis.

The following 3 chapters concern the experimental process of producing historically accurate Roman mortar and the methods by which they will be analyzed and compared with actual archaeological samples. This chapter, Chapter 3, describes the two methods by which Roman mortar was produced by experimental archeology (Sections 3.1 and 3.2), both in the field and in the laboratory as well as a discussion of the characteristic component of this type of mortar, the reactive aggregates used (the pozzolans, Sections 3.3-3.3.1).

Chapter 4 details the procedures used to test the physical and chemical characteristics of both types of experimental mortar after curing, while Chapter 5 describes the novel, comprehensive, image-based analytical protocol used on polished thin sections of both the experimental and archeological mortar. The complete experimental/ analytical process was designed to test, in parallel, the efficacy of both experimental archeology and the novel image-based protocol for understanding historical mortar. While the experimental procedure began with the production of mortar and thus this is described first, it is the development of the analytical protocol that analyze these (and potentially any other) mortars that should be considered of primary importance to this work.

3.1 Producing Experimental Mortar in the Field

The first experimental mortars to be tested were made entirely by "traditional" techniques that were available in antiquity, done in a large part to produce mortar having similar characteristics as some of those made during the Roman era. The material for making mortar (ceramic and quicklime) were fired in outdoor kilns and the resulting products were crushed, mixed and molded using hand tools. Consequently, they were left to cure in a "in-the-field" environment, covered, but without thermal control

An experimental brick oven and lime kiln built by Dr. Karl Stingl at the Mauerbach Restoration facility of the Austrian Federal Monuments Office outside of Vienna, was used to produce historically accurate bricks and quicklime. Both were of relatively simple construction (see Fig. 3.1 below), closer in design to what would have been used at the first stage of settlement in ancient times; later Roman lime kilns were much larger and more sophisticated. Brick green-ware made from local Wienerwald clay provided the source material for the bricks; a cream-colored (white to yellow) limestone from Kelheim, Germany was calcined to make quicklime. Both kilns were fired overnight, with wood being fed in periodically to maintain a

temperature between 600-800 °C for the bricks, and above 800 °C for the limestone in accordance with the common practice in producing historical quicklime [116-119]. The quicklime was then sealed in air-tight plastic containers until use, while the bricks were crushed in a jaw crusher with a maximum particle size of 4 cm (in practice a large proportion of the resulting brick dust was in the sand to silt range (see results of sieving in Section 3.4). Mixed with tap water, these were the principal ingredients for the mortar described below, although some included common mason's sand as well.



Figure 3.1: Traditional Lime Production: Clockwise from Top Left: the limekiln at Mauerbach; a "temporary Roman limekiln" per (Adams 1994); quicklime made from Kelheim limestone; Sketch of a Roman limekiln per (Adams 1994, per Cato the Elder).

Although the field-produced mortar was by definition not made in a controlled environment, most of the parameters of producing a new "Roman" ceramic-lime mortar were fixed. The

binder to aggregate ratio (b:a) was fixed at 1:3, based on both historical sources [16, 17, 34, 36], as well as previous experiments [82, 92, 107, 123]. This is a common mix proportion for mortar used by researchers and therefore there exists a large amount of data for comparison. This volumetric proportion was maintained regardless of the types of aggregate in each mix. The water to binder ratio (w:b) varied, as the most important aspect was to achieve "workability", a somewhat nebulous term that simply means that the mortar be of the correct consistency for its function. The water used was from the municipal water source. In this case, the mortar was workable when it was malleable enough to be mixed by hand and placed into 4 x 4 x 16 cm molds. The w:b was approximately 1.5:1 by volume, as ceramic aggregate absorbs large amounts of water. Although as previously mentioned Roman structural mortar would have generally relied on basket-slaking of quicklime with reactive aggregate [1, 76, 120-122], for this series of mortars, both quicklime type and slaking method (basket or putty) as well as aggregate mixture were varied to examine the effects on the physical properties and microscopic appearance of these variations; the 5 types of mortar created in this manner are listed in Table 3.2 below[4].

Mortar Label	Lime Type	Lime Technique	Aggregate Mix Type
Ton-02	Quicklime, industrial	Slaked into putty, used after 1 week	50% masonry sand, 50% crushed ceramic
Ton-03	Quicklime, industrial	Basket-slaked	50% masonry sand, 50% crushed ceramic
Ton-04	Quicklime, traditional	Basket-slaked	50% masonry sand, 50% crushed ceramic up to 20 mm
Ton-05	Quicklime, traditional	Basket-slaked	50% masonry sand, 50% crushed ceramic up to 2 mm
Ton-06	Quicklime, traditional	Basket-slaked	crushed ceramic only

Table 3.2: Mortars Produced in the Field

Since these mortars were intended to emulate those created in the past, they were not subjected to a rigid curing regime, such as those laid out in e.g., ASTM C511. While such procedures produce the ideal conditions for driving the pozzolanic reaction to its fullest, they

[4] As shown in the results sections (see especially Figure 4.9), the effect of this variance on compressive strength was minimal; thus, for the second series of mortars, only basket-slaked, artisanal lime was used with pozzolanic aggregate (sand being omitted). Since the mortar made from natural hydraulic lime or industrially produced quicklime was neither reproduced in the laboratory mortar, nor analyzed by chemical or thermal dissolution or the comprehensive image-based protocol, the discussion of these mortars TON-2,3 is not discussed further after their elimination from the test program.

are not reflective of conditions that would have been found in an ancient structure when it was built, and are in fact calibrated towards modern materials in the first place. This aside, care was taken to protect them from extreme changes in temperature and humidity, which would somewhat emulate their historical use as fill or bedding mortar that was surrounded by masonry and covered with another layer of plaster. After being placed in the mold, samples were sealed in plastic containers with damp paper to create an environment of high (over 90%) relative humidity for 28 days, which were in turn kept in a cellar-environment with relatively stable temperature during early summer. One set of mortars underwent strength testing after this 28-day period, while another was tested after 91 days (the Final Strength; see Results section 6.2). From the 91-day mortar, cross sections (shown in Figure 3.3 below) and polished cross sections were prepared for further analysis.

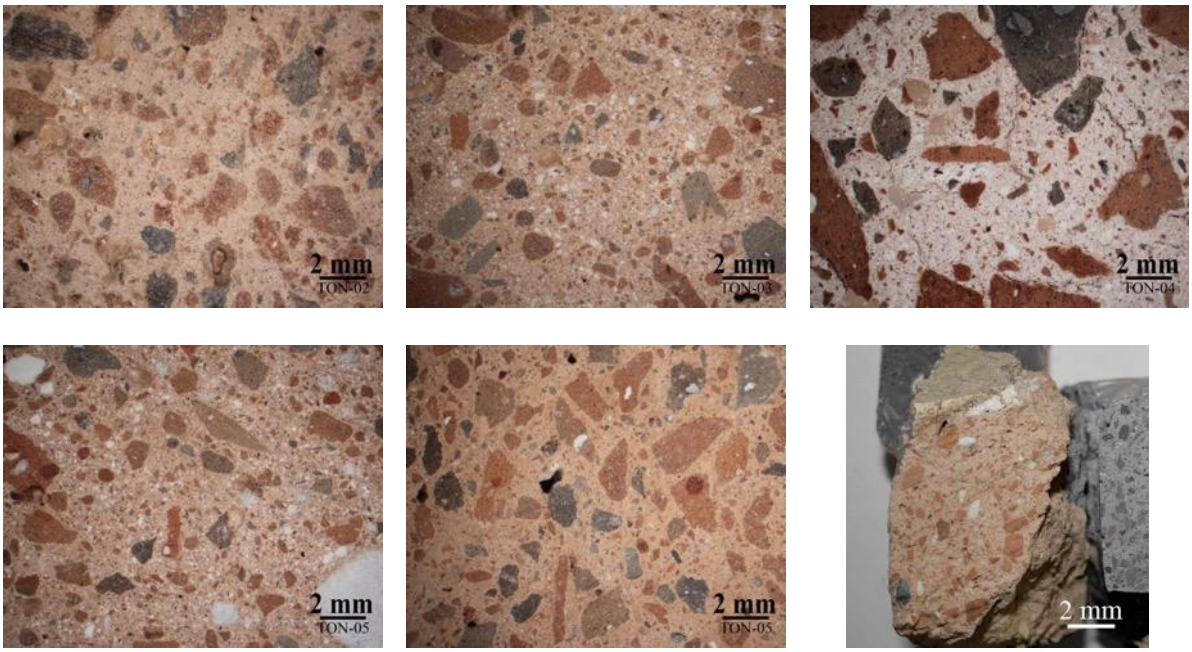


Figure 3.3: Polished cross section images of field produced mortars Ton-02-Ton-06, from top left, Archeological mortar from Aquincum bottom right for comparison. Pinkish hue is attributable to a very high load of ceramic fines. See also Figures 3.18 and 4.3.

3.2 Experimental Mortar Produced in the Laboratory

The second series of experimental mortars described in this work were produced under laboratory conditions, with special emphasis on understanding the pozzolanic reactivity of different types of aggregate. Two of the main differences for this series was that the temperature and time of firing the clay into ceramic was more rigidly controlled and the curing environment

of the mortar more closely monitored. The quicklime source and slaking method was reduced to one type (Kelheim lime and basket-slaking) based on the results of the previous series.

Laboratory production of historically accurate mortar to understand its performance is widely practiced; many modern experiments are influenced by the seminal "Smeaton Project" work by English Heritage and ICCROM [82]. Studying how different firing temperatures effects the reactivity of clay is likewise well researched [22, 23, 86-88]. The production of material to compare through comprehensive image-based analysis to archeological samples was the main goal in producing both series of experimental mortar. As noted earlier, the process of making mortar can itself be quite informative, which is discussed in Section 6.1. Additionally, this work used a unique method of molding and curing the mortar intended to better emulate conditions that would have been found historically, as described below in Section 3.5.

In contrast to the mortar produced in the field, the laboratory experimental mortar series restricted the materials used to only reactive aggregates, quicklime, and water. The water used came from municipal sources, thus remaining consistent with the previous series. Kelheim quicklime was once again used; the only difference being that the quicklime lumps were hand crushed until all pieces could fit though the 4 mm sieve.

Five types of reactive aggregate were used, four based on ceramic, which are described in much greater detail in the below. The fifth was "Terra Pozzolana" (supplied by Kremer Pigments GmbH, Germany), consisting of ground volcanic pumice and partially lithified ash deposits. Petrographic examination revealed this material to be specifically composed of palagonite tuff, an altered volcanic glass. Pozzolana has been well known since antiquity for its usefulness in construction and well-studied in modern times, it is a useful "standard" material to compare to the ceramic used in this work. It was used both in the laboratory testing and mortar production, and mortar made from this pozzolana was subjected to the same analysis as the ones made from crushed ceramic.

Historically a wide variety of clays were used to make ceramics such as bricks, roof tiles and pottery. The phyllosilicate minerals that make up clay undergo physical-chemical changes when heated, including a process known as de-hydroxylation; around 500 °C they begin to form amorphous phases that provide the reactive alumina-silicate material that can be used as a pozzolan. [22,23, 160-164]. After passing above 800 °C these same minerals start to sinter forming mullite and other glassy phases with little or no pozzolanic reactivity [ibid]. Another important factor in the firing of clay is how long it is heated at certain temperatures – the entire clay body does not completely change from amorphous to vitreous instantly above the for mentioned temperature threshold, even in the closed system described above. What is more,

the presence of flux materials can lower the temperature threshold for achieving a satisfactory ceramic body, leading to a considerable variety of phases present in the ceramic. While there is a wide variety of literature researching the optimal firing times and temperatures for turning clays into the optimal pozzolan [e.g., 22, 84, 86], clay was not fired historically to make the most reactive pozzolan, but rather to make the best ceramic for a particular use. This was done generally in a wood-fired kiln for long periods of time over a relatively wide range of temperatures. Petrographic examination of mortars made with these ceramics (such as the archeological samples shown in this work) reveals the recycling of a huge variety of ceramics as a reactive aggregate including under- and over-fired pieces that being useless in their intended function, may have been directly used as aggregate. Suffice to say, this is not a treatise on either ceramics or creating the perfect pozzolan from clay, but rather, the processes described herein can be assumed to have created a wide variety of both inert and variable reactive materials, similarly to what can be found in the archeological record, which is in fact shown throughout the results sections.

To partially emulate the historical range of wood-fired ceramics, two types of clay were fired at two temperatures in laboratory muffle ovens (Nabertherm P300, Germany). The peak firing temperatures used were 750 and 950 °C; in both cases this temperature was reached after 1 hour and held for 30 minutes, then allowed to cool slowly to ambient temperature (see Figure 3.4 for heating curve). The oven temperature remained above 500 °C for 70 minutes for the "750 degree" ceramics and 110 minutes for the "950 degree" ceramics[5]. These thermic courses were selected to emulate the variety found in historical ceramic bodies; hypothetically resulting in a mixture of potentially reactive amorphous material and material that is inert due to either not having achieved de-hydroxylation or has been (partially) sintered.

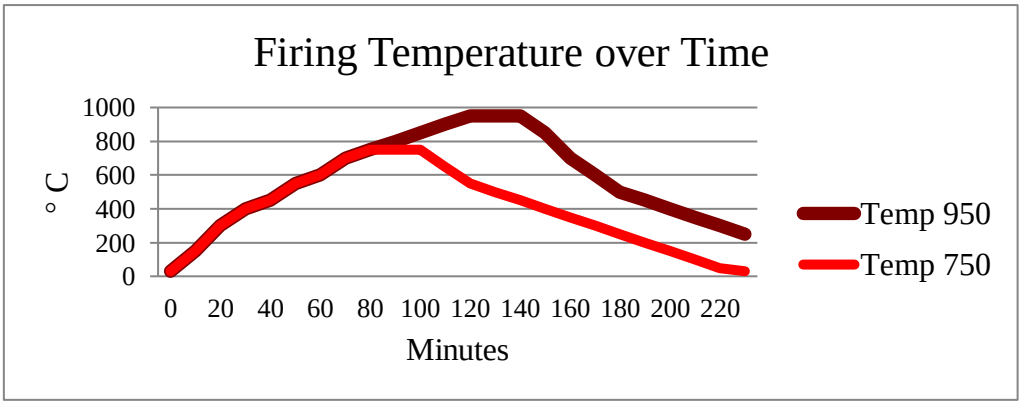


Figure 3.4: Heating curves for the firing of the "750 degree" and "950 degree" ceramics.

[5]The range of temperatures used was limited for practical purposes. For more complete studies on this phenomenon alone, refer to the literature, especially [84].

Two types of clay were selected based on their varying calcium content, to represent the range of clays used in historical times. A light-colored clay from Croatia with a calcium content of less than 0.3% ("Clay 1") and a dark grey clay from Austria with a calcium content of around 14.5% ("Clay 2") were used, representing a very low and very high range for content of these minerals[6]. These were shaped into greenware tiles roughly 40mm x 40 mm x 5 mm before firing and subsequently fired in sufficient quantities to produce the planned amount of mortar and crushed by hand to form a reactive aggregate (Detailed in Section 3.5). The resulting ceramics were examined visually, and by the use of optical and scanning electron microscopy on polished petrographic thin section, as illustrated in Figures 3.5, 3.6 and 3.7 below. Eventually, this was to see if differences in the structure of the ceramics observable in this manner could be tied to the production and performance of pozzolanic mortar made from them.

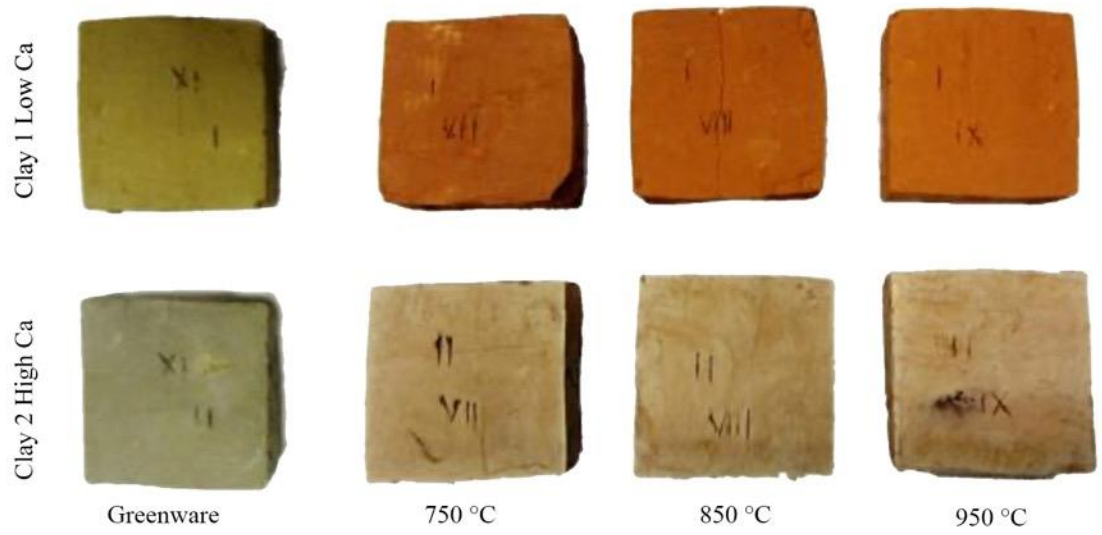
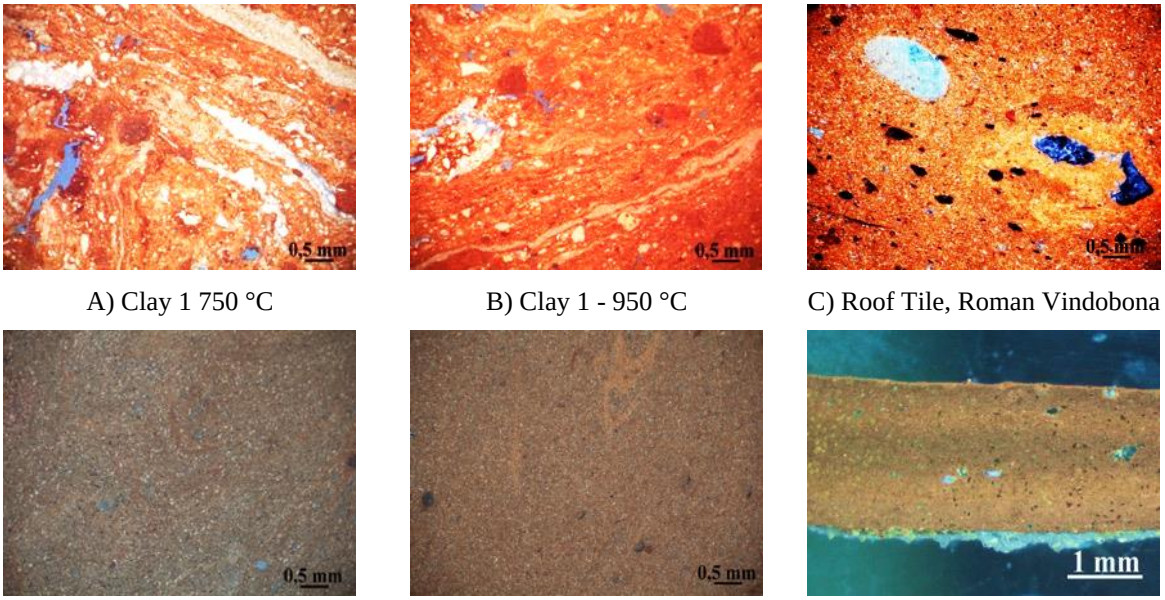


Figure 3.5: Visual appearance of the clays as greenware and fired at different temperatures.

Clay 1 produced a ceramic that was quite hard, brittle, and red. It included natural quartz temper and the matrix exhibit a foliated effect, with macro-porosity in alignment with the folia. This macro-porosity is related to the preparation of the clay pre-firing, as it was supplied as a compact solid block that could easily be cut into tile-shapes. The higher temperature firing produced greater sintering, as visible when comparing the SEM-BSE images in Figure 3.7 (A

[6] Calcium values were established by XRD, provided by the clay supplier (Wienerberger GmbH, Austria).

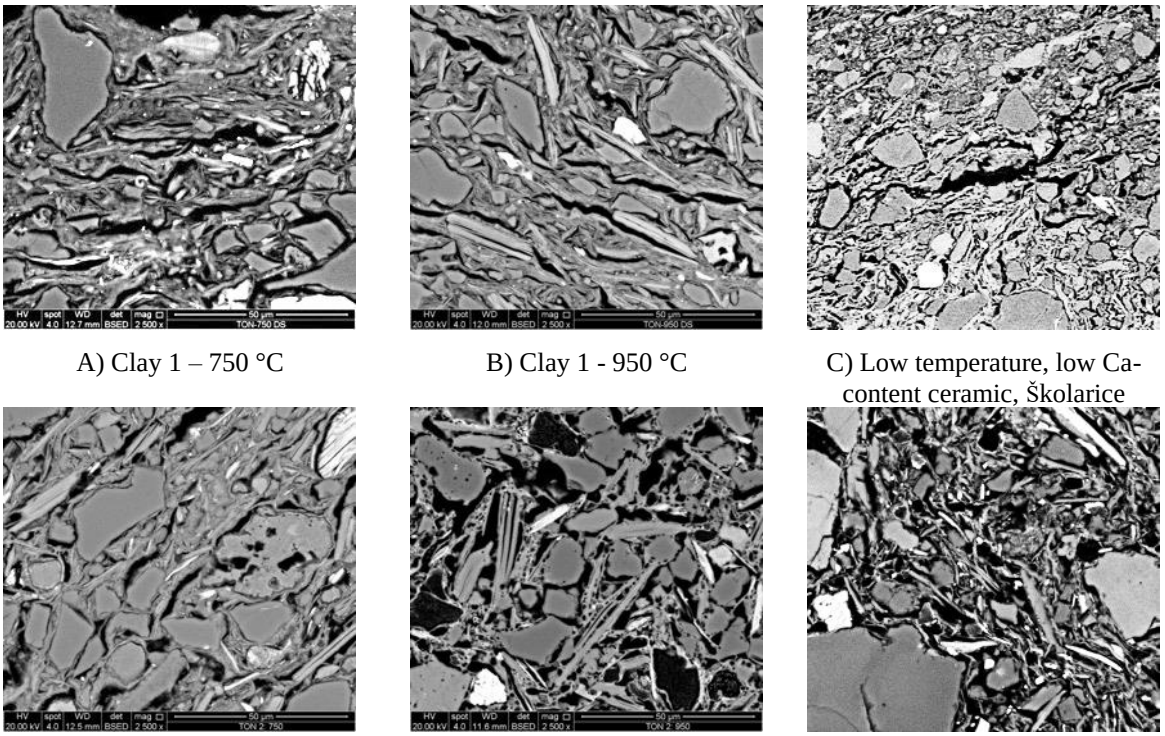
and B). Physically and morphologically these ceramics appear similar to those used in Roman construction for structural applications, i.e., bricks.



A) Clay 1 750 °C | B) Clay 1 - 950 °C | C) Roof Tile, Roman Vindobona

D) Clay 2 750 °C | E) Clay 2 - 950 °C | F) Amphora Shard, Caesarea

Figure 3.6: Polished thin sections of the four types of ceramic used to make mortar, with archeological comparisons. Observed by stereomicroscope, incident light.



A) Clay 1 – 750 °C | B) Clay 1 - 950 °C | C) Low temperature, low Ca-content ceramic, Školarice

D) Clay 2 – 750 °C | E) Clay 2 - 950 °C | F) High temperature, high Ca-content ceramic, Vindobona

Figure 3.7: Polished thin sections of the four types of ceramic used to make mortar, with archeological comparisons; SEM-BSE. Credit A, B, D, E - J. Weber, K. Kojan

Clay 2 produced a ceramic that, while brittle, was softer and had a grey-brown color. The color becomes redder (the coloration of iron oxide starts to predominate) at the higher temperature. At this higher temperature, the calcareous temper has calcined into calcium oxide (quicklime) and is no longer tightly bound to the clay mass; in the polished thick section, this "free" calcium oxide has been polished out, leaving the large pores noticeable in Figure 3.7 E. The mica shown in that image also appears to be deteriorated, but not melted. The matrix does not exhibit folia, being generally amorphous. Physically and morphologically these ceramics appear similar to those used for applications such as tableware and amphorae.

To begin to understand how these ceramics (and the pozzolana) would perform as a reactive aggregate in a mortar, both chemical and physical testing are required, with the understanding that these could then be linked to phenomena observable with image-based techniques. When the same phenomena can be observed in historical mortars through image-based techniques, then conclusions can be drawn about the reactivity of their aggregates, and how these mortars performed historically.

3.3 Characterization of the Reactive Aggregates by Reactivity testing: pH change vs. Modified Chapelle Test: Methods

There is a wide variety of methods both direct and indirect for assessing the reactivity of a pozzolan. Indirect methods include measuring the strength development over time of a mortar, and mineral phases produced as they set. These compliment the direct observations, such as the visualization of reaction rims by microscopic methods. These methods are discussed thoroughly in the Results section of this work. An important first step in understanding (and as will be seen, predicting) what is determined by these analyses is characterizing the reactive aggregates before their incorporation into mortar.

In order to directly determine the *potential* reactivity of different pozzolans, there exist a number of laboratory procedures that can be used that require little input in terms of resources and time. The pozzolans used in these experimental mortars were tested in the laboratory by two methods: the assessment of the change in pH over time of a calcium hydroxide solution mixed with pozzolan that gives results in relative terms [114], and a more precise chemical method known as the "Modified Chapelle Test" [115]. These tests were performed to produce laboratory data to compare the reactivity of the pozzolans used in both production series of

mortar, as well a wide variety of natural and artificial pozzolans, including metakaolin, which was used as a reference material.

In addition to reactivity testing, the pH when dispersed in water, sieve analysis, rate of water absorption and oxide analysis was performed on the experimental pozzolans (as well as some not used to make mortar). These data were acquired to determine what, if any, effect these properties had on the pozzolanic performance of the aggregate used in the experimental mortars. Although not directly explored herein, the greater the specific surface of a material, the higher the reactivity; this is indirectly discussed through the sieve analysis results since a finer material will typically have a larger specific surface regardless of grain morphology. Potential links between these properties and the overall mortar performance are discussed in Section 3.3.1 which follows.

The method used for the determination of pozzolanicity by the change of pH in a solution was published in 2014 as: "*New method to assess the pozzolanic reactivity of mineral admixtures by means of pH and electrical conductivity measurements in lime: pozzolan suspensions"*[114]; the procedure used is summarized in brief here. 250 ml of de-ionized water in sealed Erlenmeyer flasks were warmed on a magnetic stirrer to 35 °C ± 5. Initial testing showed that solutions of the different pozzolans tended to be variously alkaline without the addition of quicklime, as shown in Table 3.8 below. To mitigate these differences, the experiment had to be adjusted accordingly. Rather than mixing predetermined proportions of quicklime and pozzolan, 1.0 gram of fine (< 50µ) pozzolan was used in each case, and then CaO was added until the pH of the solution was above 12. This is the equivalent to the pH of a solution saturated in $Ca(OH)_2$). For each test performed, a "blank" test was performed on a saturated lime-water solution (0.2 grams $Ca(OH)_2$ - 250 ml water, i.e. saturated at 35 °C) was prepared in parallel, to determine the rate of carbonation during the experiment. Industrial grade metakaolin (provided by Professor Franz Ottner from the University of Natural Resources and Life Sciences, Vienna (BOKU, Wien)) was used as a refence material. Daily pH measurements on the continuously stirred, sealed solutions were taken with a Hanna HI 83141 pH Meter, (Hanna Instruments, U.S.A.) for one week. The reduction in pH correlates to the rate and amount of $Ca(OH)_2$ taken out of solution, i.e. it has reacted with the pozzolan to form cement hydrates (C(A)SH). After one week, the experiment was stopped with the differing reductions in pH being used to show the reactivity of different pozzolans relative to each other, with industrially produced metakaolin as the reference material. The results are given and analyzed below in the following Section 3.3.1.

Pozzolan type	pH of 1 gram dispersed in 250 mL dH_2O
Clay 1 750/950	8.75
Clay 2 750/950	10.65
Suevite (Bavarian Trass) (Kremer GmbH)	9.40
Terra Pozzolana (Kremer GmbH)	8.95
Metakaolin – Produced in the laboratory at 800 °C	9.25
Metakaolin – Industrial (BOKU, Wien)	8.15

Table 3.8: Baseline alkalinity of pozzolanic materials

The Chapelle Test is means of quantifying the pozzolanic reaction. This test is a modification of a French norm (NF P 18-513 [115]), which additionally uses metakaolin as the standard reference material. Reactivity is quantified by measuring the amount of $Ca(OH)_2$ taken out of solution by 1 gram of pozzolan over the 16 hour time frame of the test. In addition to the pozzolans used for both experimental mortar test series, many additional materials were tested. They included a powdered piece of other historical ceramic - a Roman roof tile from the site of Vindobona ("Roman-Hernals") and three naturally occurring pozzolans: suevite ("Bavarian trass") (Kremer GmbH), a meteor impact shocked quartz; tuff from Orvieto, Italy; and Santorin earth, a volcanic pozzolan from the Greek Island of Thera/Santorini. Finally, three types of metakaolin were included, one made from kaolin that was fired in the laboratory under the same conditions as the clay used for the experimental mortar production, and two industrially produced from the same source material, with different levels of amorphous content. All materials sieved (and in the case of ceramics ground to get the requisite particle sizes) so that the powder used was composed of particles in the sub-50-micron range.

1.0 gram of potentially pozzolanic material is added to 2.0 grams of quicklime (CaO) dispersed in 250 ml of deionized water (forming $Ca(OH_2)$, which has been heated to 85 °C ±5 in a closed, heated magnetic stirrer which maintains this temperature. A "blank" solution with only $Ca(OH)_2$ and water is prepared in parallel. These solutions are heated and stirred for 16 hours, after which the solution is cooled to ambient temperature and diluted with 250 ml of deionized water – sucrose solution. The solution is then filtered, and 25 ml is taken out and titrated with 0.1N HCl. The results are then determined by the formula:

$$\text{mg of } Ca(OH)_2 \text{ fixed} = 2(V1-V2)/V1 \times (74/56) \times 1000$$

Where V1 is the volume of 0.1N HCl required to titrate a blank ($Ca(OH)_2$ only) sample and V2 is the volume of 0.1N HCl required to titrate the experimental sample(s). The pozzolans tested gave a wide range of results, which are given and analyzed below.

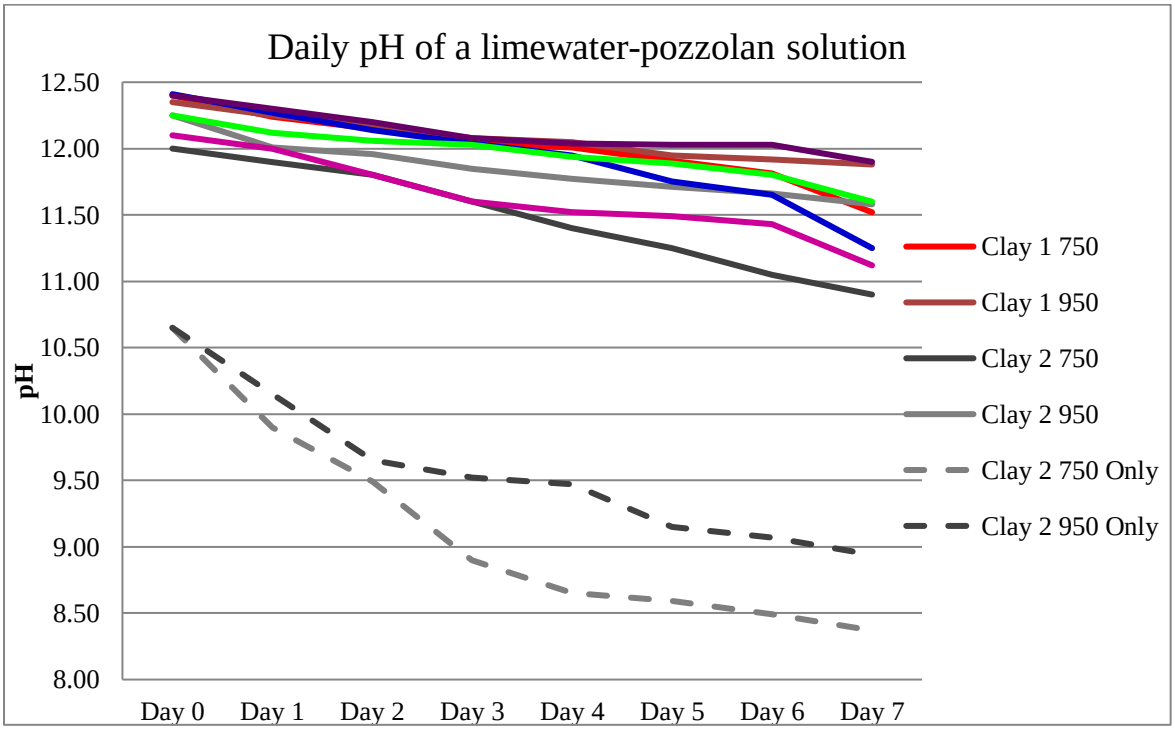
3.3.1 Reactivity testing, pH change vs. Modified Chappelle Test: Results

Of the two reactivity tests used to characterize the aggregates used in the experimental mortar samples, the modified Chappelle test gave the least ambiguous results. Both methods assume that as calcium hydroxide is used up by a pozzolan - the pH of the limewater pozzolan solution will tend towards neutralization (the pH will move from around 12.0 -12.5 towards 7), the Chappelle test takes the additional step of quantifying the amount of calcium hydroxide taken out of solution. In both cases, tests were performed with a wide range of potentially reactive materials, most notably industrially produced metakaolin, which can be considered a baseline since it is the material for which the tests were calibrated.

The results of the test based on the reduction of pH of a limewater solution [114] are shown in the graph and table in Figure 3.9 below. All 5 types of pozzolan used for making experimental mortar were tested as well as 2 types of metakaolin and suevite, a reactive impact glass. Additionally, powders from the two different firing temperatures of the calcium rich clay ("Clay 2") were tested without adding $Ca(OH)_2$ for reasons that are elaborated below. The slow rate of decline in pH for all solutions would seem to indicate that at least some of the $Ca(OH)_2$ is being taken out of solution and formed into cement hydrates (the blank $Ca(OH)_2$ solutions did not show significant carbonation).

Overall, the powders made from ceramics fired at the lower temperature exhibited a greater overall reduction in pH than the ones fired at the higher temperature, corresponding well with results found in available literature [22, 23, 84-88]. This implies that these materials would be more reactive pozzolans and form a mortar with stronger, faster initial set. The most reactive of the experimental pozzolans in this case was the low-fired (750° C) calcium carbonate-rich Clay 2, which shows a drop in pH like the two types of metakaolin, the rate represented by a steeply sloping plot in Figure 3.9 above. This is of particular interest, given the high pH of dissolved Clay 2 powder in water (without added $Ca(OH)_2$) which indicates that a certain

amount of the calcium carbonate contained in the clay converted to quicklime inside of the clay body while firing[7].



Material Name	pH Day 0	pH Day 7	Cumulative decrease in pH	Avg. Daily Change
Clay 1 950°	12.35	11.88	0.47	.067
Terra Pozzolana, Kremer	12.40	11.90	0.50	.071
Suevite, Kremer	12.25	11.60	0.65	.093
Clay 2 950°	12.25	11.58	0.67	.095
Clay 1 750°	12.40	11.52	0.88	.125
Metakaolin produced industrially	12.10	11.12	0.98	.140
Clay 2 750°	12.00	10.90	1.10	.157
Metakaolin produced in the lab	12.41	11.25	1.16	.165
Clay 2 950° no $Ca(OH)_2$ added	10.65	8.94	1.71	.244
Clay 2 750° no $Ca(OH)_2$ added	10.65	8.37	2.28	.325

Figure 3.9: Chart and Table Describing the Results of the pH test.

[7] Important note: As described in the Experimental setup (3.1.3.1), in order to compensate for the existence of CaO in the powder of clay 2 ceramic, the amount of added CaO was adjusted until a pH above 12 was achieved rather than simply adding the same amount of CaO in every solution, i.e. the pH was the standard metric, not the amount of CaO. After this a small amount of CaO is added as "excess" per the recommendation of the experimental setup.

This implies that pozzolanic reaction appeared to take place simply within materials included within the ceramic body itself. Calcium rich clay, when fired into a ceramic contains both the clay minerals capable of being tempered into pozzolanic material as well as the precursor material for forming a lime binder – in other words when this powder is mixed with water it would be somewhat self-cementing (also known as "latently hydraulic"). The high-fired (950º C) Clay 2 powder was also quite reactive; while the higher firing temperature may have reduced the amount of reactive pozzolan, it likely increased the amount of "extra" quicklime. In fact, using the performance of industrial metakaolin as a base line, as is shown in Figure 3.10 below, the low-fired Clay 2 was the most reactive material according to this test, as shown by the fact that its rate of pH change was the only one consistently below (becoming more pH neutral) that of the industrial metakaolin. A second observation of interest is the relatively "poor" performance in this test by Terra Pozzolana, a material known to have strong pozzolanic reactivity. This highlights two potential drawbacks to this type of test, firstly its short duration and secondly the potential for the results to be affected by other soluble alkali salts present in the pozzolans, which appears to be the case with Terra Pozzolana. A week is a relatively short time span for testing the reactivity of pozzolans used traditionally (which achieved final set rather slowly), but in this case studying the rate of change for the above materials is as illuminative as the overall drop in pH over the full time of measurement, as shown in Figure 3.10 below.

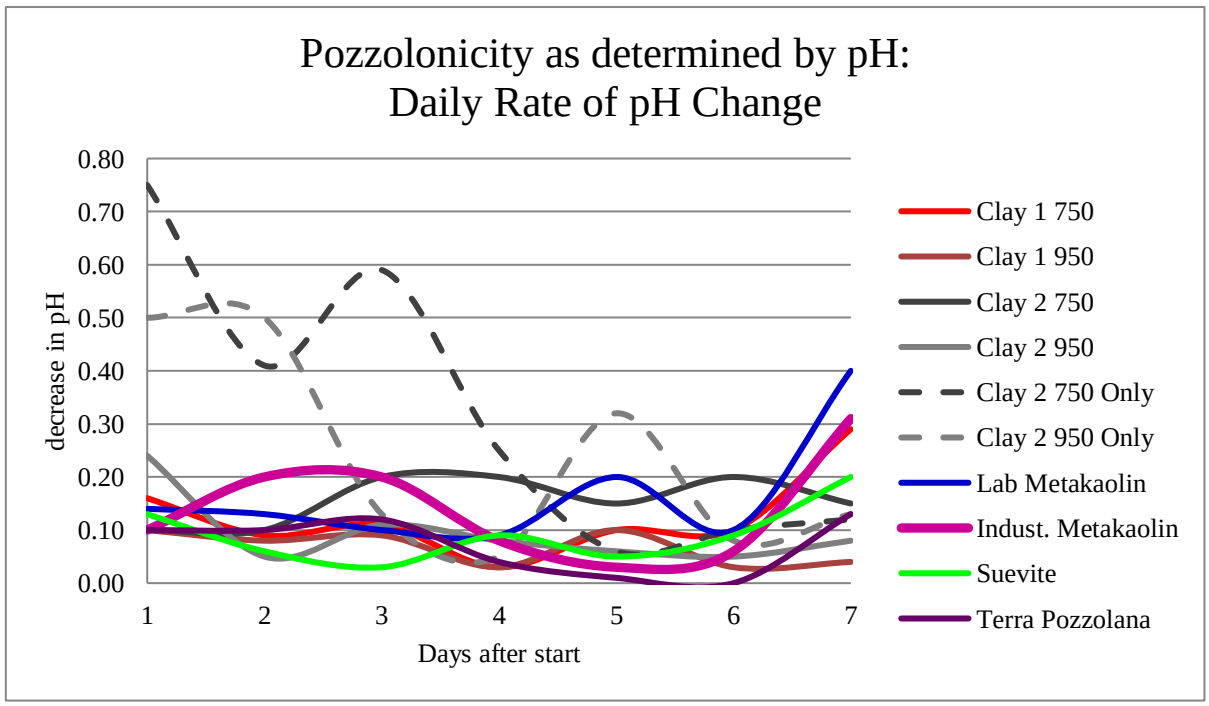


Figure 3.10: Daily Rate of pH decrease.

In Figure 3.10, rapid reactivity for Clay 2 at both firing temperatures is strongly illustrated by both the amplitude and erratic nature of the rate of change. Additionally, this is reflected at a lesser scale by the other materials, with the peaks corresponding to times when pozzolanicity has reduced the available Ca^{+} and OH^{-} ions in the system followed by a corresponding trough as more CaO from the previously super-saturated solution (referred to as "excess" lime) dissolves into ions. By the 6^{th} to 7^{th} day, the "excess" $Ca(OH)_2$ has been used up and the reaction rate is increasing. This is particularly true for the pozzolans that had had a "slow start" such as metakaolin and Terra Pozzolana. Thus, it can be seen through this method, that on a medium to long time frame (over 1 week) one could expect increasing strength development from all of these pozzolans, which is reflected in later physical testing of experimental mortars, and that is it possible that the Terra Pozzolana will eventually outperform the other experimental materials.

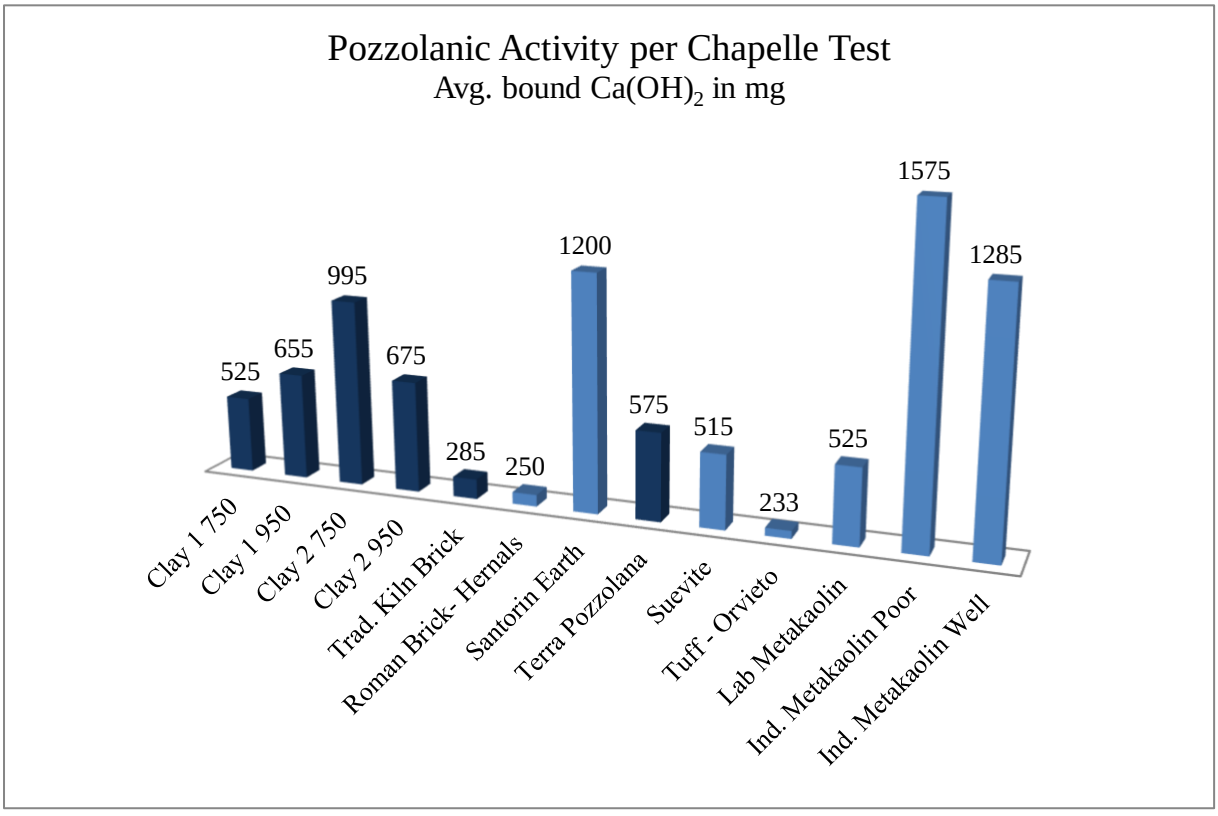


Figure 3.11: Results of the Chapelle Test for pozzolanicity,
darker blue represents materials used to make experimental mortar.

The results of assessing the pozzolanic reactivity of a variety of materials per the Chapelle Test [115] are given in Figure 3.11 above. While having the advantage of being quantitative, the modified Chapelle Test gave similarly mixed results. The performance of these pozzolanic materials can be separated into 3 groups, regardless of the origin of the material. The materials with results under 300 mg and those above 1000 mg can be said to have been found to be

minimally or strongly reactive, respectively, according to this procedure. However, over half of the materials tested fall into an intermediate range of short-term reactivity. It is noteworthy that Terra Pozzolana appears to be just as reactive as the ceramic powders and metakaolin fired in the laboratory using the same firing procedure as the clays, while the low-fired Clay 2 powder appears to be substantially more reactive. The disparity to the two different clay types fired at the same temperature seems to contradict the available literature [84, 85]. What is more, although the traditional kiln brick was found to have a low reactivity, it was found to produce a strong mortar (see results in following section). Individual tests for the three experimental ceramics besides "low fired Clay 2" and the Terra Pozzolana were within a standard deviation of each other, while low fired Clay 2 and Traditional Kiln brick were found to be more and less reactive, respectively. This is in contradiction to the strength data presented in the next section. Further, while comparing the baseline alkalinity of the pozzolans (Table 3.8) with the Chapelle test results (Figure 3.11) would seem to indicate that the more acidic a pozzolan is the higher its reactivity (partially confirmed by both strength data and image-based results), but this is not the case for the experimental clays, as Clay 2 750 °C is more reactive, yet more alkaline. These results point to the distinct possibility that these tests are underestimating the reactivity of some materials, which has been noted elsewhere [174].

Therefore, there are several factors to consider when interpreting the results of these tests. Firstly, one should avoid comparing the results between two types of pozzolans directly, i.e. if pozzolan A gives an average result of 900 mg of $Ca(OH)_2$ bound it is not necessarily "twice as reactive" as one with a result of 450 mg. This is because of the second important factor, which is that this reaction has taken place over a relatively short time. These results simply show the rate of initial consumption of calcium hydroxide by a pozzolan; in actual mortars and concrete a large amount of calcium hydroxide continues to be available for a long period of time particularly in the case of massive, volcanic pozzolan based concrete [4, 5, 62]. This aside, the short-term results are still important as in many real -life situations it is often the case that long term curing is not an option, thus making the potential long-term reactivity irrelevant.

For both laboratory-based tests it is important to keep in mind that although the short-term pozzolanicity of a reactive material may have been of vital importance to historical builders, it is only one of many methods of understanding a historical mortar as a building material. Additionally, it is one that analyzes a component of the mortar not the whole mortar. For the latter, this work relied partially on physical testing.

3.4. Additional Physical and Chemical Characterization of the pozzolans

Beyond determination of pozzolanic reactivity, additional physical and chemical data for the aggregates before their incorporation into mortar were gathered. This was done for characterization purposes, as well as to ascertain what effect, if any, these characteristics had on the experimental mortars. These consisted of sieve, water uptake, and EDX analysis.

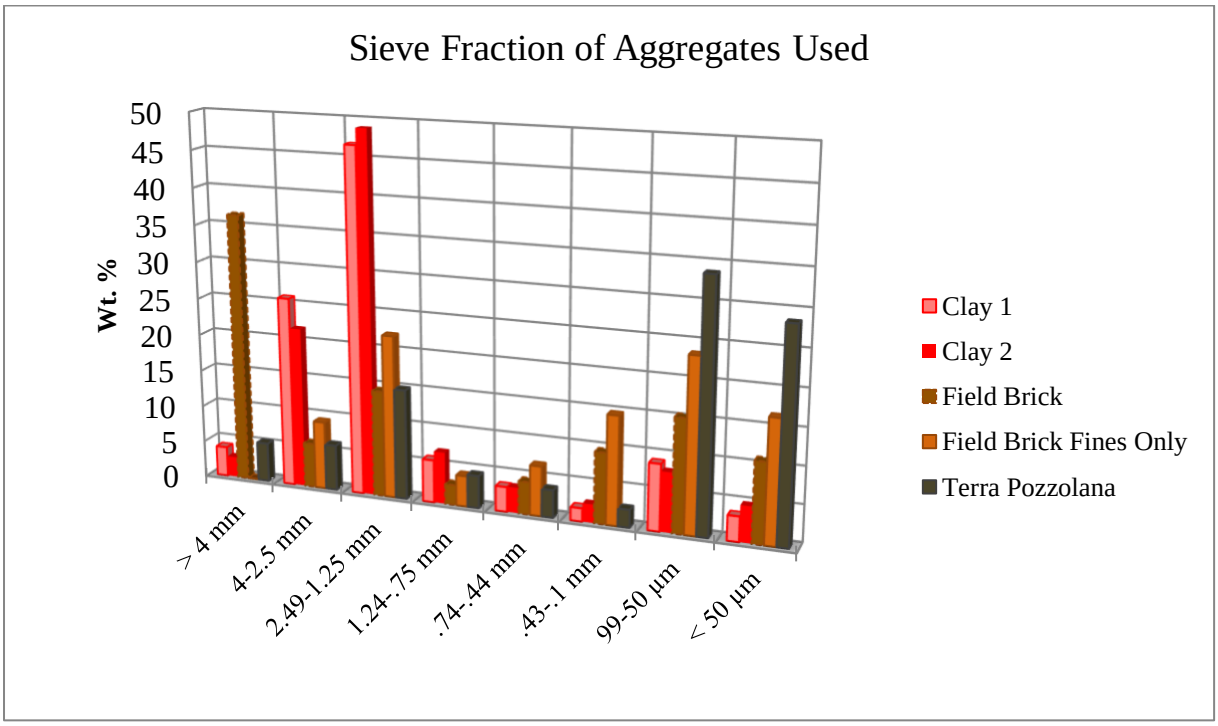


Figure 3.12: Sieve Fraction of Experimental Aggregates before incorporation into Mortar

A full 100 cc. ("a measure") volume beaker of each of the main aggregate types used to make experimental mortar were dry-sieved 3 different times through a set of standard test sieves as per *ASTM C-136.* The resulting sieve fraction measurements are compared in Figure 3.12 above. Two different fractions of the field-produced brick were tested, one more closely emulating a sieve fraction in which the product is *opus caementitium* ("Field Brick" in Figure 3.12) and the other being closer in sieve fraction to a wall covering *cocciopesto* mortar ("Field Brick Fine") as well as the two types of laboratory ceramic and the Terra Pozzolana. While the pozzolanicity testing showed the relative reactivity of fine powders of each aggregate, this test was intended to show what percentage of each aggregate was available at that fine fraction. Since the ceramics made from Clay 1 and 2 were hand-crushed, there was a lower content of fines (<.43 mm) present; to which extent this affected the short to long term performance of a mortar made from these materials is discussed further in the Results sections.

A key factor to consider when determining the water to binder (w:b) ratio when making mortar with these types of reactive aggregates is to which extent the aggregates themselves will absorb water. The more porous the aggregate is, the more water it will take to make a workable mortar, and the longer it will stay moist, as water entrapped in the aggregates can stay in a mortar system for a long time, especially when the mortar is enclosed within a wall or being cured under standardized test conditions, which advise that a test mortar be kept at a constant high relative humidity. A simple laboratory experiment was designed to test the rate and amount (in volume) of water that could be absorbed into either an 85 cm^3 piece of the ceramic, or a box of the same volume packed with the crushed aggregate (in the fraction as determined above). The amount of water in grams could then be expressed as a percentage of the known volume, which would be equivalent to the open porosity of the material. The results are given in Table 3.13 below. The experiment showed that the three lab-production series aggregates (blue rows) would be fully saturated with water within the half-hour (since the 24-hour value is the same) of mixing and slaking time described in Section 3.5 below.

Material Type	Water wt. gain grams/ 30 minutes – ambient conditions	Water wt. gain in grams/ 24 hours (porosity) – ambient conditions
Clay 1 Cocciopesto	46	46
Clay 1 Prism	6	25
Clay 2 Cocciopesto	45	45
Clay 2 Prism	15	30
Terra Pozzolana	36	36

Table 3.13: Water absorption characteristics of the lab-produced aggregates.

The final step in characterizing the aggregates before their incorporation into mortar was their analysis by energy-dispersive X-ray spectroscopy (EDX) of the SEM. Powders of the aggregates were attached to glass slides with double-sided tape and then analyzed by a Pegasus APEX Energy-Dispersive X-ray spectroscope (Ametek EDAX, U.S.A.) equipped with the Genesis SEM Quant software. The results are displayed below in Table 3.14 as oxide percentages; the results show that the silica (SiO_2) + alumina (Al_2O_3) content is well within the range of what would be considered a pozzolanic material [18-21]. Whether or not the variable CaO content or the relative levels of SiO_2 and Al_2O_3 effected the experiment or the resulting mortar, and if this can be related to historical mortar performance is discussed in further detail in the Results sections.

		Oxide Content (Mol. % - per EDX)			
Material	**Function**	**CaO**	**MgO**	**SiO_2**	**Al_2O_3**
Kelheim Quicklime	Binder	93.25	1.95	2.50	0.75
Ceramic Lab 1	Pozzolanic Agg.	1.05	1.95	79.50	13.25
Ceramic Lab 2	Pozzolanic Agg.	6.25	7.25	69.75	11.50
Ceramic Field	Pozzolanic Agg.	4.00	4.75	75.25	11.25
Terra Pozzolana	Pozzolanic Agg.	9.10	5.50	61.50	15.25

Table 3.14: Oxide content of the lab-produced aggregates.

3.5 Producing Experimental Historical Ceramic-Lime Mortar in the Laboratory

After the mortars made by traditional means, a second series of mortar was produced applying both lessons from the first, as well as observations of archeological samples. More control of the mechanism of production, both of the ceramics and the mortars, was achieved by utilizing a controlled environment. Using a laboratory environment allowed for the simultaneous testing of the materials and the mortar made from them, most notably to characterize the pozzolans as described in the sections directly proceeding, and to test the development of strength of a mortar as it was setting (Sections 4.1, 4.2).

5 types of mortar were produced in this test series, with aggregates made from the two types of ceramic fired at two different temperatures, as well as one using Terra Pozzolana. This series was also intended to represent a cross section of Roman-era mortars. The pozzolanic reaction begins immediately upon mixing of pozzolan and hydrated lime initiating the setting of the mortar. Matching the field-produced mortars, "the basket slaking" technique was used to slake the quicklime and pozzolan together. As discussed previously, most historical structural pozzolanic mortars appear to have used this slaking method or a similar method of slaking which would take place close to the application time, while lime putty would only have been used for ornamental plasters [59, 62, 63, 68, 76]. Whereas the traditional mortar production helped to illustrate several additional variables that are reflected in the examination and characterization of historic mortars, the goal of the laboratory mortar was to control these variables in a manner by which reproducible correlations could be made. The mortars produced in this campaign[8] are represented (and named) in Table 3.15 below:

Type Name	Composition
1-7	Clay 1 (Low-Ca) fired at 750 °C. : Kelheim quicklime
1-9	Clay 1 (Low-Ca) fired at 950° C : Kelheim quicklime
2-7	Clay 2 (High-Ca) fired at 750° C : Kelheim quicklime
2-9	Clay 2 (High-Ca) fired at 950° C: Kelheim quicklime
P-K	Terra Pozzolana: Kelheim quicklime

Table 3.15: Mortars Produced in the Laboratory

The mortar produced from these materials is described in the following section. Despite the laboratory setting, the work was still mostly done by hand (rather than using, for example, a mechanical mixer) in an attempt to recreate the macro- and microscopic inhomogeneity that is found in historical and archeological mortar. Subsequent testing (Section 4.2) shows that much of the mortar thus produced was not high strength. This does not undermine the usefulness of the experimental mortar; this fact assisted the interpretation of the results determined by chemical and image-based means, as discussed in the results and conclusions sections.

The mortars produced from the laboratory-fired ceramic (and terra pozzolana) were cast into plates 16 cm long by 24 cm wide by 4 cm deep in a water-resistant wooden formwork, which could then be sealed in plastic, creating a curing environment that was both high in humidity and unlikely to result in mortar carbonation. Two plates of mortar were made for each of the mortar types shown in Table 3.15 above. Each aggregates type was combined volumetrically 3:1 with quicklime and basket-slaked, which after curing yielded ten 4 cm x 4 cm x 16 cm test prisms cut from each plate. The 3-part aggregate to 1 part quicklime volumetric proportion was chosen based on both ancient sources [16, 17, 34-36], as well as a commonly used formula for restoration mortar [82, 92, 107, 123][9]. Except for weekly testing by ultrasound resistance, described in Section 4.1 below, the mortar was cured in this environment for 28 days. A model of the formwork is shown in Figure 3.16. below, as well as Figure 3.17 C, D and E.

[9] Although many structures made with pozzolana would have been considered “water work” for which Vitruvius recommends a mix of b:a - 1:2.

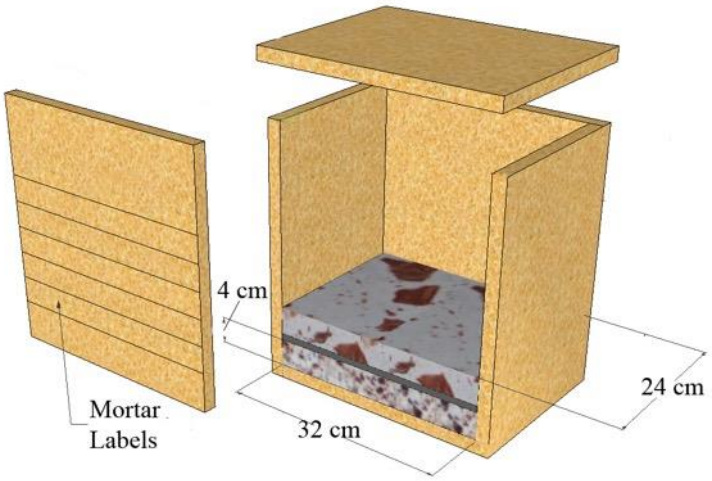


Figure 3.16: Model of the Experimental Mortar formwork

Previous research has shown that large blocks of pozzolan-lime concrete retain heat, moisture, and alkalinity for long periods of time [4, 62]. The results of these conditions have a profound effect on the curing and aging of the mortar - as can be seen through microscopy [1,122, 144] – and therefore this was considered when designing the formwork. An inserted thermocouple showed that the internal temperature of the mixture of slaking quicklime and pre-moistened pozzolan reached 300 ºC, decreasing to 160 ºC after 30 minutes. At this point the mound was both too hot and too dry to be worked by hand into mortar plates, and so additional water was added until a workable mix with an internal temperature of 65 °C resulted. In practice, making these experimental mortars required water-to-binder volumetric ratios of at least 2:1; 100 ml quicklime + 300 ml aggregate consistently required 200-250 ml of water to produce a workable mixture. This consisted of 100 ml for the lime to be fully slaked plus 100-150 ml of water for the aggregate to be "saturated" with water, which varied dependent upon aggregate porosity as shown in Table 3.13 above. The mortars were repeatedly worked with hand tools (mixing, cutting, and pounding flat) and then placed into the formwork for curing while still warm. The mortars were allowed to set in the formwork for 28 days, corresponding to the industry standard for curing concrete [166]. During this time the formwork was opened for a few minutes at 7, 14 and 28 days to measure their curing rate by ultrasonic pulse device to measure changes in the mortars' resistance to ultrasonic pulse waves as detailed in Section 4.1 [102, 103, 167]. The process is illustrated with Figure 3.17 below.



A) Ceramic Pozzolans Used



B) Slaking and Mixing



C) The Labeled Formwork



D) Placing the First Plate



E) Demolding the Mortar



F) Cutting Bars from the Plates

Figure 3.17: Photos illustrating the laboratory mortar making process, as described in this Chapter.

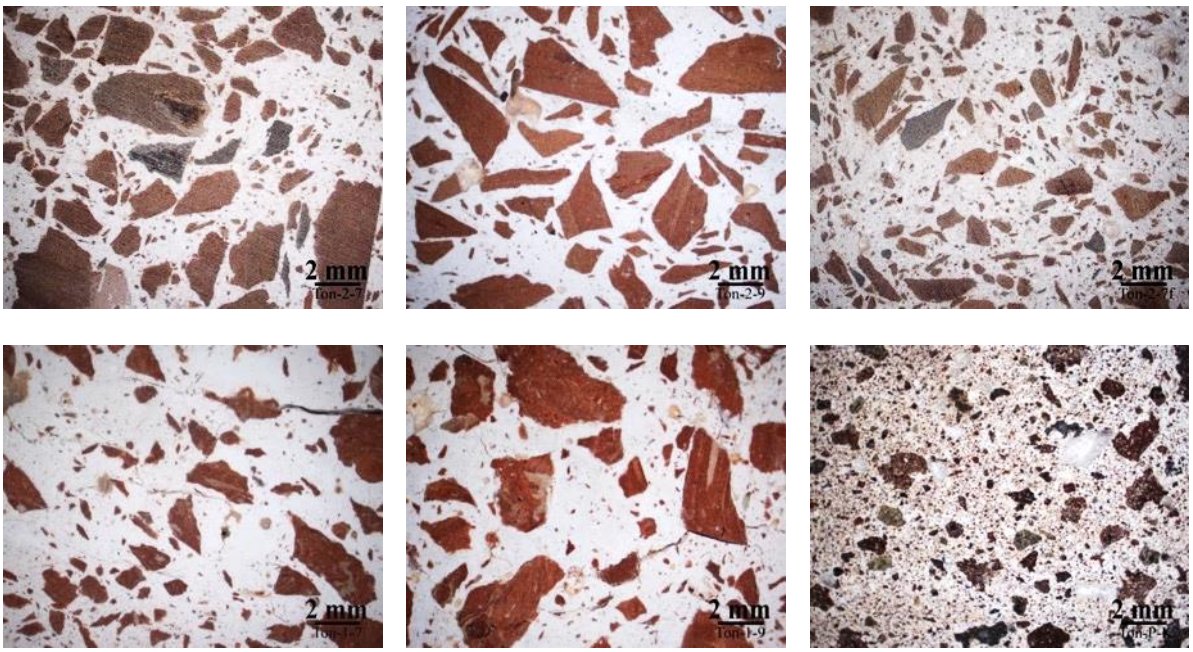


Figure 3.18: Polished cross section images of experimental laboratory mortars. From top row from left: 2-7, 2-9, 2-9 Fine Fraction only; from bottom row left 1-7, 1-9, P-K. See Table 3.12 Above.
The white binder appearance (compare with Figure 3.3) seems to indicate less binder fines and hence less potential for pozzolanicity, however strength measurement showed little indication of a direct link, especially in the case of P-K (see Figure 6.6).

After 28 days the mortar plates were de-molded and allowed to dry and carbonate on the surface under laboratory conditions. 14 days later (42 days after mixing and placing), the plates

were sawn into test bars and cubes for subsequent physical and chemical testing, and comprehensive image-based analysis, as described in the following sections. Polished cross sections (shown in Figure 3.15 above) and polished thin sections were created from each mortar type to begin the macro- to micro- based image analysis which would allow for comparison with historical mortars prepared in the same manner.

4.0 Physical and Chemical Testing of the Experimental and Archeological Mortar

Physical and chemical testing was performed on both experimental and archeological mortars for comparison with the main analytical tools used in this work, the comprehensive image-based protocol described in Chapter 5. As already mentioned, the strength development of the laboratory-produced mortars was checked during curing by ultrasonic pulse resistance, detailed below. Compressive strength testing was performed on test prisms for both series of experimental mortars after 28 days of curing and 14 days of carbonation. Finally, chemical dissolution and thermogravimetric analysis was performed on both the experimental mortars, as well as a variety of Roman-era archeological mortars. These physical and chemical tests were chosen since they are widely used, and thus provide data that can be compared with available literature. Additionally, they are used in Chapter 8 to corroborate the efficacy of the image-based protocol.

4.1 Strength Development measured by resistance to ultrasonic pulse

The ultrasonic pulse resistance of the different mortar plates made in the laboratory was tested during the mortar curing process, both before and after de-molding. The direct transmission method for testing the strength of a cementitious material by ultrasound resistance was used, measuring through both the 16 cm and 4 cm dimensions of the test plates/ prisms [167]; this was performed after 7, 14 and 28 days of curing and 7 and 14 days of carbonation. This was followed by compressive strength testing. The concept behind this application of ultrasound is that as the material gains strength, it becomes denser and more compact, and therefore an ultrasonic pulse will pass through it more quickly [102, 167].

The device used was a CONOSONIC C2-GS ultrasonic pulse generator, with portable transmission/ reception transducers. The interface with the device was an attached laptop computer that was preinstalled with the manufacturer's proprietary software named Light House Touch. Both the device and the software were developed by Geotron-Elektronik (Germany). A variety of settings was used to find a usable signal, but the most used ones were to set the transmitter frequency at 64-80 kHz, the sample rate at 4.8 MHz and the visualized amplitude at 20-50 mV. The results of this testing are given in Section 6.2.



Figure 4.1: Set up for measuring the ultrasonic resistance on cured mortar beams.

4.2 Compressive Strength Testing

After the curing period, 40 mm cubes of mortar from both experimental series were tested destructively to determine their compressive strength per international mortar testing standards [168]. On two separate occasions, 5 cubes sawn from the original 40 mm x 40 mm x 160 mm prisms were tested using a Form+Test Testing Machine (Seidner + Co, GmbH, Germany) at the laboratories of Technische Prüfanstalt (TPA), Vienna. The recorded compressive strength measurements, given in Section 6.2, helped to establish correlations with physical and chemical testing of the pozzolans and mortars, as well as phenomena observed through image-based analysis, as described in Chapter 7.

4.3 Chemical Dissolution Testing per RILEM TC-167

Traditional, laboratory-based dissolution testing was performed in parallel to the image-based analysis, in a large part to determine if there was a correlation between results obtained by both methods. Two test procedures from the RILEM technical committee publication on the characterization of old mortars (TC-167-COM Sections 2.1.1 and 2.1.1.3, Method 2) [169] were selected to characterize both experimental and archeological mortars. The first method determines the acid soluble portion of a mortar, and thus, the binder to aggregate ratio, gravimetrically. The second method determines the quantity of soluble silica by treating remnants of the previous test with a boiling alkali solution, which separates the hydraulic phases from the remaining mortar components. The results of this test are also expressed

gravimetrically. The results were refined by repeating the acid and alkali dissolution testing on the aggregates once they had been removed from the mortars, to determine how acid or alkali-soluble they were[10]. The results of these tests are given in Section 6.3. They were used to compare to the binder to aggregate ratios as determined by image analysis (by pseudo-color image editing) and the determination of percentage of hydraulic phases (such as C(A)SH) present by FTIR-m. While the dissolution tests provide gravimetric data, the image-based analysis provides indirect *volumetric* data (discussed more in Chapters 5 and 7), so for the two sets to be compared, data analysis must be applied, as described in Chapter 8.

4.4 Thermogravimetric Analysis of Mortar

Thermogravimetric analysis (TGA) is a common method used to study historical mortars, in particular to analyze the binder content [57, 77, 95, 96]. In brief, it measures the weight change of the sample as it is heated to a high temperature, as at different temperatures mortar components leave the sample. This method allows for both the identification and gravimetric quantification of the contents of the mortar [170, 171]. The components typically measured are free water until 105 °C, both bound water and organic material between 150-600 °C and release of carbon dioxide from calcium carbonate starting at 700 °C. The identification/ quantification of C(A)SH is related to the detected bound water content [57, 77, 95, 96]. Components can be identified by the temperature at which they leave the system, signified by "peaks" in the thermograph corresponding to the weight loss their leaving causes. Because there can be overlap between peaks, there is some room for interpretation by the operator, although there can be additional confirmation by mass spectrometry.

A selection of the archeological and all the experimental specimens were gently crushed in a porcelain mortar and sieved through a 0.063 mm sieve (ISO #230) to separate the binder from the aggregates before analysis. The enriched in binder fraction[11] was subjected to thermal analysis. Thermal analysis was performed using a TA Instruments Discovery SDT Q650. Approximately 20 mg of the sieved fine fraction of the sample was placed in alumina pans. The analysis was performed in a nitrogen atmosphere within the temperature interval from 25 to 1000°C with a temperature gradient of 20°C per minute. The calcium carbonate content and

[10] Thus, both the binder to aggregate ratio and the soluble silica percentages were adjusted to compensate for the weight loss of the aggregates themselves due to acid or alkali dissolution, which if unadjusted would make the mortars appear more binder or C(A)SH rich than they are.

[11] It is generally assumed that this fraction contains a small amount of pulverized aggregate as well, while beyond the scope of this work, in pozzolanic mortar, the very fine aggregate is sometimes considered part of the binder.

water bound in hydrated phases (CSH, CAH), was quantified as interpreted by the Universal Analysis 2000 software. The results of this analysis are reported in Section 6.4 and used in Chapter 8 as a comparison to the image-based methods. Ms. Dita Frankeová from the Institute of Theoretical and Applied Mechanics of the Czech Academy of Sciences performed the measurements.

5.0 Comprehensive Image-Based Analytical Protocol

The experimental procedure and physical testing described in the above sections provided a great deal of information and insight into the behavior and performance of mortar produced in a historically accurate manner. These data could then be used to further the understanding of historical mortars. This information was then used as a background for the application of image-based analytical techniques, which form the central theme of this work. Lessons learned from performing these image-based techniques on the experimental samples could then be applied to analyzing the historical samples, as well as combined with the vast amounts of extant knowledge on the analysis of historical mortar. While not every imaging technique known was used (for example Raman was specifically excluded due to fluorescent interference from clay minerals), the protocol used was intended to be *comprehensive*, fully describing the compositional and micro-structural inhomogeneity frequently encountered in all types of historical mortar.

The comprehensive, image-based analysis protocol described here was performed on high quality, polished (uncovered) petrographic thin sections. Thin sections allow for the preservation of spatial relationships and context between a mortar's microstructural features (i.e., its fabric), which is essential to understanding the methods, materials and techniques employed by an artisan in producing the mortar, as well as the alteration phenomena that have taken place since [1, 33, 128, 129]. The production of polished thin section is described in section 5.2 below. The samples were then analyzed by the following techniques *in succession* to complete the analysis using:

- Petrography by optical microscopy (OM) with both a stereo- and a polarizing light microscope (SM and PLM), which provides the bulk of the information about a mortar's texture, composition, and the condition of its fabric, as well as providing a background image by which to produce maps (detailed in 5.3)
- Scanning electron microscopy (performed in back-scattered electron (BSE) mode) combined with energy-dispersive X-ray spectroscopy (SEM-EDX), which is used to both take highly magnified images of phenomena, such as reaction rims and secondary calcite precipitation, as well as provide detailed elemental analysis of mortar components (5.4)
- Fourier transform infrared spectroscopy mapping (FTIR-m), used here in reflection mode to create spectral maps, which is particularly useful in identifying polymorphs

of mortar constituents as well as to study the location, morphology and density of reactive silicates, degradation products and hydration products, the latter of which are nearly impossible to detect and/or conclusively identify by OM or SEM-EDX (5.5).

- Image analysis, using software such as Adobe Photoshop® or freeware such as Image-J, which is used both to overlay the images taken by the other methods to help in identification as well as make comparative analysis of mortar products through color-coded pixel-counting (5.6).

Since comprehensive image-based analysis does not destroy the prepared sample, a wide variety of correlations can be made from the same preparation; however as described in 4.3 above, acid dissolution was performed on a selection of samples to produce data that could be corroborated with the image-based results. Correlations between the image-based and dissolutive techniques, meant to highlight the effectiveness of the novel, image-based protocol, are elaborated in Chapter 8.

5.1 Historical Mortars Analyzed

One of the main goals of both the production and analysis of experimental mortar is to gain insight into historical and archeological material. A wide variety of both ceramic and volcanic pozzolan-lime mortars from Roman antiquity were analyzed using the protocol described in this section. The selected mortars were used in a structural application, such as *opus signinium* floor mortar, *opus cementicium* fill mortar, bedding mortar between bricks, or as a waterproofing layer e.g., of a cistern or aqueduct. They are from a wide range geographically and in terms of building type: public baths, urban and rustic villas, aqueducts, and apartment buildings from the sites of Vindobona (Vienna, Austria), Aquincum (Budapest, Hungary), Ostia Antica (near Rome, Italy), Školarice (near Koper, Slovenia) and Caesarea Maritima (Israel). Since this work focuses on techniques to study these samples, the results presented are not discussed in terms of their meaning for the site; rather they are used to illustrate which phenomena are describable via these methods. Their provenance will be noted for each example shown.

While it is true that alteration of a mortar over even relatively short time periods can make drawing comparisons between mortars of different ages challenging, image-analysis of new mortar does give a glimpse of what the ancient mortar may have looked like before alteration.

Many types of mortar analysis such as compressive strength testing are impractical when applied to archeological samples, since acquiring a larger enough sample to test may be difficult or even prohibited[12]. Additionally, these types of tests provide little insight to how the mortar would have performed during its service life before alteration. The carbonation of a mortar over archeological time can make a mortar stronger or denser, while long-term salt attack or leaching can make it appear weaker. Therefore, on these historical mortar samples the bulk of comparative analysis was done with image-based methods.

5.2 Polished Thin Section Preparation

Most of the analysis performed in this work was performed on polished petrographic thin sections, which were produced from all of the experimental and archeological mortars discussed here. First, the sample is impregnated with blue-dyed epoxy resin (Eponal Epoxy resin, bto-epoxy GmbH, Austria and EpoBlue, Buehler GmbH, Germany) which is performed through multiple vacuum impregnations. For the most part, this inactivates the sample chemically and makes it durable enough to survive the process of becoming a thin section. Polishing the thin section, however, deposits a small amount of grinding dust in the pores. The blue dye fills the pore and crack spaces with the blue making them more easily distinguishable from solid clear minerals; even micropores below the limit of visibility by OM are discernable as various shades of blue within in the binder system. Next, the sample is glued to a glass slide with either the same epoxy or a UV-light activated polyester glue and ground mechanically to a thickness of around 0.5-1 millimeter. Finally, it is polished with diamond paste of increasing fineness made fluid with water until it is both polished and thin enough to analyze petrographically with a light microscope (25-30 μm). Samples prepared in this way can then be analyzed in succession by all of the methods described in sections 5.3-5.6 below. It is important to note that in all cases the polished thin sections are not covered by a glass slide; a glass slide or resin covering on top of the polished would make reflected (incident light) microscopy less efficient and SEM-EDX and FTIR-R impossible, as these types of analysis rely on reflected energy.

[12] See however, [104, 105] for emerging techniques for physical testing of small samples, even prepared as thin section.

5.3 Mortar Petrography – Optical Microscopy (OM)

The first step of the image-based analytical process on polished thin sections used for this work was mortar petrography. Petrography, sometimes more precisely referred to as optical mineralogy, is the qualification and description of inorganic material (mostly rocks and minerals) by means of their examination by a light microscope; the types, quantities, and shapes of aggregates in a mortar can be described and they can be identified by combining this information with their appearance in different forms of illumination [179]. Both plane-polarized and cross-polarized light are used in this manner. Minerals are identified by their morphology (both internal and external), as well as by their color and appearance when light passes through them. Due to pleochroism, anisotropic materials appear to be different colors when observed by light passing through them at different angles, especially when illuminated by cross-polarized light. Isotropic materials (such as volcanic glass) appear clear when illuminated by transmitted plane-polar light and black ("extinct") with (non-)transmitted cross polarized light. A positive identification of minerals is made by its typical interference colors (its birefringence) [180].

Beyond describing the aggregates, optical microscopy can be used in the same manner to study a mortar's binder matrix, binder source (in the case of Roman mortar this generally means studying lime lumps, although gypsum was also used) and alteration products. There are subtle changes in the color of the binder related to its density and/or the presence of different mineral phases, for example calcium carbonate polymorphs or hydrate phases. Identifying these is the key to understanding binder composition and alteration. [1, 3, 9, 129-133]. A well-made polished petrographic thin section retains the physical characteristics of the whole mortar, the condition of the mortar's constituent parts, as well as the relationship between them [129]. Each piece and how it relates to the whole is important to describing the entire history of the mortar from materials to production and use to aging and alteration. The shape of the pores and cracks and the grading of the aggregate give information about the skill of the mortar's artisan and the techniques they employed [1, 71, 123, 131]. Alteration products, such as secondary calcium carbonate and gypsum can be found in the pores and cracks, revealing some degradation processes [1,9, 128]. "Relict lime clasts" of underburned stone reveal a great deal about the skill and technique utilized in the creation of the mortar's binder, as well as potentially revealing the provenance of the source stone [1, 121, 129, 132, 133]. And perhaps most germane to this work, reactive aggregates can be first located and described by use of optical microscopy,

reaction rims on larger remaining aggregates being the first step to establishing the pozzolanicity of an ancient volcanic or ceramic pozzolan in lime mortar [1, 9, 128, 135-137].

A quick guide to the appearance of the various mortar constituents studied herein is given in Table 5.1 below.

	Appearance in transmitted light		
Mortar Constituent	**Plane Polarized Light (PPL)**	**Plane Polarized Light, Darkfield Mode (PPLD)***	**Cross-Polarized Light (XPL)**
Pores and Cracks	Light blue	Dark blue	Black
Aggregate, Quartz sand	Bright, nearly clear	Silvery	Bright, low 1st order interference colors
Aggregate, Feldpathic sand	Bright, obscured dependent on finely dispersed inclusions and alteration products	Silvery	1st order whitish gray interference colors, twinning
Aggregate, carbonate (calcite, dolomite sand and/or unburned source stone)	beige, change in relief by rotating the sample	Silvery with bright veining at grain boundaries	very high order pale interference colors
Ceramic Aggregate	Dark earth tones with silicate temper as above	Solid earth tones, mostly orange-red	Dark earth tones to black, with silicate temper as above
Glassy aggregate (pozzolana)	Clear to light yellow or brown or red	translucent dark yellow, brown or red	Pores and Matrix Extinct (black), with variously birefringent inclusions
Silica gel, secondary, alteration product	Clear to light blue (dependent on microporosity)	Dark Silver	extinct, but with anisotropic carbonate veining or nodules
undispersed lime lumps	Pale brown to brown	Milky white	Milky white, brown
Binder Matrix	Dependent on density: shades of grey for calcium rich binder, shades of brownish-grey for silicate rich binder	Milky white – high density Silvery – low density	As PPL, but darker anisotropic to opaque dependent on the amount of amorphous and crystalline phases

Table 5.1: A quick guide to the appearance of antique mortar constituents by PLM. *PPLD refers to the Nikon Stereomicroscope Only

The bulk of the petrography in this work was performed with a combination of 2 different microscopes. The first was a Nikon SMZ 1500 transmitted light, stereomicroscope (SM), with 8x eyepieces, 1x lens, and the ability to zoom from 0.75-11.25x, for range of magnification from 6-90x. It includes two attachments: an incident light source (with either direct or raking light) and a rotating polarizer. The second was an Olympus BX40 polarizing light microscope (PLM) with a 10x eyepiece and 5,10,20,50 and 100x objectives, for a range of magnification of 50-1000x and both the incident and transmitted light sources. With both microscopes, a

Canon EOS 600D DSL camera coupled with the EOS Utility software was used to capture photomicrographs. The utility of using both stereo- and polarizing light microscopes to describe the most important features of polished petrographic thin sections of mortar is given in Table 5.2 below. Thus, a large portion of the knowledge gained regarding mortars comes from this first examination by light microscope, and it forms the foundation for successive steps in the image-based analysis.

Mortar Constituent	Transmitted Light			Incident Light		
	Plane Polarized Light (PPL)	Plane Polarized Light, Darkfield Mode (PPLD)	Cross-Polarized Light (XPL)	Plane Polarized Light (IL)	Plane Polarized Light, White Background (ILW)*	Cross-Polarized Light (ILX)*
Pores and Cracks	+	+ +	+	+ +	+/-	+ +
Aggregate Characterization	+	+/-	+ +	+/-	+/-	+ +
Lime Lump Characterization	+	+ +	+/-	+	-	+
Reaction Rim Detection	-	+/-	-	+	+/-	+ +
Binder Matrix Characterization	+	+	+	-	-	+ +
Binder Matrix Density	+	+ +	+	+	-	+/-
Alteration Phenomena	+	+	+ +	+	+/-	+ +
Suitability for Pseudo-Color Editing	+/-	+ +	-	+/-	-	-

* ILW only performed with the stereomicroscope, ILX only performed with the polarizing light microscope

Table 5.2: Suitability of OM for the study of pozzolan-lime mortar

5.4 SEM-EDX: Images Combined with Chemical Analysis

After the identification of areas of interest through OM, a scanning electron microscope (SEM) coupled with energy-dispersive X-ray spectrometer (EDX) was used to make high resolution images of observed phenomena and gain chemical information in the form of elemental analysis, to further the goal of identifying complex mortar constituents. The SEM

scans the uncovered polished thin section with an electron beam that interacts with the surface atoms of the sample, causing both the reflection of electrons, both as secondary and back-scattered (BSE) electrons, and the emission of X-rays from the target atoms. The SEM-BSE creates a high-resolution image based on the contrast between the differing rates at which atoms absorb and release energy, which is element-specific. In tandem, the EDX detector uses software to analyze the X-rays emitted from these atoms when they release energy to create a spectrogram with element-specific spectra allowing elemental identification [181].

The device used for this work was a FEG Quanta 250 Scanning Electron Microscope (FEI, U.S.A.) coupled with a Pegasus APEX Energy-Dispersive X-ray spectrometer (Ametek EDAX, U.S.A.) equipped with the Genesis SEM Quant software (SEM-EDX). Images were generally taken in back-scattered electron mode (BSE) at 20 kV with a spot size of 3.5-4.0 nm and a working distance of between 12-15 mm, in low vacuum mode. EDX measurements were typically displayed as oxide analysis (omitting carbon, heavily prevalent in the epoxy resin), so that results are to be understood representing the proportion of one oxide to another in the target area.

While SEM indeed produced high-resolution images of aggregates and lime lumps, a better use of its great magnifying power was to locate and visualize much smaller constituents. Images of the binder matrix of both calcium carbonate and C(A)SH was made and then analyzed chemically by EDX. SEM-EDX in combination was of particular use in analyzing reaction rims by providing stoichiometric elemental (oxide) analysis moving from the center of a reactive aggregate through the binder-aggregate interface (reaction rim) and into the binder as a verification of pozzolanic activity [58, 58A]. This technique was also used in the same manner at the interface between the binder and relic lime clasts [72]. In addition to the imaging of the primary products of pozzolanicity, such as various forms of C(A)SH [79], degradation products of C(A)SH such as ettringite, gypsum and silica gel were studied in this manner [143, 144]. Another application of the EDX was to create elemental distribution maps, visualizing where in the SEM image certain elements occur and in which relative density. This was particularly helpful in locating degradation phenomena. When analyzing mortar in a comprehensive manner, the SEM images as well as EDX maps were also used as complimentary layers for a smaller scale, higher resolution FTIR-R image-based map. Because of spatial resolution issues when using EDX data to identify small mineral phases (there can be overlap with results from nearby minerals), FTIR was additionally employed in the following step, to compliment the EDX with molecular bonding information from the targeted phases. The usefulness SEM-EDX

in characterizing the components of a mortar and how they are related to one another spatially is summarized in Table 5.3 at the end of this chapter.

5.5 FTIR Imaging – From Chemical Detection to Chemical Mapping

The final step of data collection used was FTIR imaging. FTIR played an important role in the positive identification of compounds within the mortar sample, in particular, hydrate minerals. This allowed for the identification of many components of the binder matrix, such as portlandite ($Ca(OH)_2$) and of course, C(A)SH. FTIR has been used to study inorganic materials and cement minerals for nearly 50 years [151] and although online spectral libraries such as IRUG tend to focus on organic materials, there are sufficient publications testifying to its efficacy [152-157].

An FTIR device uses a beam of infrared light to detect molecular bonds by means of their distinctive interaction with this light. As light passes through or reflects from the target substance, a portion of it is absorbed and this reveals the content of that material, since characteristic combinations of molecular bonds can be used to identify compounds. These bonds are displayed to the user in the form of a spectrograph, which can be set to display the intensity of either absorption, transmission, or reflection of the wavelengths detectable by the device [172, 173]. The device used was a Nicolet iN 10 MX Infrared Imaging Spectrometer (Thermo-Fischer Scientific, USA), with a germanium crystal detector, cooled MCT-A linear array detector, and interfaced with OMNIC Picta software. Spectra were collected in reflection mode, spectral range 4000-720 cm^{-1}, aperture 25 µm, with 8 cm^{-1} spectral resolution, and spatial resolution <10 µm. Ultra-fast mapping mode was used for mapping larger sections. The spectra were finally vector normalized and base line corrected.

For the purposes of this work, there were 3 main types of molecular bond detected by FTIR. First were the silicates, which display a broad range of peak wave numbers between 1200-900 cm^{-1} (known as a Si=O stretching bond) and can be associated (dependent on position and shape of the peak) with a variety of silicate materials including clay, ceramic, C(A)SH and quartz. Degree of crystallinity of these silicates can also be determined by the shape of the peak. Also typical in a lime mortar are carbonates related to the binder (lumps, relict clasts, binder matrix, etc.), whose bond is displayed as a wave number peak around 1450-1400 cm^{-1}. The hydroxide anion (-OH), can be associated with portlandite (around 3600 cm^{-1}), the interstitial bound water in C(A)SH (around 1600 cm^{-1}) and gypsum (around 3450 cm^{-1}) [153-157]. Thus, the hydroxide

anion can be the key to detecting both pozzolanicity (the presence of C(A)SH) and certain degradation products (gypsum). While the acquisition of spectra is rapid, interpretation takes significant time and effort on the part of the analyst.

The samples were analyzed with a spectral imaging technique by which a large portion of the thin section was scanned creating an image made up of hundreds or thousands of point measurements. Then the target areas identified through OM or SEM-EDX are checked for spectra that match certain phenomena, for example checking a reaction rim for the combination of silicate and hydrate that would indicate the presence of C(A)SH. Once identified, the peak wave numbers selected can then be displayed across the entirety of the image, mapping by color (red= most dense, blue = least dense), the highest densities of that wave number or combination of wave numbers. These maps could then be scaled and laid over the previous images (OM or SEM) for digital image analysis. This combination of steps is central to the novel protocol used in this work.

FTIR image mapping was thus employed to confirm the identity of mortar constituents observed by the previous types of analysis as well as to study the location, morphology and density of reactive silicates, hydration products and degradation products, as the final data-collecting step of the comprehensive image-based analysis protocol. When analyzing carbonate lime lumps[13], the shift of the peak wave number was used to differentiate between polymorphs of carbonate. This gave information about the source stone and firing and slaking techniques of the lime binder (discussed in the results). Similarly, FTIR was used to study the aggregates, again by observing shifts in the peak wave number (and number of peaks) in the silicate range. These can be used to determine to which extent the aggregate is non-crystalline, information that is then paired with petrographic analysis Reaction rims observed on both aggregates and relict lime clasts were analyzed to confirm or reject the presence of cement hydrates at the rim.

FTIR imaging and mapping was found to be particularly useful in illustrating both binder matrix composition and alteration phenomena. A large part of this is due to its ability to detect hydrates, the main phases indicating, and thus confirming, pozzolanic activity. Additionally, once the presence of hydrates could be confirmed in areas where they were suspected (such as at the binder-aggregate interface) the mapping function could be used to display areas with a similar spectral signature, and thus hydrates are displayed throughout the imaged area of the sample. A critical part of the detection process involves the input of a skilled FTIR operator, who must use their experience to interpret the collected spectrographs. Part of this is taking

[13] As mentioned in Chapter 2 and discussed thoroughly in the Results sections, “lime lumps” can be both un(der)burned limestone from the production of quicklime (a.k.a. relict lime clasts) or undispersed calcium hydroxide that has since (re-)precipitated and carbonated.

background spectra of the glass slide and epoxy so that they can be subtracted from the assembled spectrograph, particularly important in the case of the slide, since the Si=O stretching in the glass can mask that of ceramic or C(A)SH silicates.

Using FTIR in this way allows a method of *semi*-quantitative analysis, in that the *surface area* of the sample that is shown to comprise of hydrates can be directly correlated to their *volumetric presence* within the binder matrix, or the whole mortar. How this works is explained thoroughly in the next section. The effectiveness of the application of FTIR imaging as the final data-collection step of comprehensive image-based analysis is reflected in Table 5.3 at the end of this chapter and discussed in the Conclusions (Chapter 8).

5.6 Composite Imaging and Digital Image Analysis, Pseudo-color Analysis

Finally, digital image analysis was performed combining the various types of micrographs and spectrographic data. This was performed using Adobe Photoshop®, although it is possible to achieve similar results using freeware downloaded from the Internet. The separate images are imported into a single file as separate layers, and then stretched to fit the same scale, anchoring on a large known[14] object from the scaled photomicrograph, for example a large piece of calcite. Then images made from the same FTIR mapping procedure representing the greatest intensity of each compound that is of interest should be inserted into this composite image on a separate layer. Done correctly, this resulting composite image will display the location of every piece of (in this example) calcite across the analyzed area, thus assigning molecular bonding data to the objects shown by OM (or SEM). It is essential that the same settings be used on all samples when the goal is to make quantitative comparisons between the resulting composite images. The underlying photomicrographs should be taken at the same magnification since the scale of the image produced by the FTIR is a constant. When this is done, an area of one composite image can be compared to the equivalent area of another, which is done by pixel-counting the areas of the highest density of a specified spectral band. Thus, the FTIR data can be effectively combined with the other image-based techniques to not only give the most complete description of the subject mortar, but it can allow comparisons with composite images of other mortars.

[14] "Known" in that the object is clearly identifiable by OM, SEM-EDX and distinctive FTIR bands.

These images can be used to analyze mortar in a variety of ways. Perhaps the simplest application is to confirm the identity of aggregates or lime lumps by overlaying molecular bonding data on top of the OM images; for example, comparing the peak wave numbers associated with two different forms of calcium carbonate can display where either calcite or aragonite occurs in the sample (see Results, Section 7.1). More complex is their use to characterize reaction rims on aggregates and the mortar's binder matrix. Reaction rims can be detected throughout the mapped area by selecting the distinctive wave numbers associated with C(A)SH, preferably from an aggregate with a large, thick rim (see Results, Section 7.2). The number of aggregates with reaction rims between two samples gives both a qualitative and semi-quantitative comparison of the pozzolanic reactivity of each mortar. Doing the same for the binder gives quantitative data about the amount of cement hydrates, i.e., the effective pozzolanic reactivity of that mortar. An example of this would be to take the density map of the peak wave intensity (colored red and orange) maps representing the bound water from two different mortars, fitting them to their respective photomicrographs at the same scale and then comparing their areas by means of pixel-counting (see Results, Section 7.6). While this is quantitative analysis, it should be understood to be a *volumetric*[15] quantitative comparison of mortar contents, as contrasted to the *gravimetric* quantitative data found by thermo-gravimetric or chemical dissolution methods. Comparisons between this method and chemical dissolution methods can be found in Chapter 8. Digital image analysis is the final step of the protocol described herein; its contribution to understanding mortar is shown in Table 5.3 below.

Historical mortar is often rendered as a pseudo-color image since this makes components of the mortar easier to visualize. This is also a prerequisite for digital quantification, which relies on pixel-counting of the pseudo-colored components so that they can be compared to each other quantitatively. The components can be colored automatically by the EDX or FTIR software when they can be positively identified, and there are examples of this in the results sections of this work. Many times, however, and in the case of coloring an OM image, it is often simply the (semi-automatic) hand-coloring using image editing software of different parts of the mortar, e.g., the binder, aggregate and porosity. The latter can be done on both OM and SEM photomicrographs, but when combing FTIR data with either, the additional step had to be taken of making sure that the FTIR map could be scaled to a photomicrograph (or an important part of it) without the map pixel density resolution losing meaning. This means that when performing *quantitative* image analysis by the image-based protocol, the FTIR map and

[15] Volumetric, in that the surface area of a mortar thin section can be directly correlated with the volume of the mortar, since the assumption is that a mortar is a homogenous mix.

photomicrograph had to be close to the same magnification, i.e., close to the 40-50x magnification of the FTIR map. Thus, for this type of analysis generally OM and FTIR results were combined (since SEM image tend to be much higher magnification).

This analysis was performed through semi-automatic image editing with the Adobe Photoshop software on overlapping images of areas of interest of a mortar, taken by OM, SEM and FTIR-m. Pseudo-color analysis allows for the volume percentage of macro-porosity or the binder-to-aggregate ratio to be quantified [1-3, 9, 33]. This latter method was used on all mortars discussed in this work, the results of which calculate the binder to aggregate ratio (b:a) of each mortar are shown in Table 7.14 in Section 7.5. The process of analyzing scaled, composite images that include information from OM, SEM and FTIR-m works on essentially the same principle (Section 7.6), in that the volume percentage of a compound detected by FTIR is calculated based on its density across the surface area of the analyzed sample. Finally, as part of the analytical procedure followed herein, both methods of pseudo-color analysis described above can be compared to the results from chemical and thermal dissolution of the mortars, thus supporting the efficacy of using image-based methods on polished thin sections alone. This comparative analysis of these techniques is done in Chapter 8.

5.7 Summary of the Comprehensive Image-Based Protocol

Every tool used in the image-based analytical protocol is very powerful individually as shown in Table 5.3 below; used together they overcome the drawbacks of each other. Optical microscopy and SEM imagery describe the mortar as a whole and its parts based on physical appearance and their interaction with light or electrons as they pass through or reflect from the polished thin section. An experienced researcher can gather a huge amount of information regarding the composition of the mortar, the skill of its artisans and its preservation state based solely on OM and SEM images. This information is then coupled with EDX (elemental) and FTIR (molecular bonding) to precisely identify the compounds contained in each sample, creating a comprehensive understanding of the mortar based entirely on a single sample preparation. This eliminates much of the uncertainty involved in making correlations between different techniques. When used together these tools provide a complete qualitative description of historical or archeological mortar. In combination with the digital image analysis method described above they also provide quantitative data, overcoming the main shortcoming of image-based techniques. In the following chapters it will be shown that this is quite effective

and can replace the destructive techniques entirely if need be. This is demonstrated with both the experimental mortars as well as archeological mortars.

	Analytical Method				
Mortar Characterization Goal	OM/PLM	SEM	EDX	FTIR	Image Analysis
Aggregate Characterization	+ +	+ +	+ + +	+ +	+
Binder to Aggregate Ratio	+	-	-	+	+ +
Lime Lump Characterization	+ +	+	+ +	+ +	+
Cracks and Porosity	+ +	+	-	+	+
Reaction Rim Detection	+	+ +	+ +	+ +	+ +
Binder Alteration Phenomena	+	+ +	+ + +*	+ + +	+ + +
Binder Matrix Density	+/-	+/-	+/-	+ +	+ +
Binder Matrix Characterization	+/-	+ +	+ +	+ + +	+ +
Suitability for Image Analysis	+	+ +	+/-	+ + +	**N/A**

* by EDX Elemental Distribution Mapping

Table 5.3: Suitability of different image-based techniques for the study of mortar thin sections

6.0 Results: Physical and Chemical Characterization of the Mortars

This chapter reports the results of the physical and chemical testing of the experimental and archeological mortars, including relevant laboratory analysis; this will be followed by results of the comprehensive image-based protocol in Chapter 7, which the laboratory analysis is intended to supplement. Generally, all mortar analysis takes one of two forms: methods that test the whole mortar, or ones that test its constituent parts individually to establish an understanding of the whole - how it came to be, and how it has changed over time. The ones used in this work are shown in Table 6.1 below. Section 6.1 describes (semi-empirical, semi-qualitative) observations made while producing experimental mortar. This is followed by results of the laboratory analysis of both mortar components (pozzolanic aggregates and binder) as well as the whole mortar (Sections 6.2-6.4). Finally, the results gained by using the comprehensive image-based protocol to describe both the mortar and its components are given in Chapter 7 to follow.

Procedure	Analysis Type	Analyzes the Components	Analyzes the Mortar
Mortar Production		-	+
Laboratory Analysis (Chapter 6)	Pozzolanicity Testing	+	-
	Strength Development by US	-	+
	Compressive Strength Testing	-	+
	Chemical Dissolution – b:a ratio	-	+
	Chemical Dissolution – Soluble Silica	+	+
	Thermogravimetric Analysis	+	-
Image-Based Analysis (Chapter 7)	Optical Microscopy	+	+
	Scanning Electron Microscopy	+	+
	Energy-Dispersive X-ray Spectroscopy	+	-
	FT-Infrared Spectroscopy	+	-
	Digital Image Analysis	-	+

Table 6.1: Types of Result by Technique.

A mortar is more than the sum of its parts, as is scientific understanding of its nature. The results will show comparisons between experimental and archaeological mortars by both laboratory and analytical equipment-based methods. The Conclusions (Chapter 8) will build upon this by highlighting correlations between the different techniques, with the aim of

demonstrating the efficacy of both the experimental archeological and comprehensive image-based analytical techniques.

6.1 Empirical Observations on the mortar making process applicable to archeological interpretation

The production of historically accurate pozzolanic mortar by experimental archeological means is informative beyond the testing of the resultant products. Table 6.2 below summarizes four observations made during mortar production that are helpful when considering the interpretation of historical mortar. They relate to workability (water-to-binder ratio, w:b), slaking method, selection/ production of (ceramic) aggregate and binder to aggregate ratio (b:a); four criteria that are considered important to the interpretation of a mortar.

Mortar Production Process	Observation	Effect on Final Mortar
Mixing in Water (w:b: ratio)	Pozzolanic Mortar has very high water requirements.	Mortar becomes more porous, slaking temperature does not remain high for long, water content and pH stay high
Basket or Hot slaking	High temperature does not remain when sufficient water is added for workability [16]	Hot slaking had minimal effect on pozzolanic mortar in this experiment.
Sieve fraction, aggregate treatment	Fine fraction difficult to create through hand crushing	Requires more experimentation, were ceramic fines from sawing or kiln waste material added, was it worked for a very long time?
b:a aggregate by volume	Historically, mortar was never produced by weight proportion, rather by volume proportion	Difficulty in comparing volumetric to gravimetric results, development of purely volumetric analysis (image-based)

Table 6.2: Observations on the mortar making process

The water to binder ratio and its relationship to workability was an issue of great practical concern. Typically, from a materials science perspective, the goal is to reduce the water input as much as possible to that which is needed to activate the binder, which is recommended in international mortar making testing standards [168]. This is reflected in many publications that deal with experimental archeological production of historical mortar, where a water to binder of about 1:1 is used [82, 83, 92, 107, 123]. For this experiment, it was found that this was

[16] This statement is based on the observations for mortar created in this work. In other scenarios where either a more massive concrete element was produced, or the mortar is placed into masonry formwork in a relatively dry and less liquid state, elevated temperatures can persist for longer periods of time.

insufficient, and w:b ratios were typically closer to 1.5:1 before the mortar could be mixed or placed effectively. This is likely due to the high aggregate porosity and large amount of very fine material used, (shown in Table 3.12 and 3.13 in sections 3.4.); it can be assumed that historical pozzolanic mortars would have also required large amounts of water to achieve a workable mix, and this would have had a drastic effect on the mortar's properties.

During the initial set of pozzolanic mortar, the reaction between calcium hydroxide and the pozzolan begins the moment it is mixed with water. Although final strength development is rather slow (as can be seen in subsequent sections), in practical terms it would not have been possible to slake the reactive aggregate and lime together for a long period of time, since it was observed that after a few hours the mortar became unworkable. Both literature and observation support that pozzolanic methods would have used a hot-slake, or basket-slake method, that is the ingredients were mixed with water shortly before the mortar's use [120-122, 144]. Heat measurements discussed in Section 3.5 show that slaking lime and pozzolanic aggregate together can generate considerable heat, but once water has been added to achieve workability, the material cools to the point at which it can be handled (to about 60º C). In massive Roman concrete this level of heat can be sustained for long periods of time [4, 5, 8, 62]; in this experiment, the mortar blocks had cooled to ambient temperature after a day. Thus, elevated temperature seems unlikely to have had much effect on these experimental mortars.

Achieving equivalent sieve fractions for each type of aggregate used proved quite difficult. Crushing ceramic in the laboratory with hand tools could not easily replicate a similar sieve fraction as the volcanic pozzolana or the field produced bricks, which had been crushed in a jaw-crusher, thus it can be assumed that in Roman mortar was either worked for a very long time or that the ceramics used were more friable. Reactivity testing of the finest fractions of all types of ceramic (Section 3.3) and the final strength of the field and laboratory produced ceramic mortars were nonetheless similar (Section 4.2), which raises the question of whether or not certain fractions of material were used preferentially historically. This would require additional experimentation. The coloration found in the mortars shown by Figure 6.3 below would seem to indicate a very high proportion of ceramic fines, illustrating that the field production mortar technique may have produced mortar of closer equivalence to the historical types than those made in the laboratory. While empirical observations are important, they are not intended to replace scientific analysis, especially in cases where observations seem contradictory to other available evidence.



Figure 6.3: An archeological mortar visually compared to an experimental archeological mortar Left: A wall rendering mortar from Aquincum (Budapest) Right: Ton-06, Made in the Field

6.2 Mortar Strength: Strength Development as measured by ultrasound resistance and Compressive Strength

In addition to reactivity testing of the aggregates used in the mortar, two types of physical testing were performed to provide information on the strength of the cured mortar. These were the measurement of strength development by ultrasonic resistance and industry-standard compressive strength testing after curing and carbonation of the experimental mortar samples. These were performed to support the results found by image-based analysis found in Chapter 7.

The results given in Figure 6.4 are from a novel application of the measurement of ultrasonic pulse resistance, used to measure the strength development of large blocks of experimentally produced, historically accurate opus caementitium[17]. The measurements were taken after 7, 14, 28 days while the samples were curing in a high-humidity setting, and then after 35 and 42 days after removal from that environment. These correspond roughly with the intervals used for compressive strength testing (per ASTM-C109/M, EN-998, see below) [168] as well as by ultrasonic device [102, 167] (per ASTM C597, EN-12504-4-2004). This method was applied to the mortars made in the laboratory setting only.

[17] Although the particulars of the mortar tested and how and when they were tested are novel, it is similar to previously published work dealing with testing cured mortar prisms with ultrasound [105].

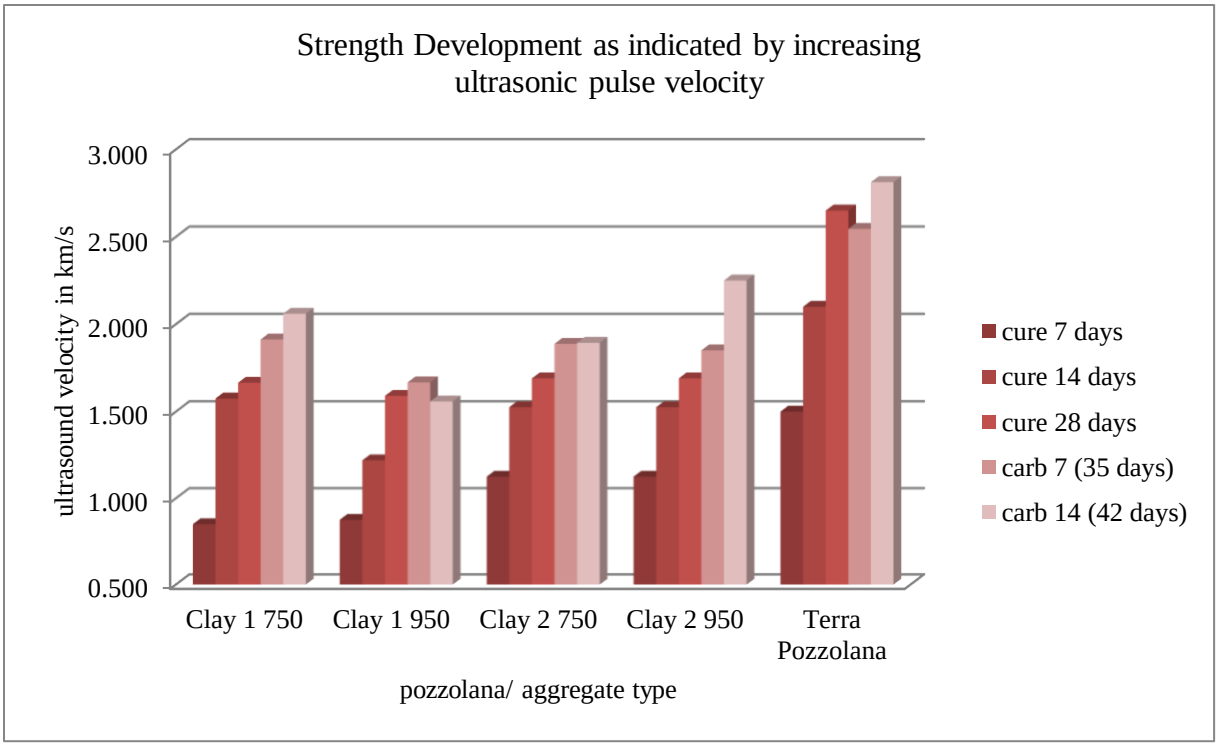


Figure 6.4: Ultrasound Pulse Velocity During Mortar Curing/ Carbonation for the laboratory mortars. During curing the mortar plates remained in a high-Rh environment, and during carbonation, they were removed and kept at ambient conditions.

In interpreting these results, it is important to keep in mind that there is not necessarily a direct correlation to compressive strength (as will be discussed in the next section), but it is nonetheless informative as a measure of how strength is developing over time. This can be qualitatively compared between different types of mortar. The measured ultrasound pulse velocity increases the most rapidly and achieves the highest final rate in the Terra Pozzolana-lime mortar ("P-K" when prepared as a polished thin section), with the ceramic-based mortars developing both more slowly and to a lower final measured ultrasound pulse rate. Thus while the Chapelle test (see Figure 3.11) seemed to show that pozzolana was equally reactive as the ceramic powder, when the pozzolana was actually used in mortar, the mortar gained more strength, more rapidly than any of the ceramic-based mortars. This corresponds well with the well-established behavior of volcanic pozzolana as noted since Vitruvius to the present-day state of the art[18]. What is more noteworthy is the seeming discrepancy between the strength development, where mortar made from the low-fired calcium free Clay 1 and the high-fired calcium-rich Clay 2 achieve the best results. The first result appears to conform to the expected performance, that the lower firing temperatures result in higher pozzolanicity (as measured by strength development) [22, 23, 84-88]. Contrarily the high-fired Clay 2 produced the stronger

[18]As thoroughly reviewed in Section 2.2 of this work.

mortar. A possible reason for this is the partial conversion, especially at the *higher* firing temperature, of a percentage of Clay 2´s calcium carbonate content to calcium oxide, which then combines with pozzolanic material. In other words, because the clay is calcium rich, high temperature ceramic made from it is slightly self-cementing and air-hardening.

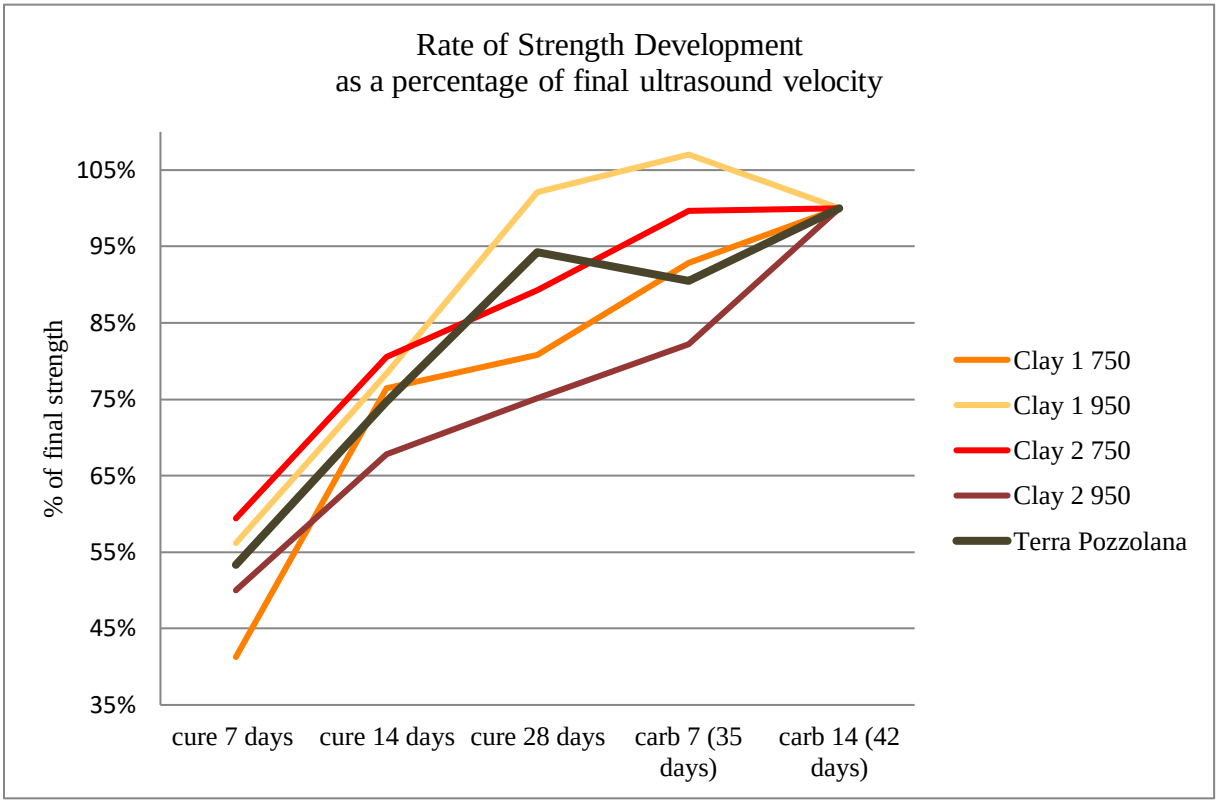


Figure 6.5: Rate of Strength Development as a percentage of final ultrasound velocity during mortar curing for the laboratory mortars.

Figure 6.5 shows this strength development over time as a percentage of final measured ultrasound velocity. The decrease in rate between 28 and 35 days (sometimes into a downslope) can be attributed to the time of de-molding (end of curing, beginning of carbonation). When water leaves the pore system of the mortar, ultrasound transmission drops (as the material is less dense); these results are more representative of the mortar alone (without being filled with water)[19]. While these results show a loose correlation with the final compressive strength, as shown in the next section, they indicate that regardless of mineralogy and treatment of clay materials, from a practical standpoint the resulting mortars could be expected to perform in a similar fashion, with the volcanic pozzolana generally outperforming all of them.

[19] This effect is most noticeable in mortar "Clay 1 – 950" where the combination of water loss and mortar shrinkage give an apparent value of 105% of final strength.

The results of the compressive strength testing per ASTM C- 109/ EN998 are shown in Figure 6.6 below. They reveal both that the laboratory mortars are relatively low strength, and that there is a relatively strong correlation between the final measured ultrasonic pulse velocity and the compressive strength of the mortar, shown in Table 6.7.

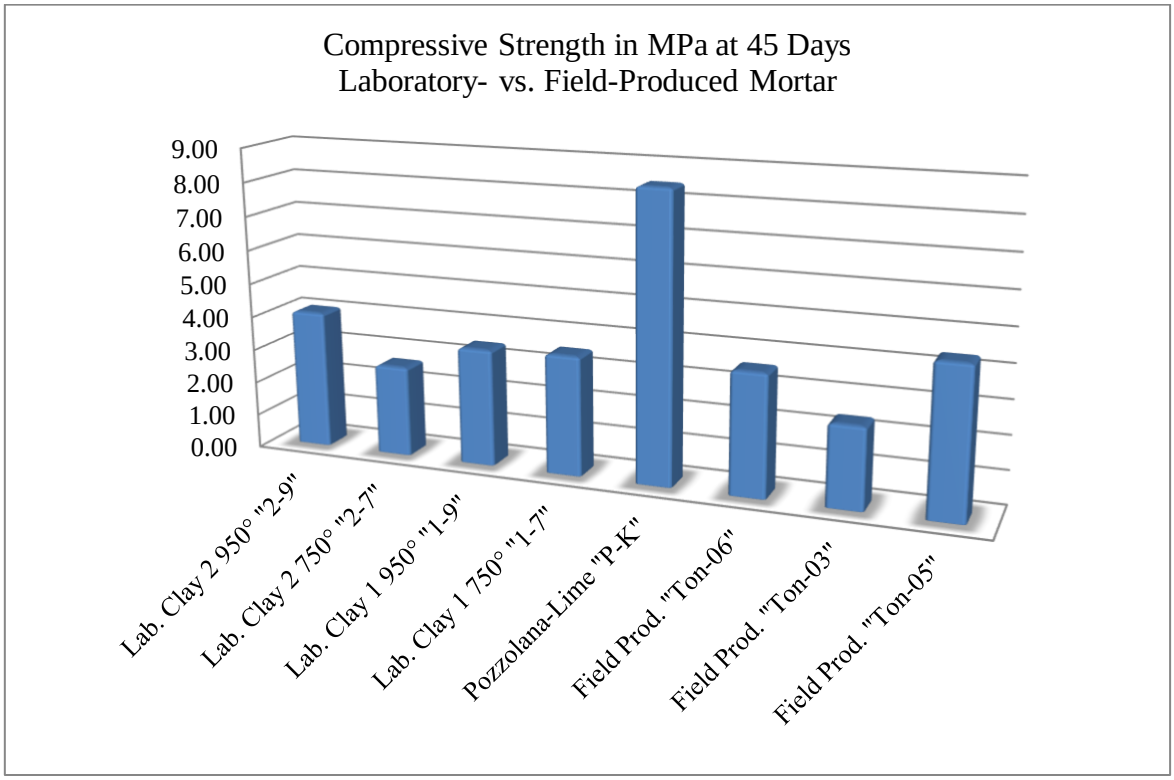


Figure 6.6: Compressive Strength of Mortars from both Experimental Mortar Programs, tested at 45 days (+/- 3 days) Compositions found in Tables 3.2 and 3.15.

Overall, the experimental mortars from both production series gave relatively consistent compressive strength results, in the 2.5 to 4.5 MPa range for the mortars that used both basket-slaked air lime and ceramic aggregate. These values correspond to a lower range of replacement mortars found in the literature, but a relatively high range for young, lime-pozzolan only mortar [74, 82, 83, 182]. The two with higher average compressive strength were “Ton-01” which used a hydraulic lime burned in a small-scale traditional kiln[20] with ceramic powder and the volcanic pozzolana-lime mortar “P-K”. The two with the lowest strength values contained less reactive material, “Ton-3” which included inert sand, and “1-9” which had a larger proportion of over-fired ceramic.

Mortar Type	US Velocity in km/s 42 days	Comp. Strength in MPa 42 days
Clay 1 750° "1-7"	2.061	3.53
Clay 1 950° "1-9"	1.558	2.68
Clay 2 750° "2-7"	1.894	3.46
Clay 2 950° "2-9"	2.250	4.06
Terra Pozzolana "P-K"	2.813	8.47

Table 6.7: Comparison of ultrasound velocity to compressive strength at 42 days

The testing methods correlate: the higher final ultrasound velocity, the higher the final compressive strength, with the pozzolana "P-K" mortar clearly developing a higher strength over 42 days. While testing the laboratory – made mortar by ultrasonic transmission velocity proved informative for measuring strength development, these results show relative strength development, consistent with similar experiments on mortar beams [102,103]. From these data, it cannot be inferred that a mortar with a US resistance velocity of "X" will have a compressive strength of "Y" MPa, rather that there is general trend of higher resistance indicating greater strength.

Taken all together, the combination of reactivity and strength testing of the experimental mortars served as a background for understanding what could be observed through image-based methods, a background that could then be applied to understanding the behavior of archeological mortars during their service life (i.e., before they were archeological remains). In Chapters 7 and 8 it will be shown that both the reactivity of pozzolans and the strength of mortars made from them can be clearly correlated with the data elaborated by the comprehensive image-based analysis protocol.

6.3 Chemical Dissolution Test Results

Chemical dissolution testing of the experimental and historical mortars was used to describe the binder to aggregate ratio as well as the soluble silica proportion gravimetrically. As a wet-chemical procedure, chemical dissolution testing is inexpensive and can be done with common laboratory equipment; the RILEM TC-167 technique, while not a standard, is widely used in preparing reports on ancient mortar. These results provided an important point of comparison to the results obtained through image-based analysis, the binder to aggregate ratio being compared to the image-based pseudo-color analysis and the soluble silica to those results given by FTIR imaging, which are given in Sections 8.3. and 8.5 respectively.

The results of determining the binder to aggregate ratio gravimetrically by this method are given in Table 6.8 below. The results given are the average of values obtained from running the analysis on 5 pieces of the sample. Although they were mixed to the same volumetric proportions using very similar aggregates, the average binder to aggregate values of the experimental ceramic-lime mortars show quite a wide range, from 22 to 52%; this is also reflected in the archeological ceramic-lime mortars which show values of binder weight percentage values of 36% and 67%. Similarly wide ranges of results can be found in the relevant literature [7, 15, 57, 78, 81, 183][21]. The standard deviation of these averaged data is much higher for the archeological samples, showing that the experimental mortar is in fact more homogenous. A reasonable conclusion from this is that historical mortars were produced with much less adherence to any particular b:a "rule" than those produced in the lab in modern times, and the wide variety of b:a could be attributable to sample bias.

Name	Description	b:a proportional	Binder as wt. % of mortar	Standard Deviation
Experimental Mortar				
P-K	(Volcanic) Pozzolana-Lime Mortar, Lab	1:1.57	39%	1.8
1-7	Ceramic-Lime Mortar, Lab	1:2.02	33%	2.3
1-9	Ceramic-Lime Mortar, Lab	1:0.89	52%	3.3
2-7	Ceramic-Lime Mortar, Lab	1:1.55	39%	2.4
2-9	Ceramic-Lime Mortar, Lab	1:1.74	36%	2.7
Ton-03	Ceramic-Lime Mortar, Field	1:1	50%	3.5
Ton-04	Ceramic-Lime Mortar, Field	1:3	25%	1.5
Ton-06	Ceramic-Lime Mortar, Field	1:3.5	22%	
Archeological Mortar				
Pozzalana-Lime, Ostia	(Volcanic) Pozzolana-Lime Mortar	1:1.6	40%	8.1
Pozzolana-Lime, Caesarea	(Volcanic) Pozzolana-Lime Mortar	1:1.75	36%	5.3
Ceramic-Lime, Aquincum	Ceramic-Lime Mortar	2:1	67%	5.6
Ceramic-Lime, Školarice	Ceramic-Lime Mortar	1:1.76	36%	7.2

Table 6.8: Binder to aggregate ratio and weight percentage for both Experimental and Archeological Mortar per RILEM TC-167

The average values for all tested samples tabulated above are illustrated in Figure 6.9 below. They are listed from left to right by increasing level of the weight percentage of binder, with

[21] While individual studies may show a narrower range of results, comparing between studies can give b:a ranging from .25-.67 for ancient ceramic-lime mortar; whether this is due to regional building variation or sampling bias is an open question. This discrepancy is thus inherent to the materials studied, and not likely a source of experimental error.

their symbols color-coordinated by pozzolan type and provenance (as described in Section 5.1). The results from archeological sites represent average values for several different mortar samples (themselves tested three times) and those of the experimental mortars are averages of repeated tests on different mortar prisms (at least 5 times). The graph shows that there is little correlation between mortar provenance and type and the results to be gained through this type of analysis. Correlations between this technique and image-based ones will be discussed further in Chapter 8.

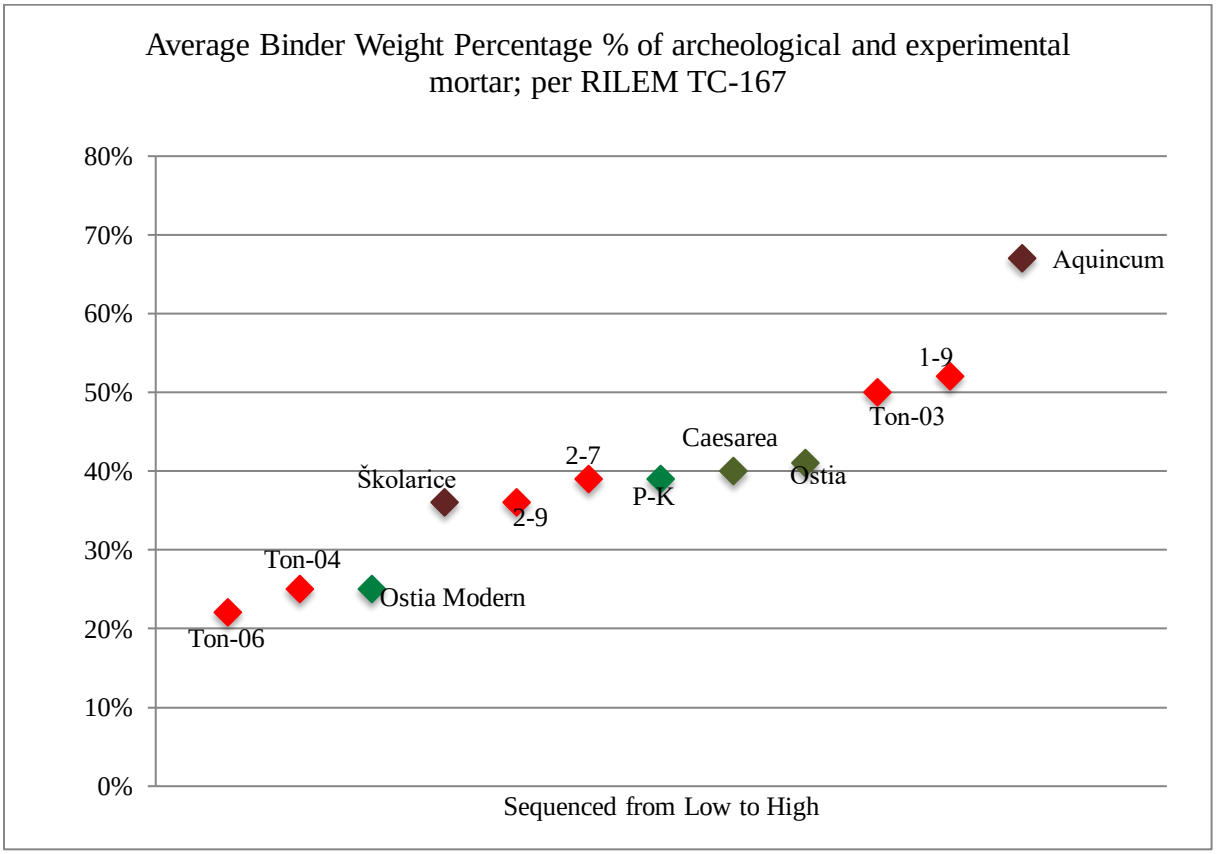


Figure 6.9: Scatter Chart of Binder to aggregate ratio (mean values), expressed as a weight percentage, for Experimental and Archeological Mortar per RILEM TC-167.
Red – Ceramic Aggregate, Green - Volcanic Aggregate (both: light experimental, dark archeological)
Samples arranged left to right in ascending order to allow for quick comparisons to b:a as determined by pseudo-color image analysis (see Section 7.5 and Conclusions).

The second step of the chemical testing was the treatment of the remnants from the previous step with alkali to determine the soluble silica content of the mortar. The alkali disassociates (referred to as "cracking") soluble silica and bound hydrates (such as C(A)SH), thus the sample loses the weight associated with these products. As in the previous step, this test was repeated 5 times per sample; the values given are averages. These data are particularly important when working with pozzolanic mortar as they speak to the issue of hydraulicity of the mortar, i.e.,

how strongly the mortar would have exhibited the pozzolanic reaction and produced C(A)SH. These data are then used to compare the subject mortar to others, particularly those analyzed by other researchers and/or test methods. The results of this analysis are given in Table 6.10 below, both in terms of the gravimetric percentage of the whole mortar, as well as adjusted by combining it with the previously determined binder to aggregate ratio to show the percentage of the binder that is C(A)SH by weight, and again track well with other studies that utilize the same technique [6, 7, 15, 57-65, 78, 81, 183]. Both the raw volcanic pozzolana and ceramic pozzolans were found to be alkali soluble - 18% and 5% by weight, respectively; the numbers presented below represent an adjustment.

Name	Description	Soluble Si wt.-% of mortar	Soluble Si wt.-% of binder
Experimental Mortar			
P-K	(Volcanic) Pozzolana-Lime Mortar, Lab	7.8%	19.4%
1-7	Ceramic-Lime Mortar, Lab	4.2%	12.8%
1-9	Ceramic-Lime Mortar, Lab	5.1%	9.3%
2-7	Ceramic-Lime Mortar, Lab	4.3%	9.5%
2-9	Ceramic-Lime Mortar, Lab	8.8%	22.0%
Ton-03	Ceramic-Lime Mortar, Field	6.8%	12.1%
Ton-04	Ceramic-Lime Mortar, Field	8.9%	25.6%
Ton-06	Ceramic-Lime Mortar, Field	3.5%	13.5%
Archeological Mortar			
Pozzalana-Lime, Ostia	(Volcanic) Pozzolana-Lime Mortar	11.1%	27.0%
Pozzolana-Lime, Caesarea	(Volcanic) Pozzolana-Lime Mortar	10.1%	31.0%
Ceramic-Lime, Aquincum	Ceramic-Lime Mortar	9.3%	13.3%
Ceramic-Lime, Školarice	Ceramic-Lime Mortar	8.0%	19.5%

Table 6.10: Soluble Silica proportion by weight for both Experimental and Archeological Mortar per RILEM TC-167

Soluble silica content determined in this way gives high values relative to those determined by thermo-gravimetric analysis (see following section), which could be partially due to the solubility of the aggregates, as noted above. Regardless, the volcanic pozzolanic mortar generally has greater soluble silica content (even after adjusting for aggregate solubility) than the ceramic pozzolanic mortar, thus more C(A)SH, and corresponding well with the physical testing from the previous sections. The main exceptions to this are Ton-04 which has a very high ceramic fine fraction, some of which may be dissolving and contributing to the soluble silica value, and sample 2-9, which as previously discussed exhibits some self-cementing properties. These results are shown graphically in Figure 6.11 below as tests of individual samples. The green-shaded symbols represent volcanic pozzolanic mortars, which clearly dominate the higher range of soluble silicate content by binder percentage weight; this result

similarly corresponds with available literature [57-65]. Correlations between this technique and image-based ones, in particular FTIR-mapping, will be discussed further in Chapter 8.

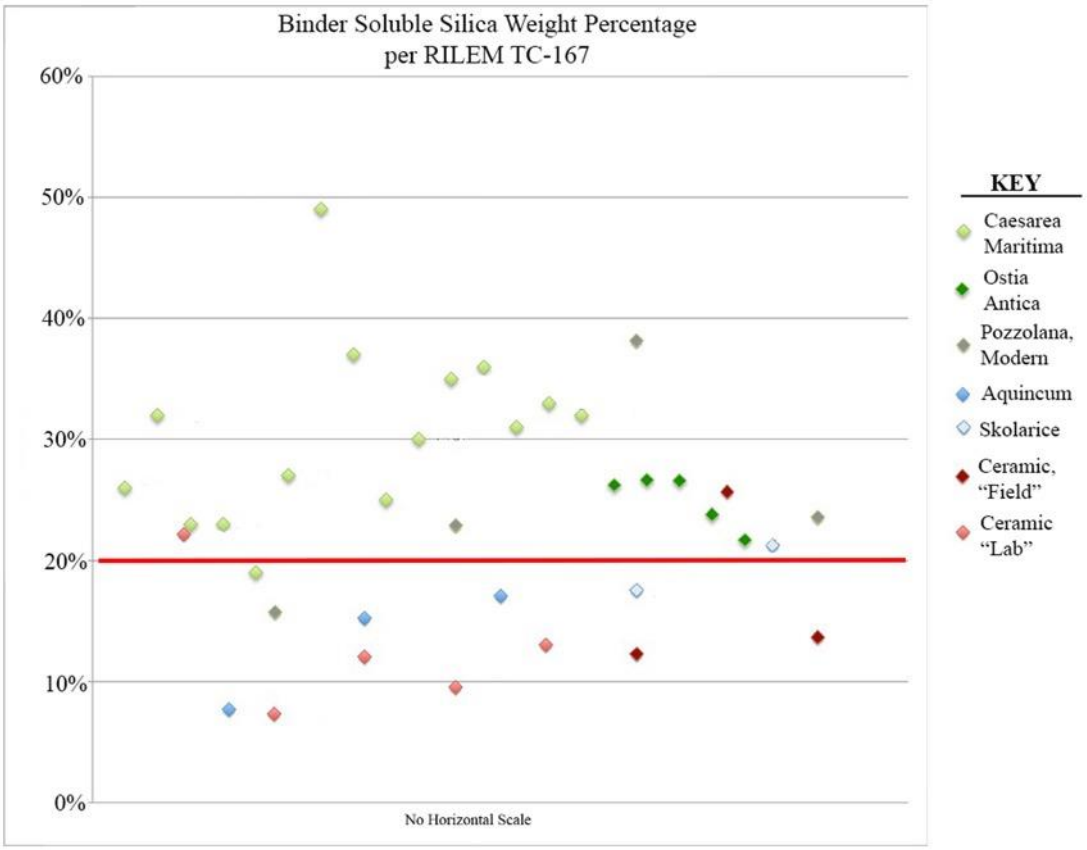


Figure 6.11: Scatter Chart of Soluble Silica in Experimental and Archeological Mortar per RILEM TC-167. The binder from volcanic pozzolanic mortar (green shades) tends to contain over 20% soluble silica by weight, while that of ceramic pozzolanic mortar (red and blue shades) tends to be below 20%
Note: Averages of Individual Samples, color-coordinated by site/ provenance

6.4 Results of Thermogravimetric Analysis of Mortar Binder

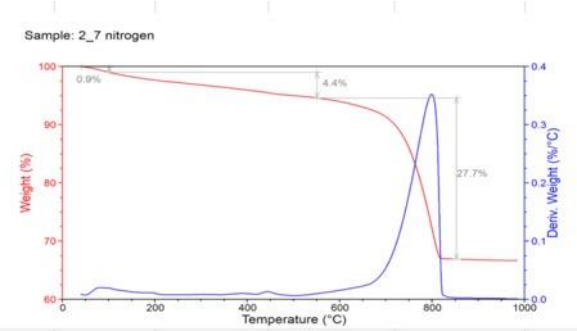
Thermogravimetric analysis was performed on the binder fraction of all the experimental mortars and a selection of the historical ones, as per the methodology often (?) used in archeological science [110, 112]. For the pozzolan-lime mortars, there were three main areas of weight loss, free water (up to 105 °C), carbon dioxide from calcium carbonate (between 600-800 °C) and a variety of types of chemically bound water in the temperature ranges in between. This middle area presents a challenge for interpretation, as the chemically bound water can be found in cement hydrate (C(A)SH), unreacted portlandite and/ or the alteration product gypsum, although the latter two generally have a distinctive range of thermal degradation around 400 °C

and 150 °C respectively.[22] In the case of gypsum, there is no way to determine whether the gypsum was an original part of the binder, or an alteration product. However, this can be seen in image-based analysis, which shows the localization and density of the gypsum and/ or the presence of relic clasts of gypsum binder source (see Figures 7.10 and 7.11). This uncertainty lead to a novel method of interpretation of these results; rather than express the hydraulicity of the binder as the proportion of *calcium carbonate to bound water* (per Moropolou 2004 [15]), the hydraulicity is expressed as the proportion of the bound water found in the sample in the range of temperatures up to 550 °C, divided by the total weight loss due to binder degradation over the full range of the thermogravimetric measurement (wt. loss % 150 - 550 °C / wt. loss % 150 – 800 °C), i.e., it gives the hydraulic portion of the binder as a percentage the *total binder (both hydraulic and non-hydraulic portions)*. In this manner, both calcium hydroxide and gypsum are included in the hydrated phases of the binder, therefore remaining C(A)SH and one of its main alteration products are counted together. This makes the results more directly equivalent to both the chemical dissolution (since these materials would also dissolve in acid and alkali) and the image-based (since FTIR would also determine all phases with bound water) methods used throughout this work. As shown in Table 6.13 below, in most cases this calculation is closely equivalent to the established method, with some exceptions in the case of heavily altered historical mortars. To create a more approximate equivalence between the two methods of interpretation, the ratio used in the traditional method was reversed so that the index of hydraulicity is expressed in terms of bound water to carbonate.[23]

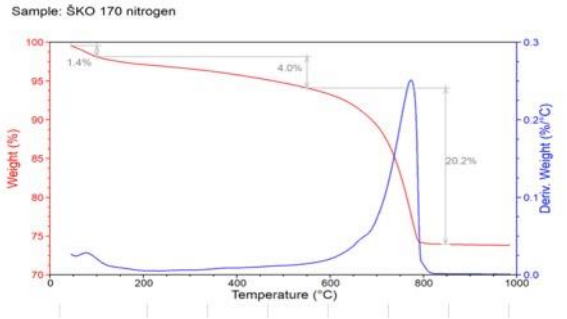
Four examples of thermographs from this procedure are shown in Figure 6.12 below, comparing the experimental mortars to the archeological ones, with both pozzolan types represented. The total weight loss for the experimental ceramic - lime mortar "2-7" and the archeological ceramic – lime mortar from Školarice "SKO-170" is roughly equivalent (4.4% to 4.0%). However, larger percentage of weight loss occurred for 2-7 in the carbonate region than the hydrate region, as opposed to SKO-170, which lost more weight associated with the hydrate regions (10.3% to 16% (see Table 6.13)). Therefore, it is can be said that SKO-170 has a higher index of hydraulicity, per TGA-DSC. Whether this hydraulicity is due to long term or short-term reactivity is not knowable. Other additional interesting points of comparison between the experimental and archeological ceramic – lime mortar thermographs are the small peak around 400 °C for 2-7, indicating the presence of unreacted and un-carbonated portlandite and the

[22] Unfired clay and organic material would also "burn off" in this temperature range; these are not present in the experimental mortar and likely minimally present in the archeological mortar.
[23] Binder hydraulicity index per Moropolou [15] is expressed as CO_2 loss to (bound) H_2O loss. This is reversed to compare with the "total binder" method proposed here to (bound) H_2O loss to CO_2 loss.

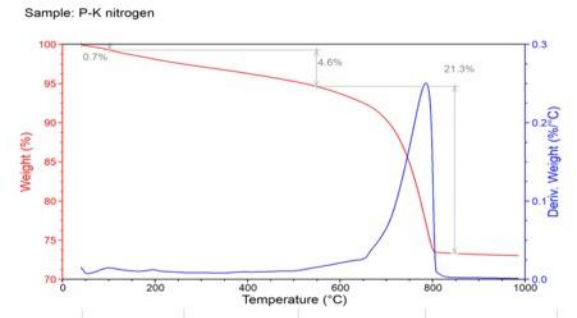
"shoulder" between 600-700 °C in sample SKO-170. The latter is likely indicative of the breakdown of aragonite and vaterite (which happens at a lower temperature than calcite), both of which are likely alteration products of C(A)SH. This can be compared to the smooth shoulder for Sample 2-7, indicating a lack of these carbonate polymorphs. For the pozzolana mortars, the laboratory produced "P-K" sample has a similar, if slightly higher, bound water content than both ceramic-lime mortars previously discussed.



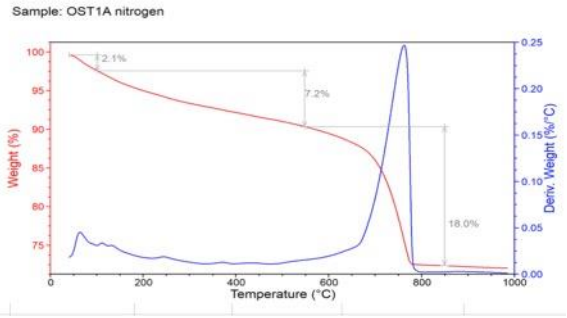
2-7 Experimental Ceramic-Lime Mortar Binder



SKO-170 Archeological Ceramic-Lime Mortar Binder



P-K Experimental Pozzolana-Lime Mortar Binder



OST-1a Archeological Pozzolana-Lime Mortar Binder

Figure 6.12 – Example thermographs of experimental (left) and archeological (right) mortar binder types.

The ancient pozzolana-lime mortar from Ostia Antica ("OST-1A") displays nearly twice the bound water as the other samples. There is also a large discrepancy between the two different methods of interpretation of results (shown in Table 6.13 below, in red). Close examination of both volcanic pozzolana-lime thermal degradation curves reveals that the range between 150-550 °C has a variety of small peaks not found in the ceramic-lime mortars representing a wider variety of cement hydrates.

The results of all samples examined by this method are shown below in Figure 6.13 as a scatter chart of the "total binder" method and a table indicating the percentage of hydraulic binder, by both methods. Due to time and financial considerations, fewer repetitions of this destructive technique were performed. There appears to be little to no statistical pattern beyond

the general observation that the pozzolana mortars have a higher percentage of bound water (thus likely C(A)SH) than the ceramic mortars, which corresponds with the results gained by

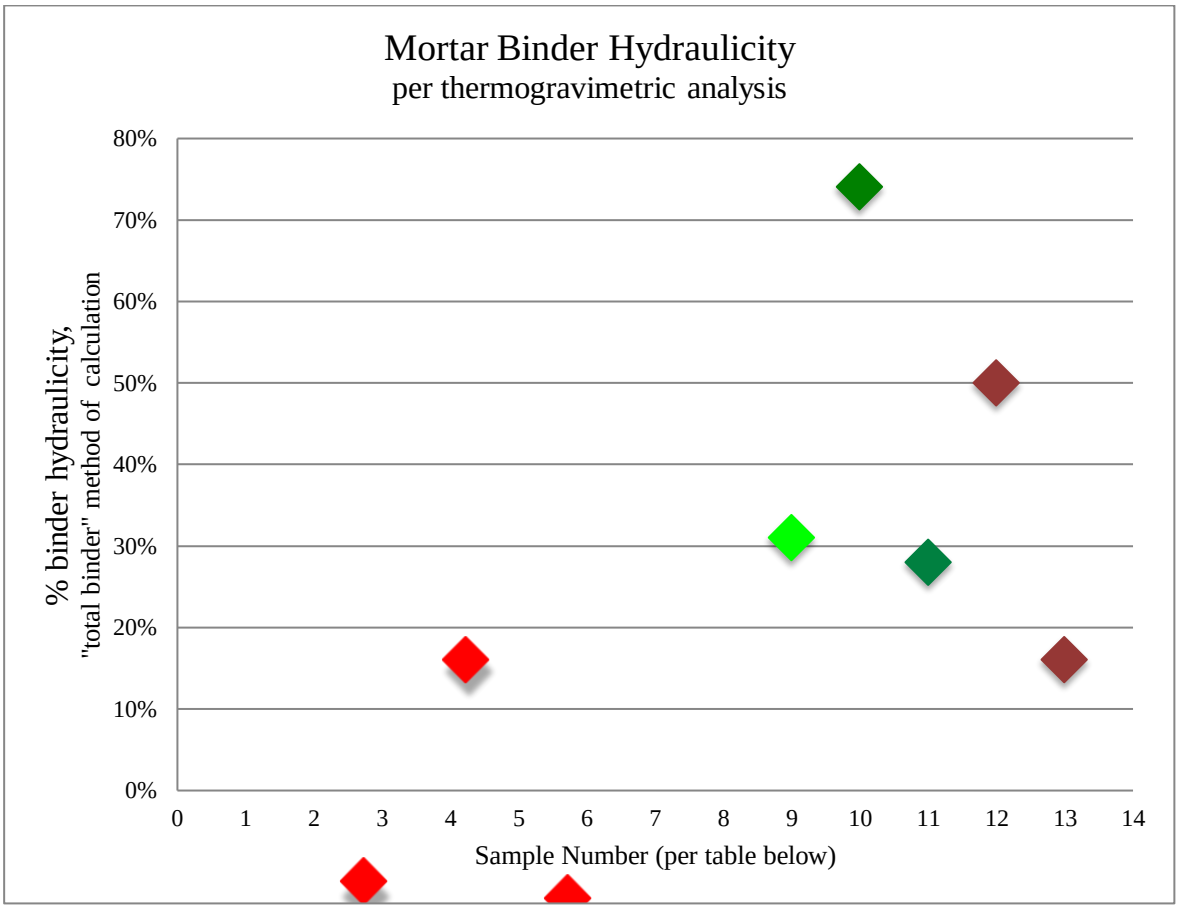


Figure and Table 6.13: Scatter Chart of percentage weight loss in bound water in the binder of a selection of experimental and archeological mortars. "Total Binder" Calculation Method, Sample numbers correspond with table below (right column). Red shades – ceramic pozzolan, green shades volcanic pozzolan.

Sample Number: Name	Description	Bound H_2O: CO_2 (Moropolou method)	Bound H_2O: CO_2 Total binder method
Experimental Mortar			
1: Ton-03	Ceramic-Lime Mortar, Field	25.5%	24.2%
2: Ton-04	Ceramic-Lime Mortar, Field	38.5	42.5%
3: Ton-06	Ceramic-Lime Mortar, Field	18.9%	22.9%
4: 2-9	Ceramic-Lime Mortar, Lab	7.8%	6.0%
5: 2-7	Ceramic-Lime Mortar, Lab	6.9%	10.3%
6: 1-9	Ceramic-Lime Mortar, Lab	11.1%	9.0%
7: Ton-05	Ceramic-Lime Mortar, Field	10.5%	12.0%
8: 1-7	Ceramic-Lime Mortar, Lab	16.7%	14.1%
9: P-K	(Volcanic) Pozzolana-Lime Mortar, Lab	21.5%	17.0%
Archeological Mortar			
10: Pozzolana-Lime, Caesarea	(Volcanic) Pozzolana-Lime Mortar	64.0%	74.0%
11: Pozzalana-Lime, Ostia	(Volcanic) Pozzolana-Lime Mortar	**40.1%**	**28.0%**
12: Ceramic-Lime, Aquincum	Ceramic-Lime Mortar	**17.0%**	**50.0%**
13: Ceramic-Lime, Školarice	Ceramic-Lime Mortar	19.8%	16.0%

other methods, and the literature [57-65, 77, 95,96]. This said, correlations could be made between the thermogravimetric and image-based results, as discussed in Chapter 8.

Both chemical dissolution and thermogravimetric analysis are powerful tools for the analysis of mortar and other cementitious materials. They can gravimetrically quantify binder to aggregate ratio, as well as different types of hydrate in a binder with great accuracy. However, they cannot locate where these materials are within the structure of a mortar, which can be the key to understanding the mortar's history and performance. For this it is necessary to turn to image-based analytical methods. While image-based methods typically are thought of as being able to perform qualitative, but not quantitative analysis, the following chapter shows that they can in fact do both when combined with image-analyzing software.

7.0 Results: Mortar Characterization through Comprehensive Image-Based Analytical Protocol

This chapter displays the results that were achieved through the application of the comprehensive, image-based analytical protocol described in Chapter 5. They are meant to illustrate that the protocol is the most effective way of studying mortar: not only can the maximum amount of information be extracted by the study of petrographic thin sections, but the sample is additionally preserved for future study. The sections that follow give examples of when the entire, comprehensive protocol is the most effective tool to qualifying or quantifying with the highest degree of certainty several important characteristics of the mortars analyzed. Sections 7.1 and 7.2 deal with the identification and characterization of lime lumps and evidence of pozzolanicity (reaction rims on aggregates), respectively. Together, studying these two mortar constituents can reveal the extent and source of binder hydraulicity, whether it is from pozzolanicity or not. The other three sections deal with the entire mortars, with Section 7.4 giving results for evaluating binder to aggregate ratio by image analysis (which does not require the use of FTIR and hence does not employ the entire protocol), and Sections 7.5 and 7.6, which deal respectively with characterizing the binder matrix and its alteration phenomena and quantifying its hydraulic content. In Chapter 8, these results will be compared with those in Chapter 6, demonstrating the great utility of the image-based protocol.

	Analytical Method				
Mortar Characterization Goal	OM/PLM	SEM	EDX	FTIR	Image Analysis
Aggregate Characterization	✓	✓	✓	ø	ø
B:A Ratio –Section 7.4	✓	ø	ø	ø	✓
Binder Characterization through lime lump Analysis	**Comprehensive Image Analysis – Section 7.1**				
Cracks and Porosity	✓	✓	ø	ø	ø
Detecting Pozzolanicity through Reaction Rim Characterization	**Comprehensive Image Analysis – Section 7.2**				
Binder Alteration Phenomena	**Comprehensive Image Analysis – Section 7.5**				
Binder Matrix Density	✓	✓	ø	ø	✓
Binder Matrix Hydraulicity Characterization by FTIR imaging	**Comprehensive Image Analysis – Section 7.6**				

Table 7.1: Mortar Analysis Goals and those achieved by Comprehensive Image Analysis

7.1 Binder Characterization through lime lump Analysis

Perhaps the most important questions in studying any mortar or cementitious system revolve around the origin and condition of the binder, i.e., what makes the mortar turn into a solid mass rather than a collection of aggregates. For the purposes of this work studying Roman-era mortar and experimental samples emulating them, this means the study of lime lumps, relics from the process of burning calcareous stone, slaking the resulting quicklime and what they say about the binder formed. The study of lime lumps in historical mortar gives insight into the technological level of the society that created the mortar [1, 3, 9, 121, 122, 129, 132-135, 144, 177]; studying the chemistry and morphology of lime lumps in experimental mortar provides a window into the likely appearance and performance of historical mortars, as well as the source material for the quicklime. The key to positively identifying the lime lumps in a mortar is the combination of OM, SEM-EDX and FTIR on a representative sample of lumps to determine their morphology, crystallinity, and often their level of hydration and carbonation. The following two figures demonstrate the use of comprehensive image-based analysis to describe several features in lime lumps from an experimental mortar made in the field from quicklime and ceramic, both of which were made in wood-fired historically inspired kilns, as described in Section 3.1.

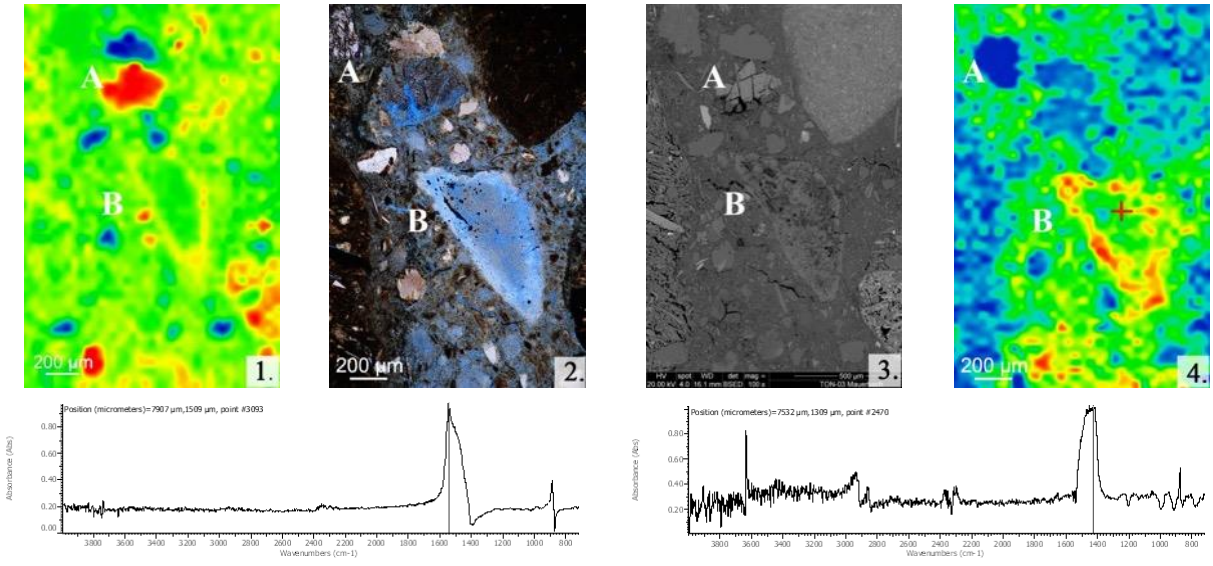
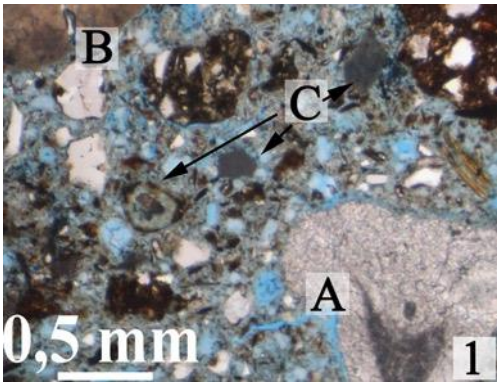


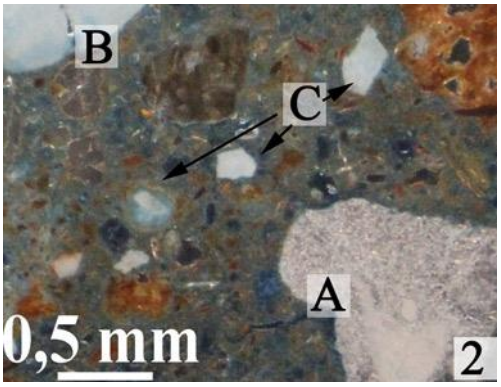
Figure 7.2: Two lime lumps in experimental mortar "Ton-03". A- relict lime clast (unburned limestone) and B – quicklime/ calcium hydroxide lump. **1)** FTIR image created by mapping the density (red – highest to blue lowest) of wavenumber 1396 cm^{-1} (bottom left spectrum – carbonate); **2)** PLM image, transmitted light, plane polars; **3)** SEM-BSE image, the differences in density and crystallinity are evident in the brightness of the greyscale image; **4)** FTIR image created by mapping the density of wavenumber 3436 cm^{-1} wavenumber (water, associated with band 1411 cm^{-1} (aragonite) (spectrum bottom right), indicative of a mixture of $CaCO_3$, CaO and $Ca(OH)_s$.

Figure 7.2 above demonstrates the differences between two different types of lime lump within the same mortar as shown by optical microscopy, SEM and FTIR within a ceramic-silica sand-lime mortar. Lump "A" is the type known as a relic lime clast, that is an underburned piece of the source stone, while lump "B" has a different appearance that is not as easily classifiable. While the PLM and SEM images (center) show the clear structural differences between the two lumps, and EDX proves the high calcium content of lump B, it is the FTIR results that confirm the chemical difference between these lumps. The left FTIR composite image (with spectrum below) shows that while lump "A" is strongly carbonate with the typical spectrum with peaks at wavenumber 1396 cm^{-1} and 896 cm^{-1}, lump "B" is much less so, as shown by the dense red center of lump A and the green center of lump B. Mapping spectra taken from the center of lump "B" (right image and spectrum) show a shifted carbonate band (to 1411 cm^{-1}) with a large amount of "noise" in bound water (-OH) area. Creating an image from the wavenumber 3436 cm^{-1} clearly displays a rim of hydrated product which is generally associated with $Ca(OH)_2$ [152-157 157a, 175]. Thus, it can stated that lump "B" is an "undispersed" lime lump, with a calcium carbonate – calcium oxide core (partially burned and partially slaked limestone) with an outer surface of uncarbonated, hydrated lime that is minimally reactive within the mortar (see also section 7.2.1 below). The presence of this calcium hydroxide in a young mortar that was turned into a polished thin section is not surprising.

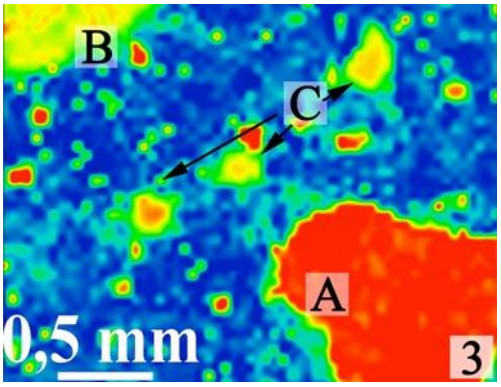
A second example of this type of analysis is given in Figure 7.3 below, which illustrates positively identifying and differentiating the same two types of lime lumps based on maps showing wavenumber shift alone in the same mortar as above. The positive identification not only applies to the two main lumps shown by SM with SEM details (top left images and bottom row), but also to the smaller lumps in between the two, which are not so clearly identifiable by OM. The large relic lime clast in the bottom right-hand corner ("A" in Fig. 7.3 1-4) exhibits the classic FTIR signature for calcium carbonate with a band centered on 1397 cm^{-1}, whereas the one in the top left ("B" in Fig. 7.3 1-4) shows the highest concentration of the band shifted to 1411 cm^{-1} [158]. The crystal structure of each lump is thus likely different, and again it can be inferred that the 2nd (top left) lump, is likely poorly burned, slaked, or dispersed quicklime, some of which has re-crystalized into calcium carbonate (as aragonite). The mapping of the 1411 cm^{-1} band across the entire area shown in the SM images allows the identification of the three smaller central lumps as undispersed lime lumps ("AC" in Fig. 7.3 1-4).



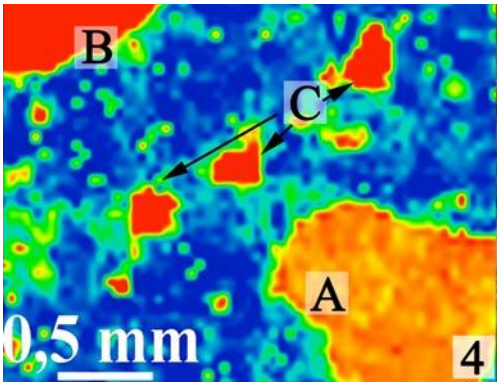
Ton-03 by SM, PPL



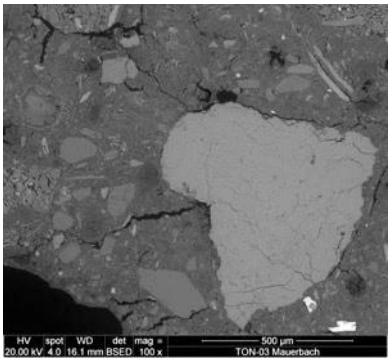
Ton-03 by SM, PPLD



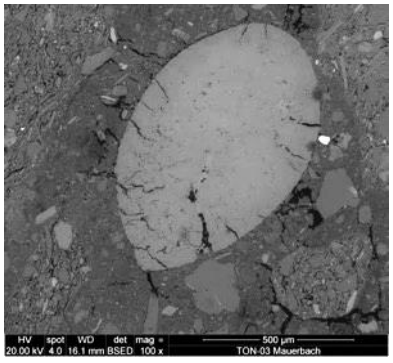
FTIR image of Ton-03,
wave number 1397 cm^{-1} ($CaCO_3$ - calcite)



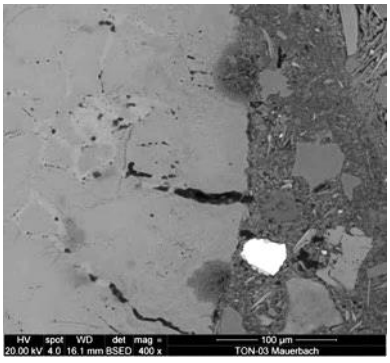
FTIR image of Ton-03,
wave number 1411 cm^{-1} ($CaCO_3$ – aragonite)



SEM of relict lime clast “A”, crystalline unburned limestone, Ton-03



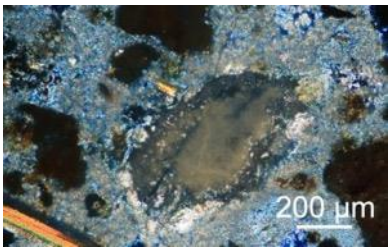
SEM of lime lump “B”, undispersed slaked lime, Ton-03



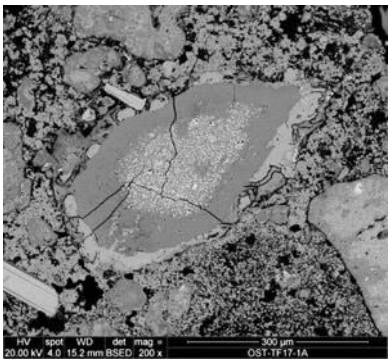
Detail of undispersed slaked lime “B”, Ton-03

Figure 7.3: Two lime lumps in experimental mortar, detection, and imaging by wavenumber shift, description as follows in text.

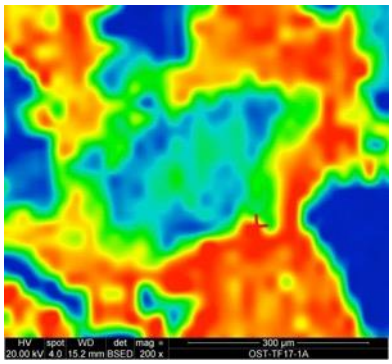
A simpler application of the same principle is shown in Figure 7.4 below, which depicts a part of an archeological mortar from Ostia Antica (“Ost-1a”). Both optical microscopy and SEM-EDX appear to show an object that is a lime lump. The grey-brown appearance of the object that is surrounded by calcite – rich binder shown in the PLM image is typical for an undispersed lime lump. SEM-EDX analysis shows that the bright core of the object is calcium-rich, although confusingly also rich in fluorine.



Ost-1a PLM (XPL) of a lime lump?



Ost-1a SEM of a lime lump?



Ost-1a FTIR image of wavenumber 1425 cm^{-1} (CO_3, likely carbonated binder): not a lime lump, as carbonate is only found outside of the lump in the binder matrix.

Figure 7.4: Using FTIR to correctly identify an object previously characterized as a lime lump.

The FTIR image of the same object, however, shows no presence of carbonate inside of the object. It is in fact a piece of volcanic pozzolana, low in silicate, but rich in fluorite (CaF_2) that is surrounded by reaction product and carbonated binder as part of a pozzolana-lime mortar. The red binder matrix demonstrates a carbonate wavenumber shift to 1425 cm^{-1} (again, likely aragonite), indicating carbonated C(A)SH [1, 30-33]. This example demonstrates the importance of using the wide variety of tools that are part of this protocol when confronted by a question that can only be answered by combining petrography, elemental analysis (EDX) and chemical bonding information. Additionally, it illustrates information that would be completely lost through dissolutive testing.

7.2 Detecting Pozzolanicity through Reaction Rim Characterization

An ancient pozzolanic mortar's defining characteristic is the fact that it has hydraulic properties due to the formation of cement hydrates (C(A)SH) in an interaction between calcium hydroxide and reactive siliceous aggregate [18]. Therefore, it is natural that the study of pozzolanic mortar revolves around the study of reaction rims at the binder-to-aggregate interface. One important goal is the ability to determine if these rims are truly the result of pozzolanicity, or if they were caused by lime-rich water from the binder precipitating in the surface porosity of the aggregate, often called "precipitation rims". It is possible to see both by the naked eye as a color change of a thin portion of the aggregate where it meets the binder, or

as a dark area of the binder where there is a lower concentration of binder matrix (for example in "2-7" in Figure 7.5 below). To obtain further evidence of a reaction, such as the partial dissolution of the aggregate, requires microscopic analysis, done here by applying the image-based protocol.

Using OM and then SEM-EDX is the typical state of the art for the detection and description of reaction rims [29, 79, 141-144, 176]. This can be made more exact using point-by-point EDX measurements, line scans, or EDX mapping which can detect the occurrence and measure the thickness of rims [58, 157A]. What the examples below demonstrate is the novelty of combining OM and SEM with FTIR and image analysis (on both archeological and experimental mortar) to provide further detail of the physical and chemical nature of such rims, (previously advanced by this author [1, 128]). Using the protocol allows for the discrimination between precipitation rims and true reaction rims. While microscopy (OM and SEM) can examine the aggregate's physical condition, and EDX and determine if both calcium and silica (and alumina) are in a rim, FTIR is then used to detect if silica, carbonate, and hydroxyl bonds are present and co-molecular, indicating the presence of C(A)SH.

Figure 7.5 below gives examples of the application of comprehensive image-based analysis being used to study the reaction rims on three types of mortar produced in the laboratory, made from two types of ceramic ("1-9" and "2-7") as well as volcanic pozzolana ("P-K"). Two different FTIR methods were used to make the reaction products visible, one of which focused on the detection of interlayer bound water (-OH stretching ~ 1600 cm^{-1}) and the other that combines the peak density of co-molecular carbonate (~ 1400 cm^{-1}) and silicate (~ 995 cm^{-1}) [152-157A]. The first example, 1-9 shows a SM and SEM image of a piece of reactive ceramic that was fired at 950 °C from calcium-free clay. It was first considered as (potentially) reactive by the darker "halo" in the binder surrounding the aggregate and the fact that it has partially detached from the binder matrix, both indicative of a change in binder density and composition. FTIR imaging of the area allowed for the confirmation of pozzolanic activity, by the detection of the Si-O stretching vibration associated with C(A)SH mentioned above. This image was then fitted to the SEM image by setting them to the same scale, creating map of the reactive aggregate. The highest density of C(A)SH can then be shown to be just at the surface "rim" of the ceramic (Figure 7.5 top row).

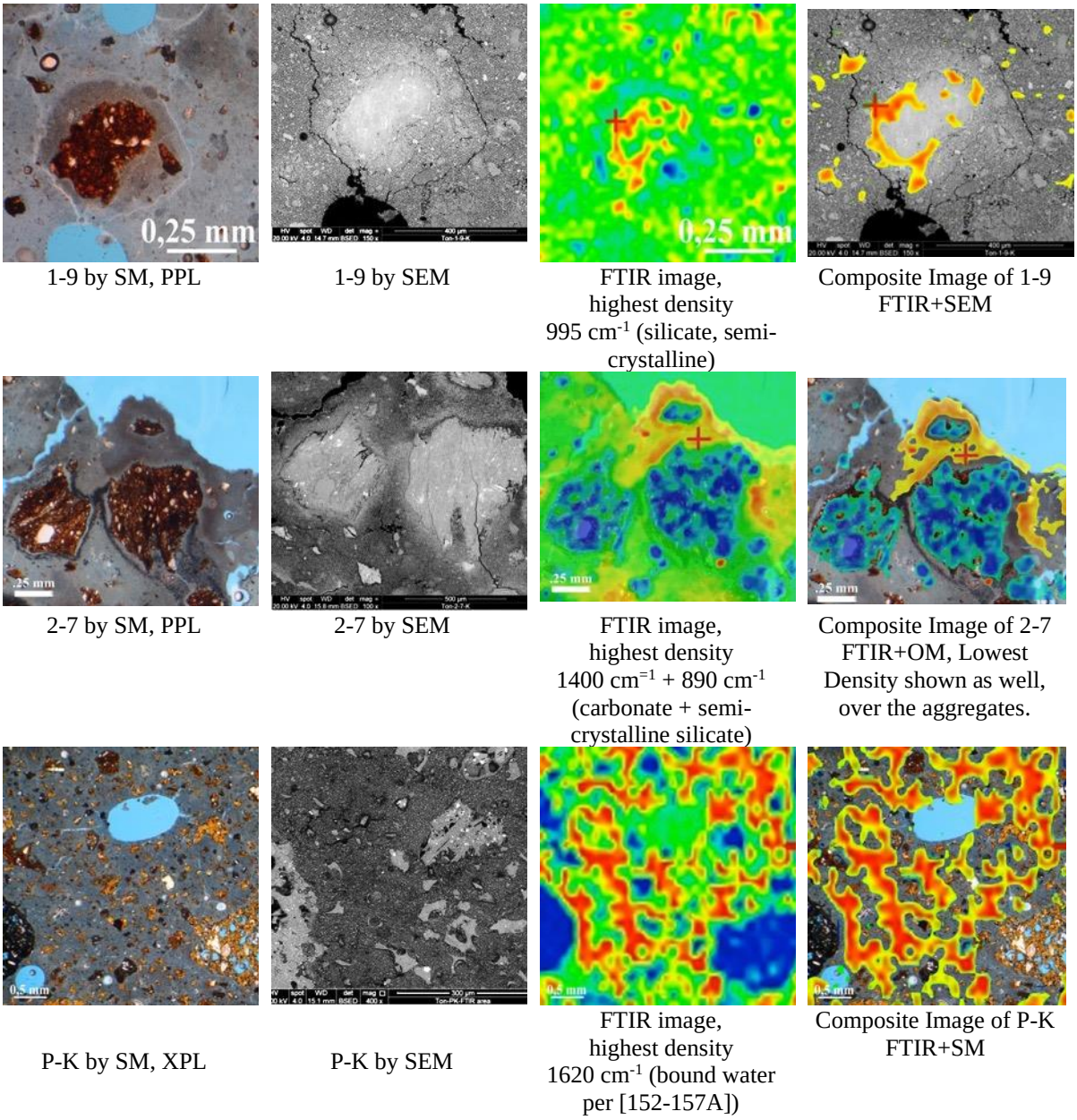


Figure 7.5: Reaction Rims in experimental mortar.

Top Row: Investigation of a ceramic aggregate featuring a "cloudy" feature in the surrounding binder matrix, seen by SM and SEM. FTIR mapping of the 995 cm^{-1} band associated with silicate stretching in CASH seems to show a reaction rim, which can be seen in the FTIR-SEM overlay image at right.
Middle Row: A group of ceramic aggregates with differential binder density visible in both PLM and SEM; FTIR imaging combined with the composite image in the right two images locate carbonate (1400 cm^{-1}) and silicate (890 cm^{-1}) bands in the area of the binder beyond the rims, an area of pozzolanic activity.
Bottom Row: An experimental volcanic pozzolana mortar that does not show clear reaction rim by stereomicroscopy or SEM, but in which FTIR imaging of the intermolecular bound water found in C(A)SH (at around 1600-20 cm^{-1} shows that it is prevalent (red – high density) in the binder matrix, associated with very fine pieces of aggregate.

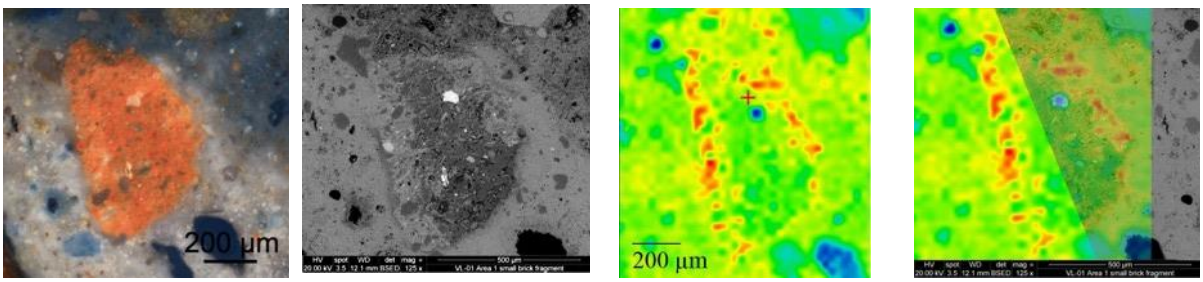
The area of the binder just outside the aggregate is in fact quite poor in these compounds, which would seem to indicate that the lime-rich water from the binder matrix infiltrated the ceramic's

pore structure, which in turn contained both the requisite material and a place in which a dense amount of C(A)SH could form (and be detected).

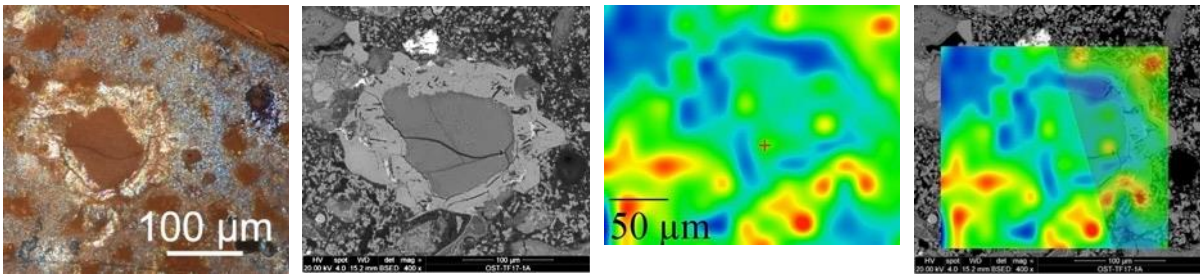
The middle row in Figure 7.5 shows "2-7", which used ceramic made from calcium-rich clay fired at 750 °C as the aggregate. OM and SEM imagery seems to indicate that the two ceramic fragments featured had reaction rims, indicating the presence of C(A)SH. The dark areas surrounding the aggregates are in fact areas of lower concentration of binder matrix, contrary to the previous example. In this example, the FTIR image represents the highest density of both the peak intensities of both the carbonate band (~ 1400 cm^{-1}) and the silicate band (~ 890 cm^{-1}), overlapped (where both bands occur with the highest intensity). This method was selected because of difficulties detecting the more typical C(A)SH silicate band at 995 cm^{-1}. Silicate stretching is detectable in all samples in a band with wavenumbers from 800-1000 cm^{-1}, after which there are additional bands which are difficult, if not impossible, to differentiate from other silicates, i.e. the aggregate or the glass slide, hence the need to focus on very specific silicate range. The dark areas shown by OM and SEM in fact have a lower concentration of reaction products than the surrounding binder matrix; FTIR showed they were poor in $CaCO_3$ and $Ca(OH)_2$ as well. The binder area beyond these calcium-poor regions appears to be most rich in C(A)SH, particularly between the smaller aggregate towards the top of the image and the middle aggregate. It is of note that the C(A)SH seems to have formed preferentially within the binder, away from the aggregate, perhaps resulting in this mortar's relatively low strength (discussed in the previous chapter).

In the final example ("P-K" Figure 7.5, bottom row), that shows mortar made from ground volcanic pozzolana and lime, there are no reaction rims on the aggregate clearly identifiable by OM or SEM. Strength values for this mortar are consistently higher than any of the mortars made with ceramic aggregate (see Figure 6.6 and Table 6.7 above), indicating that the aggregate is clearly reactive. FTIR imaging holds the key to understanding this. In this case the often difficult to detect bound water in C(A)SH (1620 cm^{-1}) is easily visualized by FTIR. Combining the imaging result with the SM micrograph allows for the localization of the C(A)SH thus detected, showing it heavily concentrated just outside the aggregates in the binder matrix, and likely interconnected throughout the matrix leading to high strength.

The lessons learned from using this method on experimental mortar can then be applied to the analysis of historical mortar. Figure 7.6 below shows the application of the image-based protocol on an ancient ceramic-lime ("VL-01") and a pozzolana-lime ("OST-1a") mortar to analyze reaction rims



VL-01 by PLM, ILXP Ceramic pozzolan | VL-01 by SEM | FTIR image, highest density 1400 cm^{-1} + 890 cm^{-1} | Composite Image of VL01 FTIR+SEM



OST-1a by PLM, ILXP Volcanic pozzolana, largely vitreous | OST1a by SEM | FTIR image, highest density 1400 cm^{-1} + 890 cm^{-1} | Composite Image of Ost-1a FTIR+SEM

Figure 7.6: Reaction Rims in ancient mortar. Methods as noted, displaying similar locations of pozzolanicity as described in the experimental samples in 7.5 above, i.e., at the rim for the ceramic aggregate, in the matrix beyond the rim for the volcanic aggregate.
Top: Ceramic Pozzolan – lime mortar from Vindbona, 1st Century A.D.
Bottom – Volcanic Pozzolan – lime mortar from Ostia, 2nd Century A.D.
Both image sets previously published in (Baragona 2019[128])

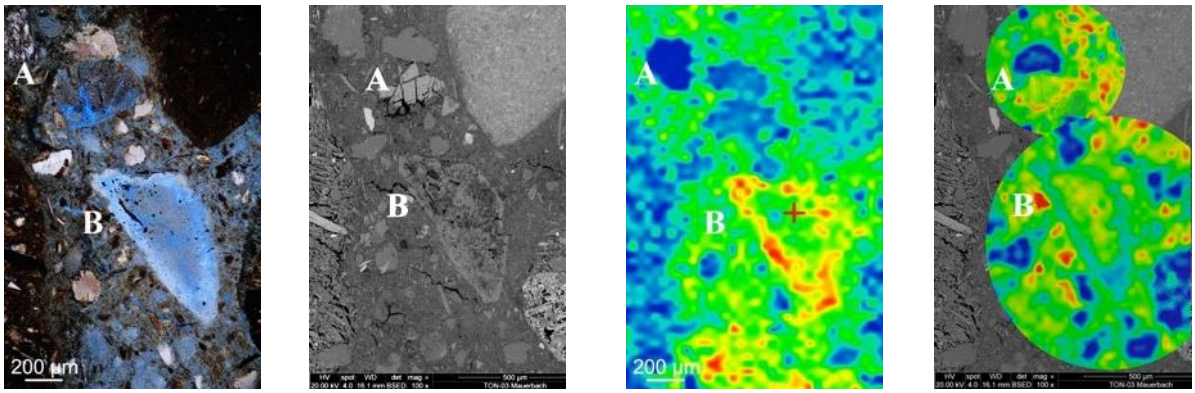
In both cases, an aggregate with a reaction rim visible by OM and SEM was further analyzed by the application of FTIR imaging. Maps were created by combining the FTIR image for the combination of the peak concentration of the overlap between wavenumbers 1400 cm^{-1} (carbonate) and 890 cm^{-1} silicate) and scaling and overlaying these images to fit the SEM image taken of each aggregate. These bands were chosen because of the difficulties in discovering bound water, which in an ancient mortar may no longer be present in large quantities due to binder alteration.

The results are strikingly similar to those found for the experimental mortar. C(A)SH appears to be localized directly at a semi-dissolved border area in the case of the ceramic pozzolan mortar from Vindobona, while it is more prevalent in the binder matrix of the volcanic pozzolana mortar (away from the glassy core of the pozzolana). In the example of the volcanic pozzolan, C(A)SH is concentrated in the matrix with a (clearly visible) compact area of calcium carbonate which forms an interstitial interface between the aggregate and the binder, which may indicate a higher density of C(A)SH at the rim which has since carbonated. Whether this translates directly into a more reactive aggregate and thus stronger mortar is not entirely clear.

However, this finding, in combination with the strength testing from the previous chapter appears to confirm much of the literature on the subject, as well as the writings of ancient authors [4, 5, 8, 16, 17, 34, 36] and will be discussed in the Conclusions.

7.2.1 Lime Reaction Rims

Following the same procedure, a very similar phenomenon was observed at the binder to lime lump interface, hereafter referred to as "lime reactions rims". In these instances, large lime lumps are behaving more like the aggregate portion than the binder portion, showing again that line between what is binder or aggregate in a pozzolanic mortar is blurry at best. What is more, they perfectly exemplify the exact type of information that would be lost through mechanical, thermal, or chemical dissolution of the sample material, as they are chemically identical to the binder despite their aggregate-like behavior. Lime reaction rims show that in the case of pozzolan – lime mortar, C(A)SH is formed in any place where there are the requisite chemical building blocks and a place for the minerals to form. Determining whether these compounds form preferentially in these areas or are simply easier to detect goes beyond the scope of this work. This phenomenon was first observed in the experimental mortar samples, with two examples given below in Figure 7.7. Observations on the experimental samples were then instrumental to interpreting what was being discovered within the historical samples, with an illustrative example shown in Figure 7.8 that uses the entire comprehensive protocol to analyze a lime reaction rim in an historical sample.



Ton-03 by PLM, TL

Ton-03 by SEM

FTIR image, highest density 3436 cm^{-1} ($Ca(OH_2)$)

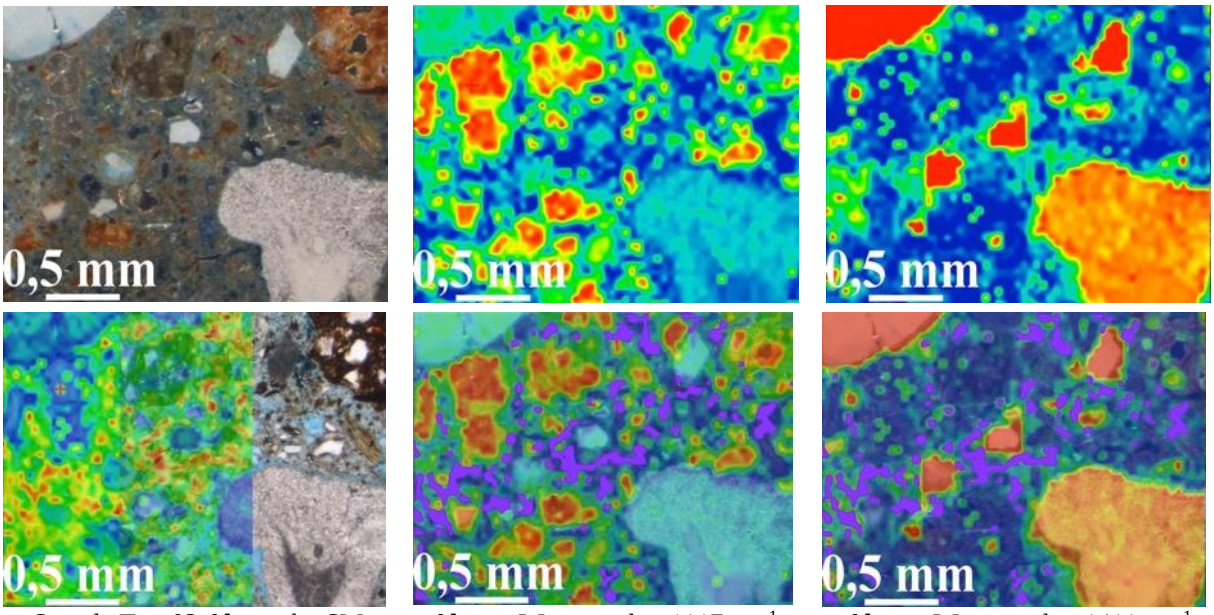
Composite Image of Ton-03 SEM+ FTIR, highest density 1400 cm^{-1} + 890 cm^{-1} (carbonate and silicate)

Figure 7.7: Reaction Rims near lime lumps in experimental mortar. Methods as noted. A "stronger" rim is noticeable around the underburned calcite grain (A) than the undispersed lime lump (B).

The first example (Figure 7.7) re-examines the two lime lumps found in the field-produced ceramic lime mortar, previously examined in Figure 7.2 in Section 7.1. The first three images show the relic lime clast "A" and the partially slaked and undispersed lime lump "B" by optical microscopy, SEM and an FTIR image of the highest density of the –OH band associated with $Ca(OH_2)$, which can be seen forming a distinct ring around lump B. While this indicates that the potential for forming C(A)SH existed at this location, further exploration was needed to determine which exact reactive products were present. Following the same procedure as for reaction rims on aggregates, a point in the FTIR image was located near a reaction rim where a spectrum distinctive of C(A)SH (with peak wavenumbers near the carbonate (1400 cm^{-1}), silicate (850-1000 cm^{-1}) as well as bound water of various types and intensities) were located, indicating likely co-molecularity. In order to confirm that the carbonate and silicate were co-molecular, an overlap image for 1400 cm^{-1} and 890 cm^{-1} was produced, and this highest intensity image was scaled and overlapped with the SEM image, shown in the fourth image. While pores (epoxy and amorphous silicate – glass slide) and crystalline silicate aggregates (quartz) read as dark blue (lowest concentration), the red regions showing the highest concentration cluster around a large ceramic aggregate (top right) *and* cluster around the relic lime clast A. Although (perhaps because of) the highest concentration of calcium hydroxide is around lump B, the highest concentration of C(A)SH is found elsewhere in this example.

The second example, depicted in Figure 7.8 below, is from a different region of the same sample, also first introduced in Section 7.1. The image features both types of lime lumps, the largest relic clast in the bottom right and the largest undispersed lump in the top left, with a variety of smaller lumps in between as well as both pure silicate and varying grades of ceramic aggregate throughout. In all, images from three different bands were considered: first the 995 cm^{-1} C(A)SH silicate band (composite image bottom left), secondly, ceramic fines were identified by creating an image of the 1117 cm^{-1} wavenumber (top middle) and the third image was made from the carbonate band centered on 1411 cm^{-1} (top right), which displays both types of lime lumps, with the less crystalline undispersed ones showing up in solid red. For this analysis, the higher densities of the C(A)SH silicate band were overlapped with both the previously located ceramic fines and lime lumps, resulting in the in the composite images in the bottom row, center and right. Colored purple, these areas of intense C(A)SH development appear more localized near the lime lumps, rather than the ceramic grains, underscoring the point made above, that perhaps this environment is more conducive of C(A)SH development. In other words, the highest density of C(A)SH, shown in red in the bottom left image and purple

in the bottom center and right images, shows a higher concentration near the small lime lumps in the center of the image, than the small pieces of aggregate on either side.



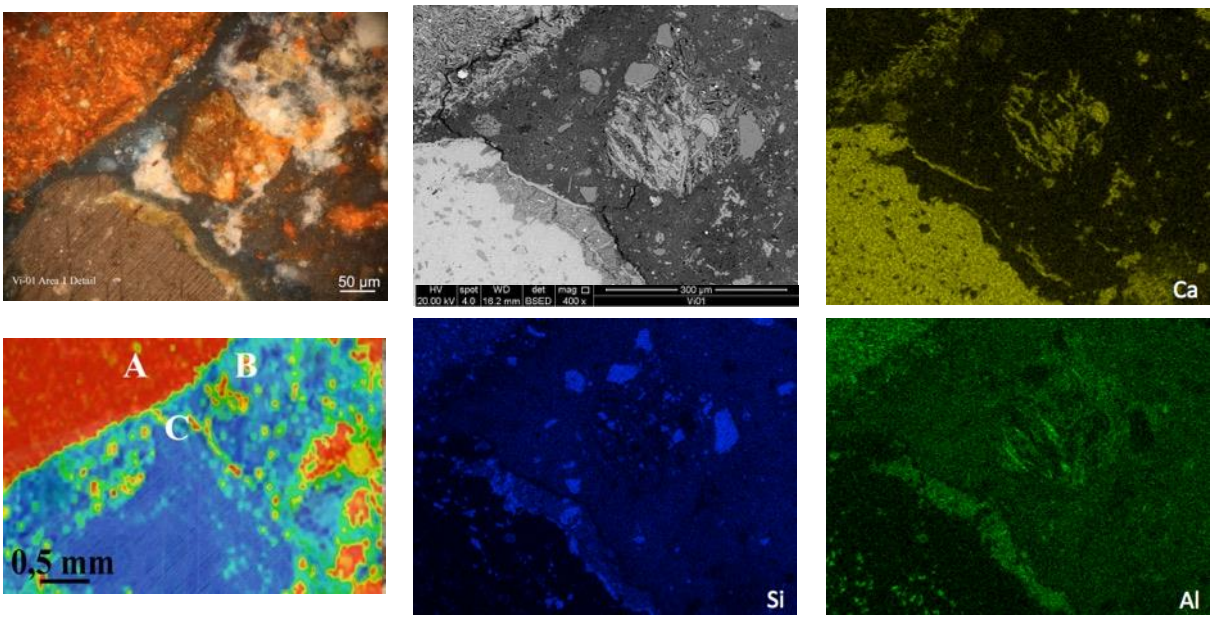
Sample Ton-03 **Above**: by SM, PPLD
Below: Composite Image of SM and FTIR for Si-O 995 cm^{-1}

Above: Wavenumber 1117 cm^{-1} associated with ceramic fines
Below: Location of wavenumber 995 cm^{-1} (purple) relative to 1117 cm^{-1} from above.

Above: Wavenumber 1411 cm^{-1} associated with lime lumps
Below: Location of wavenumber 995 cm^{-1} (purple) relative to 1411 cm^{-1} from above.

Figure 7.8: Reaction Rims preferentially near lime lumps relative to ceramic grains in experimental mortar; the purple areas in the bottom right two images show that there is a closer association of the silicate stretching band associate with C(A)SH (995 cm^{-1}) with lime lumps (bottom right composite image) than ceramic grains (bottom center composite image).

The last example, depicted in Figure 7.9 below, uses the method described above to describe a similar phenomenon in an historical ceramic – lime mortar, in this case with supplementary imaging provided by EDX mapping. OM (Figure 7.9, top left) revealed what appeared to be a reactive ceramic aggregate (center) surrounded by altered, two-tone binder. The large calcite relic bottom left also clearly displayed a rim, but of uncertain composition. In this case, both SEM-EDX mapping and FTIR imaging could be employed in order to characterize this part of the sample, with the EDX mapping in fact being used after the FTIR. A FTIR image of the peak density of the 995 cm^{-1} band was again made and overlapped with the OM image (bottom left). Although this indeed shows silicate located at the rim of the calcite grain ("C"), the same band is present both the original reacting ceramic ("B") and seems to compromise the entirety of a larger ceramic "A". FTIR results in this case are somewhat inconclusive.



Vi-01 Aqueduct Vindobona
Above: by PLM, ILXP
Below: FTIR map of silicate: a broad band around 995 cm^{1}.

Vi-01 Aqueduct Vindobona
Clockwise from Top Left: SEM image showing reaction rims on both a ceramic aggregate and a lime lump; EDX map of Calcium; EDX map of Aluminum; EDX map of Silicon

Figure 7.9: Reaction Rims on large calcite grain, ceramic – lime mortar from the lining of a Roman aqueduct

EDX mapping is generally more time intensive and does not provide a similar ability to detect compounds and polymorphs as FTIR does but does have enhanced imaging capabilities of its own. SEM-EDX shows the central aggregate has indeed dissolved with calcium penetrating it completely and the large ceramic piece shows a concentration of calcium on both sides of a piece that has broken off from the main body, perhaps providing enough space for C(A)SH to be produced and detected throughout the part visible, hence the previously mentioned FTIR results. Most remarkable is the visualization/ detection of what has occurred at the rim of the calcite. The SEM image and the detection of calcium shows that a thin piece has broken off from the main body, similarly to the large ceramic above. In this case the EDX mapping shows why: both silica and alumina are shown to be heavily present in the rim indicating expansive growth of C(A)SH in this area, that by chance happens to show the crystalline structure of C(A)SH in cross-section. This example of a lime reaction rim reinforces the need to utilize the entire compliment of image-based techniques described within this work when describing particularly complex phenomena within historical mortar.

7.3 Binder Matrix and Mortar Characterization - Overview

Moving from characterization of the lime and aggregates used, and how they interacted to form a pozzolanic mortar, the next step involves methods that characterize the entire binder. While studying reaction rims gives an idea of *if* a mortar can be considered pozzolanic, the next step of describing *how pozzolanic a mortar is,* requires the study of its binder. Since it is indeed the binder that is used to classify a mortar, the study of not just how it came to be formed, but also how it has changed over time, how much of a mortar is binder, and what makes up the binder are of utmost importance. Hence the final three sections of results below focus on using image-based methods to describe a mortar's binder.

Alteration phenomena, while not present in the fresh experimental samples, hold the key to understanding the "life story" of an archeological or historical mortar. They can be detected, identified and both qualified and quantified by the comprehensive image-based protocol, as is shown in Section 7.4. Calculating the binder-to-aggregate ratio gives clues to the intent of the builders as well as the performance that can be expected of a mortar, both historically and as it ages. While the determination of binder to aggregate ratio (b:a) is often done gravimetrically, image-editing software allows for relatively fast pseudo-color image editing that can then utilize pixel counting to provide a volumetric binder-to-aggregate ratio.[24] This provides for an interesting comparison to historical mortar recipes, which were also generally formulated volumetrically. The results of this application of imaging to understanding a mortar are given in Section 7.5. Finally, determining the level of pozzolanicity (hence hydraulicity) requires the quantification of the cement hydrates within a binder system. This is generally quantified and referred to as a "hydraulicity index". While this is often performed by chemical and thermal dissolution giving gravimetric results, proposed herein is a means for the volumetric quantification of these materials by utilizing FTIR-imaging and image analysis software, and is the subject of Section 7.6, and its efficacy is discussed in the Conclusions (Chapter 8).

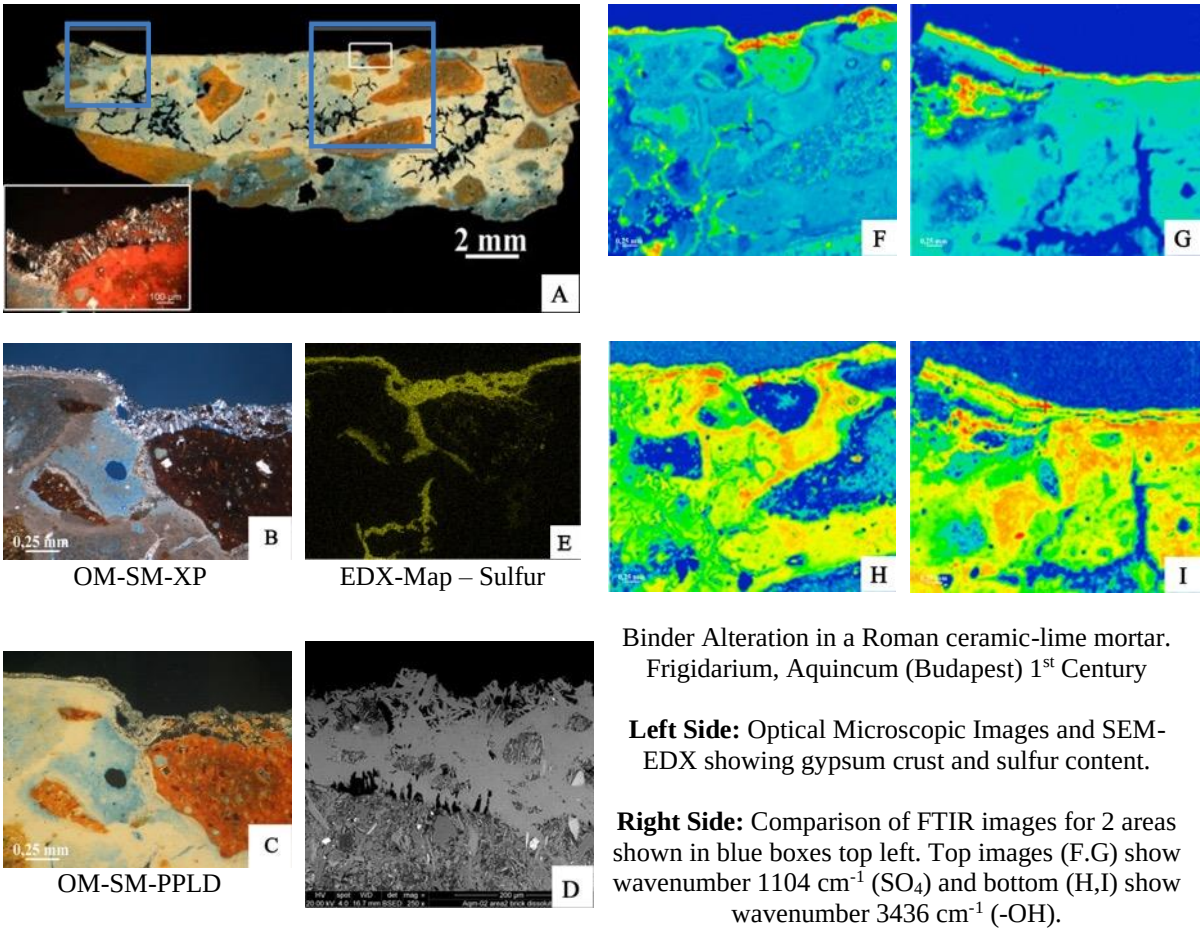
7.4 Binder Alteration Phenomena

For the great majority of the archeological mortars studied, the fabric of the mortar and the binder is greatly altered from how it would have been in historical times. Part of the rationale behind the production of experimental mortars was to help with the identification of true

[24] Both methods were performed for this work; how comparable they are is discussed in the Conclusions.

alteration phenomena (by their absence) and to locate in which part of a fresh mortar the alteration products are likely to occur. The study of binder alteration also serves a very important practical role from a preservation/conservation perspective in that it can identify and locate potentially damaging alteration products, the first step in their mitigation. The first two examples shown below deal with the potentially damaging sulfate-hydrate products, gypsum ($Ca_2SO_4 \cdot 2H_2O$) and ettringite ($Ca_6Al_2(SO_4)_3(OH)_{12} \cdot 26H_2O$), which can be either primary or secondary (alteration) products in historical mortars. One example is given from a ceramic - lime pozzolanic mortar and another from a volcanic pozzolana-lime mortar. The third example examines an alteration process observed in ancient pozzolanic mortars – the separation of a hydraulic binder where C(A)SH was the main cementing product into a binder matrix that appears to consist of a patchwork of calcium carbonate and silica gel [9, 13, 21, 144, 177, 178]. In each case, it was the combination of all parts of the comprehensive image-based protocol that led to the most complete understanding of the observed binder alteration products.

Figure 7.10 below shows a heavily altered ceramic-lime mortar from a Roman archeological site in Budapest, Hungary. Optical microscopy shows both a two-tone binder matrix (in this case likely due to a carbonation front) as well as a weathering crust. Both stereomicroscope and polarizing light microscope images (inset on larger scale image top left) clearly show that crust exhibits the distinctive interference colors typical of gypsum in cross-polarized light. To search for the presence of this compound throughout the sample, both FTIR imaging and EDX mapping (two blue boxes and small white box, respectively on SM image 7.5A) were used. These methods were also employed to determine if the sulfate forming the gypsum was of recent or original, that is if the gypsum had re-crystalized from ettringite that had formed throughout the sample during the hydration of the binder, or if it appeared later as a weathering product in modern times. In other words, EDX and FTIR were used to find out whether the alteration product was forming *at* the surface, or from the inside *to* the surface. EDX mapping of the sulfur content of the sample (central image) showed that whichever sulfurous material was in the sample was almost totally confined to the surface and cracking originating at the surface. This was corroborated by FTIR imaging of both the sulfate and bound water bands of gypsum throughout two regions of the sample, shown in images G and I in Figure 7.5. Bound water is found throughout the binder (Figure 7.10, H,I), most heavily present in the binder areas closer to the aggregates.



Binder Alteration in a Roman ceramic-lime mortar. Frigidarium, Aquincum (Budapest) 1st Century

Left Side: Optical Microscopic Images and SEM-EDX showing gypsum crust and sulfur content.

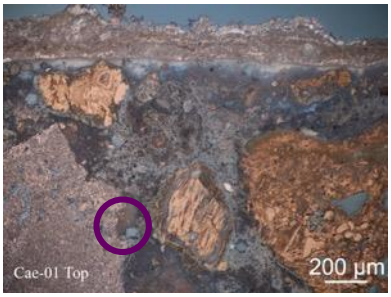
Right Side: Comparison of FTIR images for 2 areas shown in blue boxes top left. Top images (F.G) show wavenumber 1104 cm^{-1} (SO_4) and bottom (H,I) show wavenumber 3436 cm^{-1} (-OH).

Figure 7.10: Binder Alteration on a ceramic lime mortar. While hydrated compounds are found throughout the mortar (red and orange areas of the middle FTIR images showing hydroxyl density), sulfate is found predominately at the surface (top FTIR images).

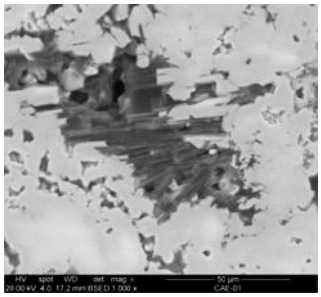
The higher percentages of sulfate are only found in the crust (Figure 7.10 F,G). The presence of sulfate (-SO_4) mostly at the surface indicates that the gypsum is likely of recent provenance, and that little to no gypsum has formed deeper in the mortar, despite the presence of bound water (-OH) throughout. This indicates that the bound water is typically integral to C(A)SH and not gypsum. C(A)SH. Had ettringite been an original component of the binder of the mortar when formed, both sulfate and bound water would have been present in much greater proportions than detected throughout the sample; this result would have also been evidence of the sample being replacement mortar that used Portland cement.

Figure 7.11 below shows binder alteration in a volcanic pozzolana – lime mortar from the site of Caesarea Maritima, Israel. Optical microscopy was used for the initial description of the sample, which exhibits binder inhomogeneity with bright patches and glassy dark patches and a carbonate crust - the deposition of calcium carbonate that has dissolved out of the binder and precipitated on the surface. While studying the reaction rim of the central piece of pozzolana

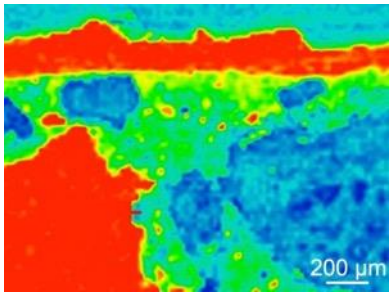
with SEM, an interesting formation of crystals was found in the pore space of the large relic lime clast (top center, purple circle on OM image) that warranted further investigation.



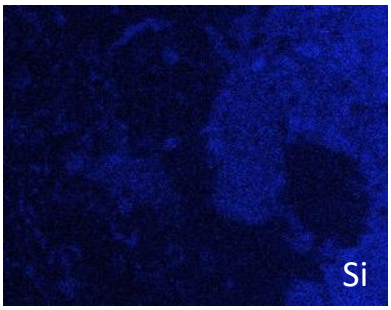
Cae-01: Roman pozzolana-lime mortar, Caesarea Maritima 1st century A.D. PLM-PPL.



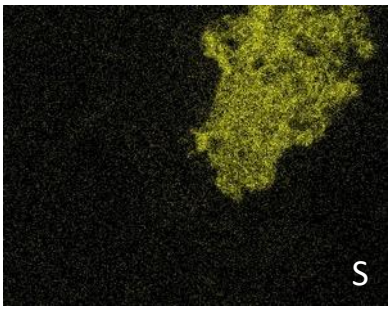
Cae-01 SEM detail of hydrate phases at rim of calcite (purple circle left)



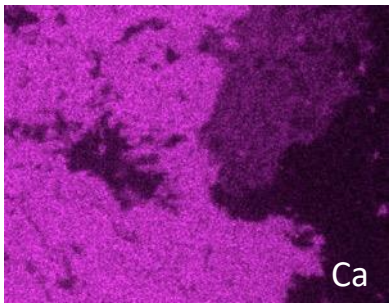
FTIR image of carbonate at wavenumber 1397 cm^{-1} (calcite)



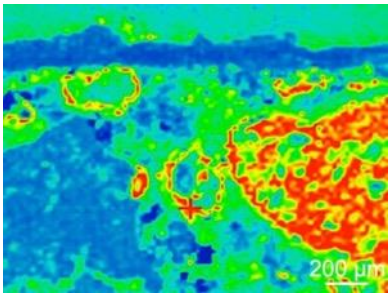
EDX-Map – Silicon (purple circle)



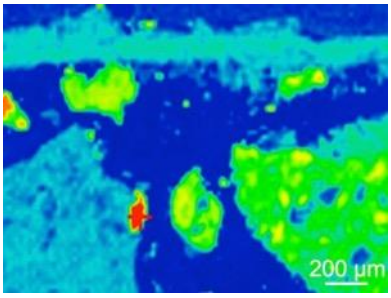
EDX-Map – Sulfur (purple circle)



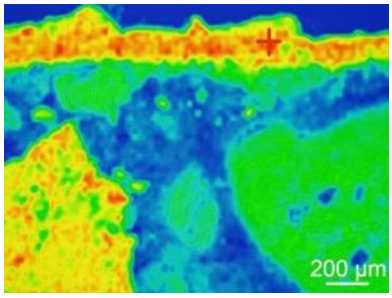
EDX-Map - Calcium (purple circle)



FTIR image of silicate wavenumber 995 cm^{-1} (semi-crystalline, CASH)



FTIR image of sulfate wavenumber 1124 cm^{-1} (ettringite – likely primary)



FTIR image of carbonate at wavenumber 1433 cm^{-1} (aragonite - secondary)

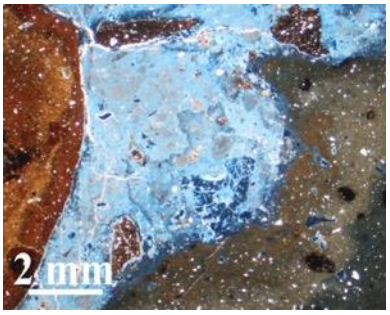
Figure 7.11: Binder Alteration on a pozzolana - lime mortar, ettringite (center three images and EDX maps) and secondary $CaCO_3$ - aragonite.

The area was then examined through EDX mapping to investigate this clump of crystals further, as the displayed morphology does not necessarily preclude calcite. The map of silicon shows both the silica-rich nature of the binder both inside and outside of the relict lime clast, while a large amount of sulfur is found only outside of the clast (Figure 7.11 center row). The lack of sulfur inside the clast points to the formation of the silica-rich area as being primary and the sulfur rich area being secondary (and as shown by the FTIR results that follow, not

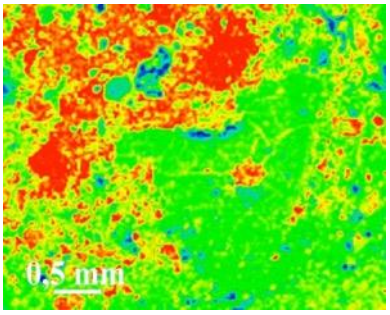
prevalent); therefore, this can be seen as an example of a "lime reaction rim" where C(A)SH has formed. It is likely that the position of the C(A)SH protected it from alteration and thus facilitating its detection. FTIR imaging was performed on the equivalent area as the photomicrograph to complete the analysis by providing identification and distribution of compounds throughout the sample. Two types of carbonates were mapped by highlighting the two peaks found in the carbonate band of spectra found in both the relict lime clast and the carbonate crust (1397 cm^{-1} and 1433 cm^{-1}; Figure 7.11 top and bottom right). From this, two things are striking. Firstly, both calcite and aragonite, polymorphs of calcium carbonate, are distributed throughout the sample, although with a much higher concentration of the 1433 cm^{-1} in the surface deposit. This wavenumber peak is typical of aragonite, an alteration product of C(A)SH as it ages [158]. Secondly, the sample shows large areas of binder that contain little to no carbonate. This points to the near complete alteration of the binder into Ca-poor areas with silica gel and (perhaps) magnesium silicates. It is possible the magnesium content is attributable to the use of seawater in slaking the quicklime used to make this mortar [4,5]. This image made from the often-discussed 995 cm^{-1} silicate band indicates that C(A)SH is still present in the reaction rims of the pozzolana, including the one that the original focus of interest. Finally, the overlap of the sulfate and silicate bands (bottom 2 images from the left) shows only localized distribution of ettringite, i.e., that it is not an original part of the binder system.

In the last example, shown in Figure 7.12 below, the topic of the dissolution of C(A)SH into calcite-aragonite regions and silica gel regions is examined more closely. The sample shows a 2nd Century Roman floor mortar made from ceramic and lime, where mostly only larger fragments of ceramic are clearly visible. Despite this, OM and SEM-EDX examination shows evidence (high silica content of the binder, gel-like areas) of a highly hydraulic mortar making it likely the fine siliceous aggregate has mostly dissolved over time. The center of the large-scale OM image displayed a rather dramatic example of binder alteration in a large, cracked area that was glassy in appearance (left side images). That this was sort of binder alteration product seemed highly likely; the challenge was in identifying the nature of the product. This seemed particularly true since EDX point analysis showed that many areas of the mortar to be highly enriched in magnesium. Both EDX mapping and FTIR imaging were employed to further explore this phenomenon. FTIR imaging (Figure 4.28, top center) clearly showed the lack of carbonate in the gel-like area, whereas the determination of the nature of this silicate gel was less apparent. The inability to detect any type of bound water points to the determination that cement hydrates were not present, though this does not mean that they were *never* present.

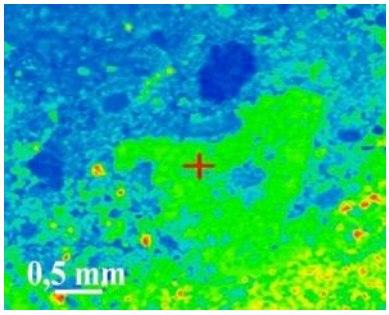
EDX mapping was similarly inconclusive; the gel area was shown to be silicon and magnesium rich and calcium poor.



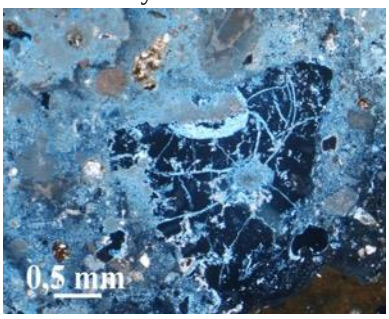
Sko-239: Roman ceramic – lime mortar, Školarice, Slovenia 2nd century A.D. SM-XPL



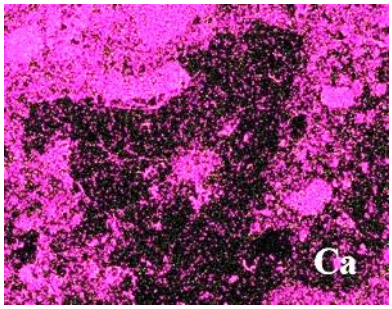
FTIR image of carbonate at wavenumber 1433 cm^{-1} (aragonite - secondary)



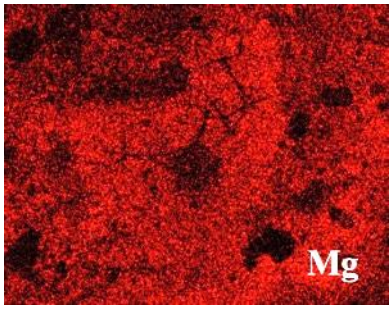
FTIR image of silicate wavenumber 1050 cm^{-1} (gel-like to semi-crystalline).



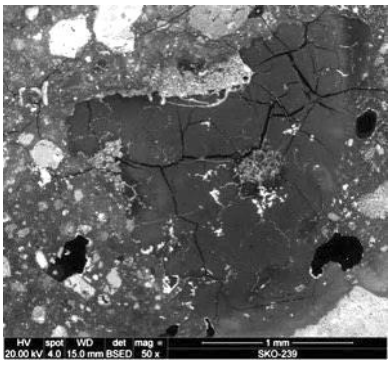
Detail of gel area near center of above. SM-XPL



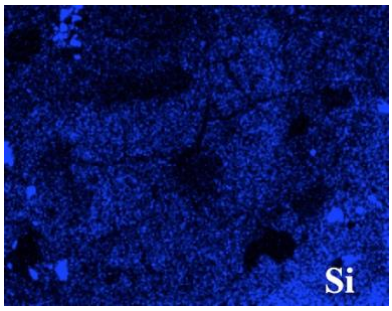
EDX-Map – Calcium



EDX-Map – Magnesium



SEM image of Mg.-Si gel with Ca in pores, cracks and periphery.



EDX-Map – Silicon

Binder Alteration in a Roman ceramic-lime mortar.
Opus Caementitium, Školarice Slovenia

Binder has altered into areas of Magnesium rich gel (possibly Mg-S-H) and Calcium and Magnesium Carbonate

Figure 7.12: Binder Alteration on a ceramic lime mortar, binder separation into silica gel and Mg, Ca – CO_3

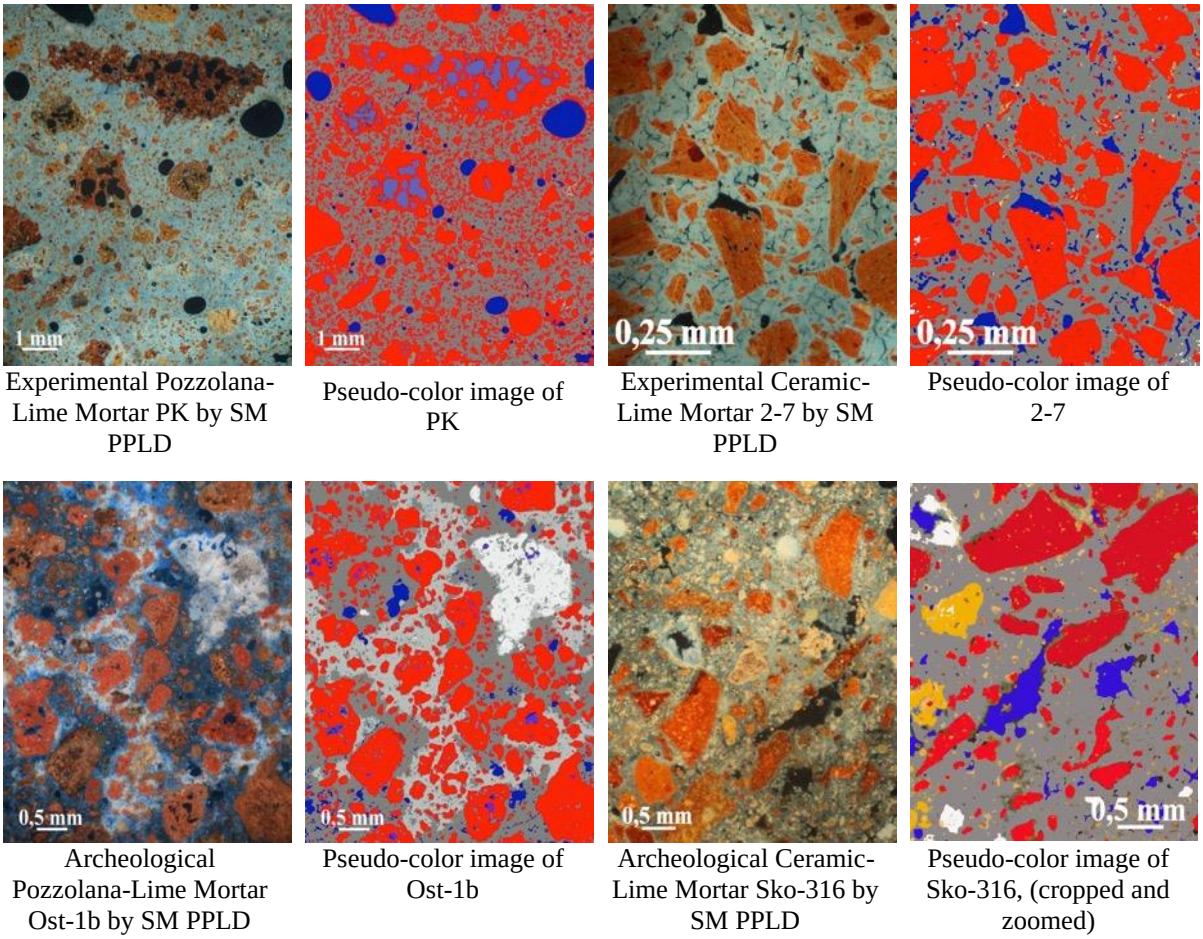
At the time of writing, there is growing interest in the examination of magnesium-rich, ancient pozzolanic binders (M-S-H in conjunction with C(A)SH) [184] and as such, areas such as these will continue to be the subject of future research. A key to qualifying these binder areas could be identification of spectra distinctive of magnesium silicate hydrates, and

carbonated versions of this material; the example shown in Figure 7.12 is a good candidate for future research into this subject.

7.5 Mortar Characterization by Image Analysis – pseudo-color analysis

Pseudo-color analysis was performed on photomicrographs of polished thin sections of each of the laboratory mortars as a method of determining the volumetric binder-to-aggregate (b:a) ratio. This was already known as the mortar was produced in both the laboratory test series and the one made in the field was mixed to a controlled b:a of 1:3 (25% binder by volume). These data serve a three-fold purpose. First, they serve as a test-of-concept of the use of image analysis to determine the volumetric b:a of a mortar, both since the mix volumes are known and as a comparison to the results of gravimetric methods. Secondly, they provide an important data point for comparison between different mortar types. Lastly, they are instrumental in interpreting other results, such as the adjustments to the FTIR results described in the following section. Four examples of this technique applied to both experimental and historical mortar are shown in Figure 7.13 below. In the images shown in Figure 7.13, red and yellow are used to show aggregates, grey tones for binder of various compositions, and blues to show different types of porosity (dark blue for binder porosity, indigo for internal aggregate porosity). Semi-automatic pixel counting was used to create proportions between each colored element, providing the typical b:a ratios for all types of mortar, both experimental and historical. The averages of these are given in Table 7.14 below. What is most significant, is that despite the use of the same volumetric b:a when producing the experimental mortar, there is a sizeable difference in the resultant b:a between mortars made with the two different types of aggregate (from 25% to 33% for volcanic, from 25% to 48% for ceramic). They consistently appear more binder rich than the original mix, most likely because the binder increases in volume while the aggregates do not[25]. Further, this difference is echoed with the ancient mortars (despite the advice of Vitruvius), suggesting a relatively authentic replication by the laboratory mortar production. The finding that ceramic pozzolan mortars appear more binder-rich than volcanic ones is echoed in the analysis of the ancient samples, possibly since some of the very fine ceramic particles being counted towards the binder, due to limits in device resolution.[26]

[25] The binder converts from solid CaO to $Ca(OH)_2$ to $CaCO_3$ and C(A)SH; it is also much more porous.
[26] At a certain point, fine ceramic particles behave more like binder than aggregate, especially when they are reactive.



Experimental Pozzolana-Lime Mortar PK by SM PPLD | Pseudo-color image of PK | Experimental Ceramic-Lime Mortar 2-7 by SM PPLD | Pseudo-color image of 2-7

Archeological Pozzolana-Lime Mortar Ost-1b by SM PPLD | Pseudo-color image of Ost-1b | Archeological Ceramic-Lime Mortar Sko-316 by SM PPLD | Pseudo-color image of Sko-316, (cropped and zoomed)

Figure 7.13: Pseudo-Color Analysis of Experimental and Historical Mortar, used to determine binder to aggregate ratio through pixel counting. (Mertens 2009)

In other words, both the ancient builders as well as this experiment had a similar result, in that due to the differences between the sorting, grading, and packing ability of volcanic versus ceramic aggregates, when mortars are made with a "1:3" volumetric proportion the resulting cured mortars show that ceramic-lime mortars appear to be significantly more binder-rich by image analysis 17-19%[27]. A similar difference in the gravimetric results can be found in Section 6.3, showing a rough parity in experimental techniques. This is shown in Figure 7.15 below, which overlaps the results from both techniques and is further discussed in Chapter 8. While this process is relatively simple, if time consuming, from a technical standpoint, pseudo-color imaging proves its worth in terms of analytical results.

[27] Whether this is due to differences in binder matrix or aggregate densities (or both) was not determined, but it is important to notice that the effect was found in both experimental and archeological mortars.

Mortar Type	Binder to aggregate ratio By pseudo-color analysis	Binder % by pseudo-color analysis
Experimental Mortar		
Volcanic Pozzolana-Lime Mortar, New (mixed 1:3)	"1:2"	33%
Ceramic-Lime Mortar, New (mixed 1:3)	1:1	48%
Archeological Mortar		
Volcanic Pozzalana-Lime, Ancient	1:2	34%
Ceramic-Lime, Ancient	1:1	53%

Table 7.14: Binder to aggregate ratios of Experimental and Historical Mortar as determined by pseudo-color analysis.

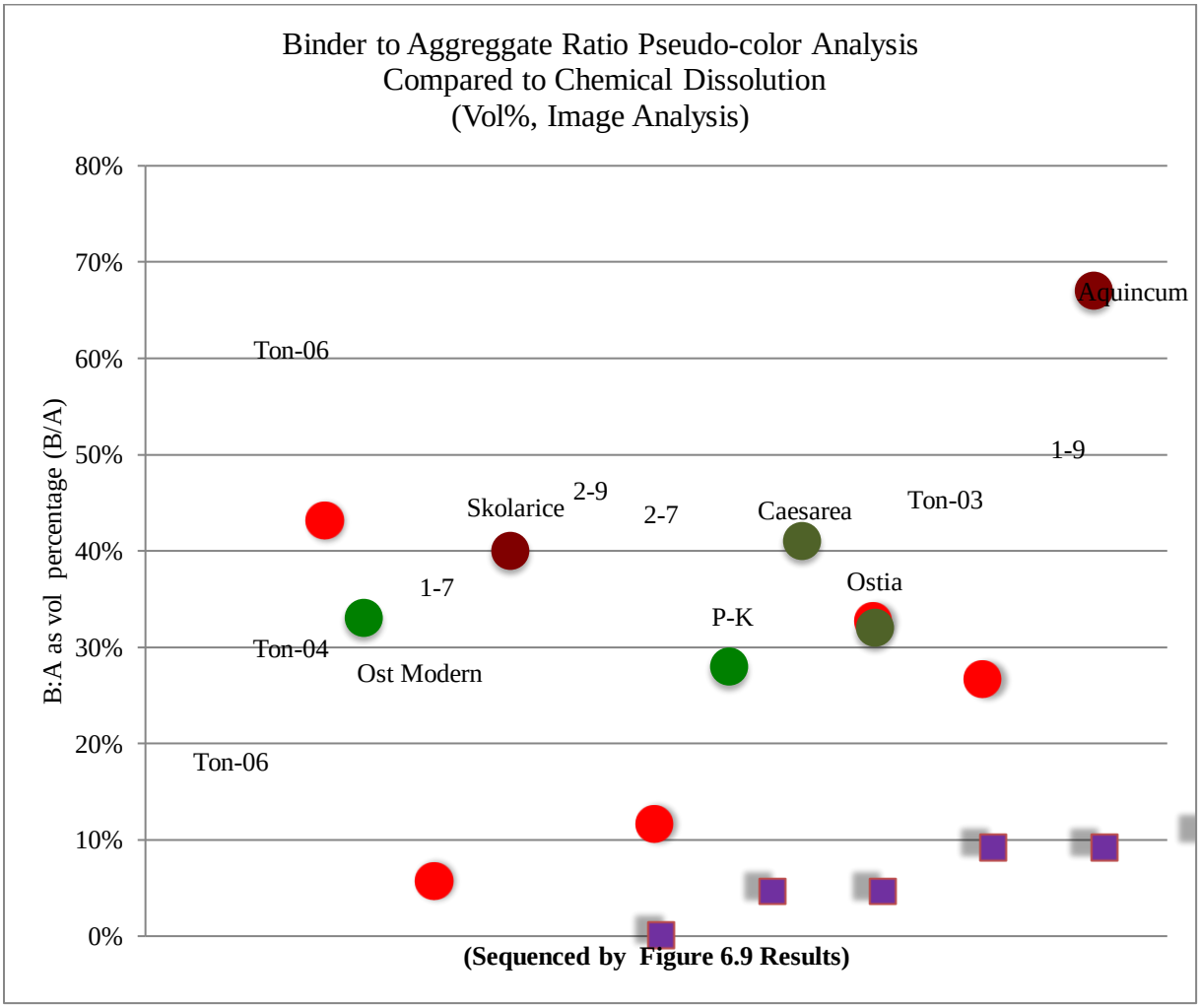
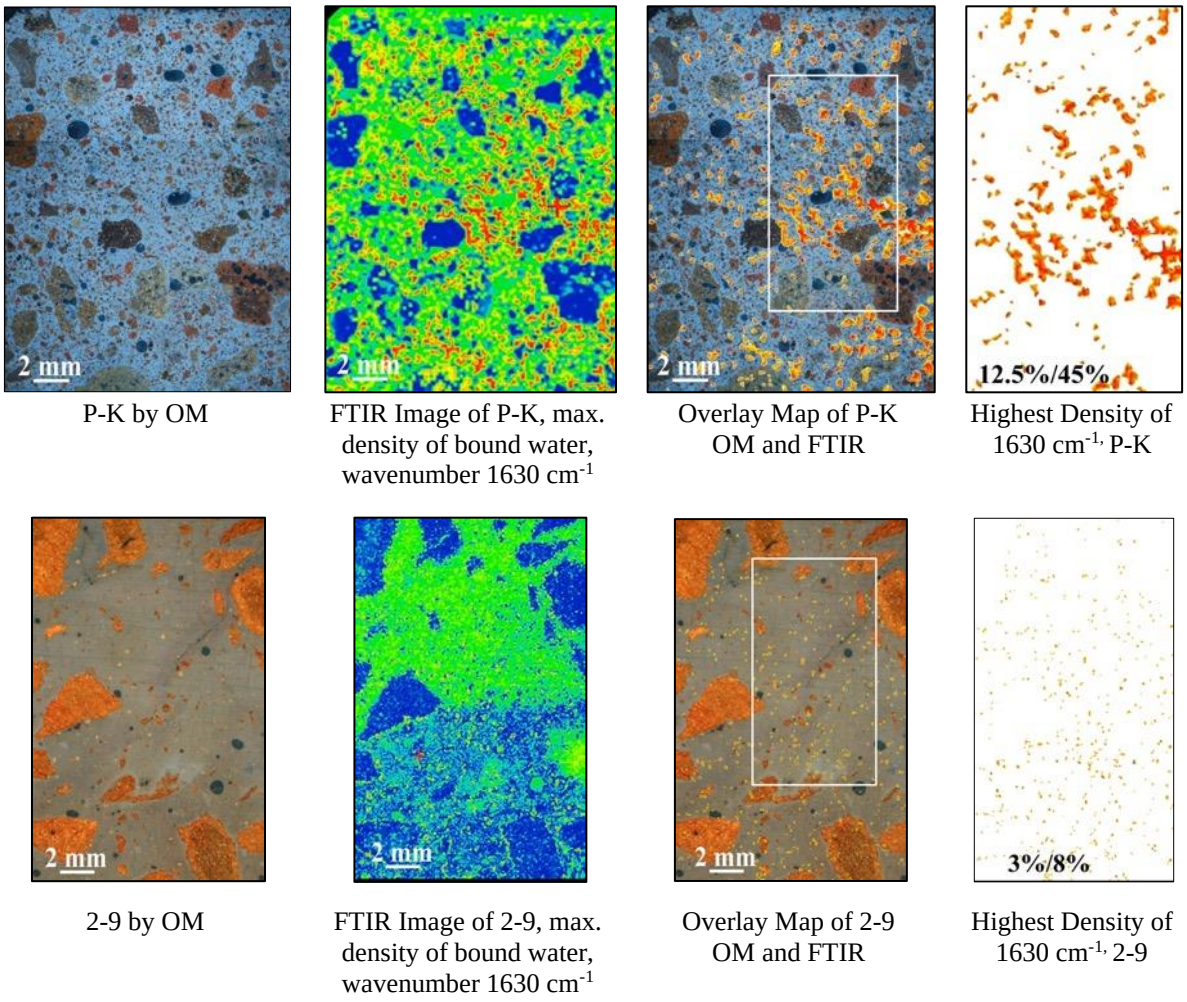


Figure 7.15: Binder to aggregate ratios of Experimental and Historical Mortar as determined by pseudo-color analysis, rendered as a percentage, and overlaying the same samples as analyzed by chemical dissolution (purple) from Figure 6.9

7.6 Binder Matrix Hydraulicity Characterization by FTIR imaging

In a manner similar to the pseudo-color imaging process described above, it is also possible through the use of image-editing software to combine SM/PLM, SEM-EDX and FTIR to provide qualitative and *quantitative* information about the mortar's binder. Contrary to pseudo-color imaging that relies in a large part on the analyst's ability to distinguish optically between mortar constituents and then pixel counting to determine something about the physical nature of the mortar (for example binder to aggregate ratio or porosity), this comprehensive protocol method uses the image created by the FTIR software based on detected molecular bond intensity combined with the other microscopic techniques determine something about the chemical content, by volume, of a mortar. This section gives examples of how this was done for detecting the C(A)SH content of a mortar's binder. Described in full in Section 5.6, this method relies on overlaying an FTIR image describing the peak intensity of a band that is characteristic of the target compound with a scaled image of the same area of the mortar. As determining the hydraulicity of pozzolanic mortars, especially ancient ones, is the most difficult question to answer by optical microscopy and SEM-EDX, the target bands were those associated with C(A)SH, either the bound water signified by –OH stretching around 1600 cm^{-1}, or a combination of carbonate found around 1400 cm^{-1} with the silicate band typically found within C(A)SH around 995 cm^{-1} [152-158]. In other words, this analytical method was used to quantify the volume of reaction products within each mortar, based on its quantification on the surface of a thin section. This is done by pixel counting the areas of highest density of C(A)SH on the surface of the scaled, composite image of the FTIR and OM or SEM of a mortar polished thin section. The color scale of the FTIR image denotes increased intensity of the targeted bands, this corresponding to both the likelihood and density of that bond being present. Red and Orange represent the high point of the scale, therefore it has been interpreted that these are the areas that contain (in this case) the most C(A)SH. This method was applied to all experimental mortars and enough of the archeological ones to provide not just a comparison between the two mortar types, but also to provide enough data to perform a statistical analysis of the technique itself, relative to destructive techniques (described in Chapter 8). Three examples of the use of this method are illustrated in Figures 7.16-7.18 below.



P-K by OM | FTIR Image of P-K, max. density of bound water, wavenumber 1630 cm^{-1} | Overlay Map of P-K OM and FTIR | Highest Density of 1630 $cm^{-1,}$ P-K

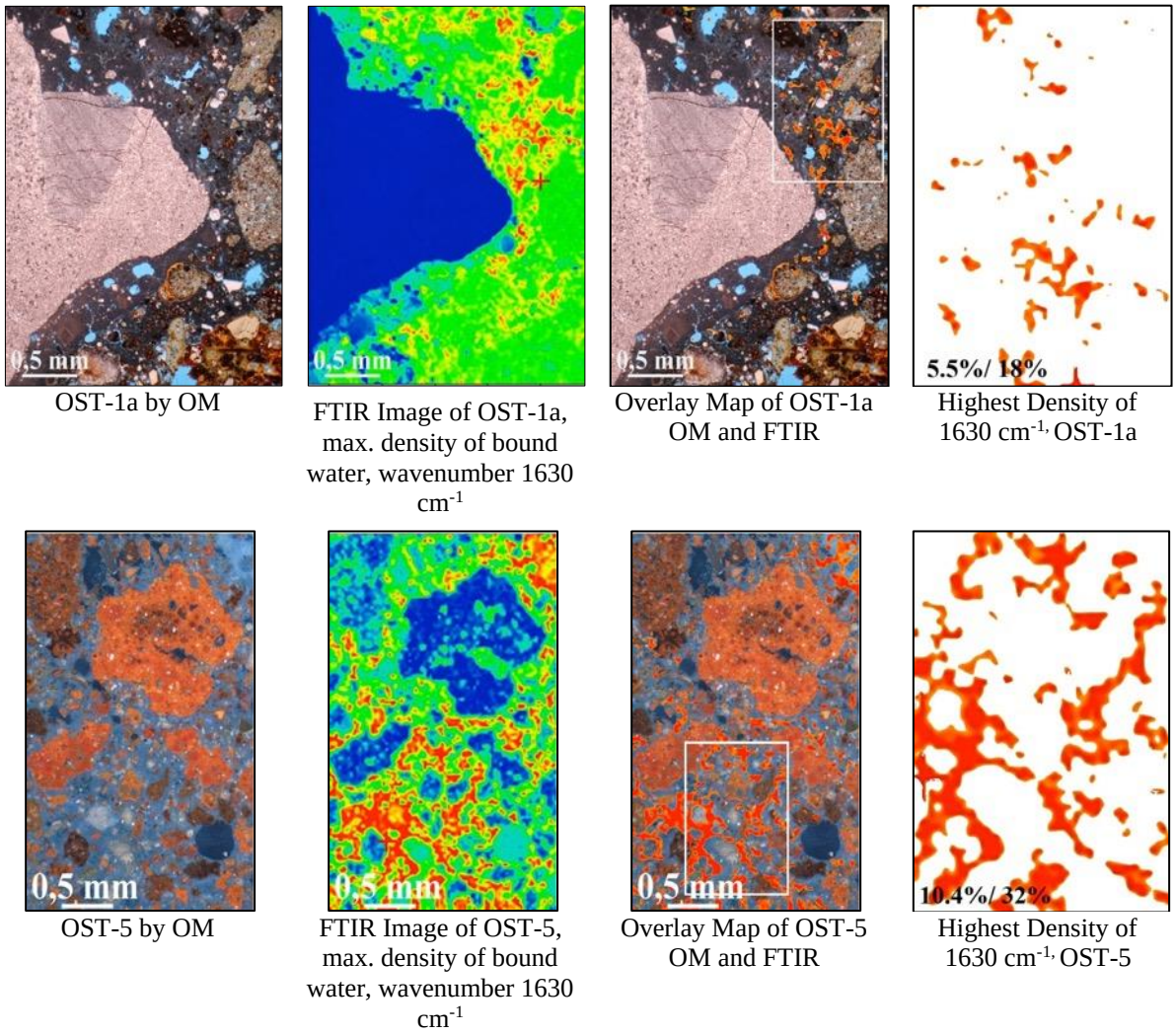
2-9 by OM | FTIR Image of 2-9, max. density of bound water, wavenumber 1630 cm^{-1} | Overlay Map of 2-9 OM and FTIR | Highest Density of 1630 $cm^{-1,}$ 2-9

Figure 7.16: Comparison of the areas of highest density of reactive products, as determined by FTIR imaging of the bandwidth associated with bound water in C(A)SH (~1630 cm^{-1}), combined with scaled stereo-microscope images of two experimental mortars
Top: a volcanic pozzolana-lime mortar; Bottom: a ceramic pozzolan-lime mortar.

Figure 7.16 above compares the binder C(A)SH content of two types of experimental mortars produced in the laboratory, one made from pozzolana and lime ("P-K") and one from ceramic and lime ("2-9"). Two equal-sized representative areas (50 mm^2) of the mortar were compared by pixel counting the highest density of the signature band for bound water in C(A)SH. This shows a very high density of the band for mortar "P-K" covering 12.5% of the surface area of the mortar, equivalent to 45% of the binder surface area, a much larger amount when compared to mortar 2-9 which exhibits 3%/ 8% respectively. This does not necessarily mean that there is four to six times the amount of C(A)SH present, just that there is a larger amount. This is because while the FTIR detects a higher density of the bonds associated with C(A)SH in those regions, the density itself cannot be given a numerical value. However, the area that is red and orange of the image of "P-K" is clearly much greater than the corresponding image for "2-9". Pixel counting shows that it is in fact about 5 times greater. This was

interpreted as showing that "P-K" has 5 times as much bound water, much of it is likely C(A)SH. This result corresponds well with both the higher compressive strength and soluble silica content of mortar type "P-K" as compared to mortar type "2-9". This is described in sections 6.2 (Figures 6.4-6.7) above. The FTIR image of 2-9 clearly displays the depth of carbonation of the sample; the darker blue area at the bottom is towards the outer surface of the mortar and carbonated sooner, hence less pozzolanic reaction product is detected.

Figure 7.17 below shows results for following the same protocol to compare an archeological mortar (OST-1a) with a restoration mortar (from the 1960s) (OST-5) of the same composition, volcanic pozzolana and lime, from the same archeological site, Ostia Antica in Italy.

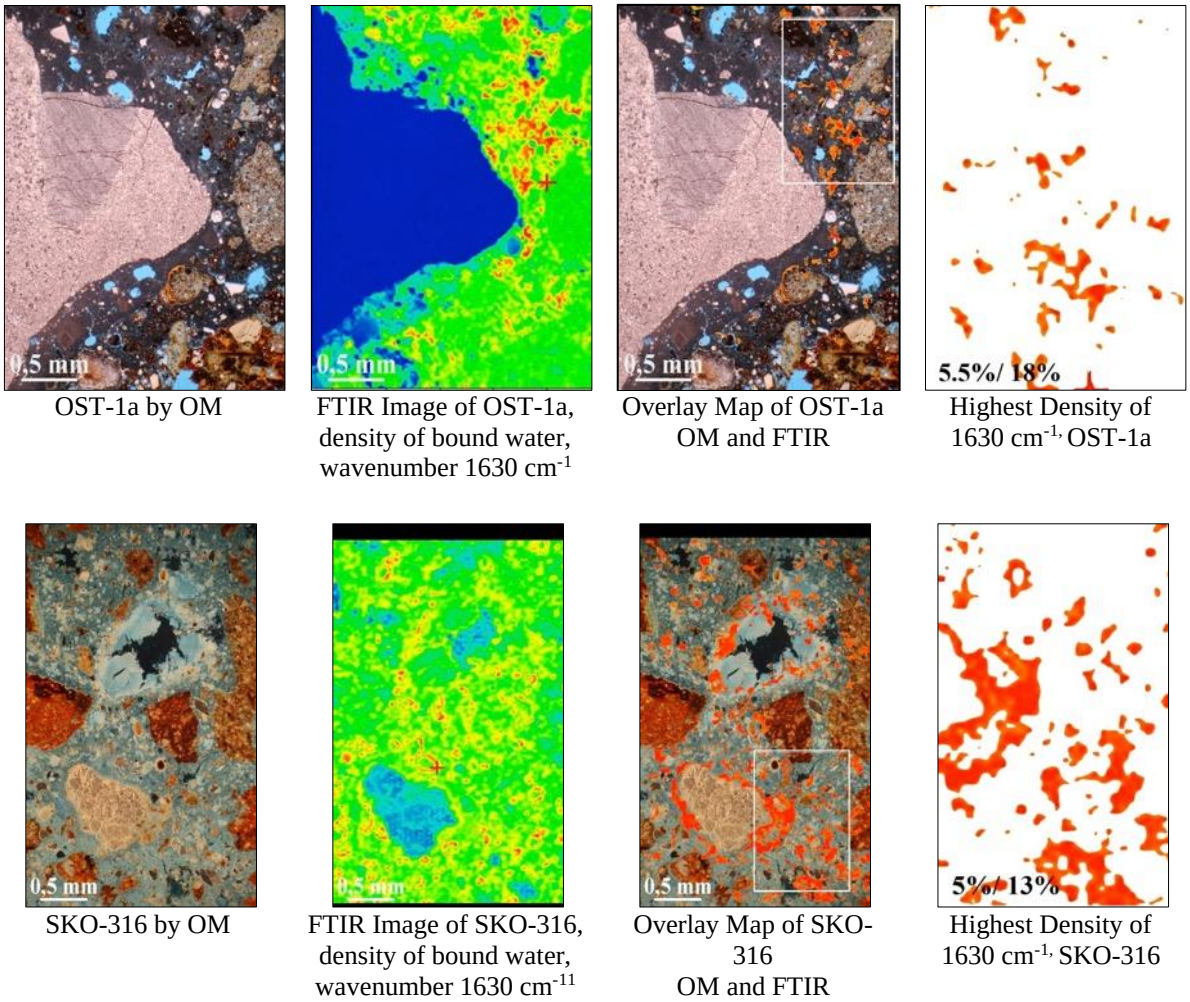


OST-1a by OM | FTIR Image of OST-1a, max. density of bound water, wavenumber 1630 cm^{-1} | Overlay Map of OST-1a OM and FTIR | Highest Density of 1630 $cm^{-1,}$ OST-1a

OST-5 by OM | FTIR Image of OST-5, max. density of bound water, wavenumber 1630 cm^{-1} | Overlay Map of OST-5 OM and FTIR | Highest Density of 1630 $cm^{-1,}$ OST-5

Figure 7.17 Comparison of the reactive products of an archeological mortar (top) and a restoration mortar (bottom) of similar composition, mapped by combining FTIR and scaled stereomicroscope images, method as 7.16 above.

This example illustrates a potential issue with using this application of the protocol, but then shows how it can be resolved with information taken from another step in the mortar's analysis. While the composite map of the detected bound water in OST-5 displays a very high density of reaction product, the area analyzed, has a significantly higher binder-to-aggregate ratio, i.e., it is more binder-rich. Therefore, it is important to always express the proportion of C(A)SH detected in an image of the whole mortar in terms of what proportion of the substance is present in the binder (not the image). Even after this adjustment, it is clear that the restoration mortar is significantly richer in hydrated reaction product (32% vs. 18% of the area of the binder). The probable cause of this disparity is the vast difference in age; the restoration mortar is less altered (decomposed) C(A)SH, which tends to separate into (calcite and aragonite) $CaCO_3$ and silica gel over time [1, 9, 128].



OST-1a by OM | FTIR Image of OST-1a, density of bound water, wavenumber 1630 cm^{-1} | Overlay Map of OST-1a OM and FTIR | Highest Density of 1630 $cm^{-1,}$ OST-1a

SKO-316 by OM | FTIR Image of SKO-316, density of bound water, wavenumber 1630 cm^{-11} | Overlay Map of SKO-316 OM and FTIR | Highest Density of 1630 $cm^{-1,}$ SKO-316

Figure 7.18: Comparison of the reactive products of two archeological mortars mapped by combining FTIR and scaled stereomicroscope images, as in previous two Figures. **Top:** a volcanic pozzolan-lime mortar; **Bottom:** a ceramic pozzolan-lime mortar.

The final example demonstrating this technique, Figure 7.18 above, compares the same ancient volcanic pozzolana-lime mortar sample as mentioned previously (OST-1a) with a nearly contemporaneous example of a ceramic pozzolan-lime mortar sample from a Roman villa in today's Slovenia (SKO-316). This example illustrates both the differences between the two pozzolans, as well as the need for adjustment by binder to aggregate ratio when using this technique.

Upon initial inspection, the ceramic-lime mortar appears to have a much higher concentration of reactive products. The region analyzed is dominated by a large field of binder, thus when adjusted for binder to aggregate ratio, the relative percentage of C(A)SH is significantly reduced into the range more typically seen for this mortar type, both by this technique and by thermal and chemical dissolution techniques. The higher detected intermolecular water found in C(A)SH in the volcanic pozzolana sample, OST-1a, corresponds to a higher reactivity of this aggregate. This in turn can be compared with the results for the experimental mortar; therefore it can be deduced that for the ancient mortars, the volcanic pozzolanic-lime mortars would have set more quickly and to a higher strength than the ceramic pozzolanic - lime ones, corresponding with the strength testing results (Section 6.2 above) and the results found by comprehensive image analysis. While it is important to compare FTIR results from the same bands when comparing between samples, it is also important to note that the band used above is not the only option. It is additionally possible to perform the same analysis selecting a different band associated with C(A)SH, such as the 995 cm^{-1} Si-O stretching band, or to compare bound water content from other molecules, such as broad "-OH" band around 3400 cm^{-1}.

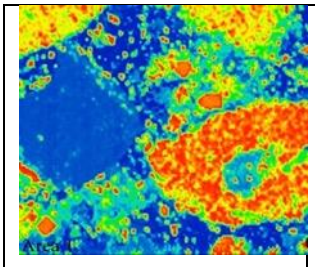
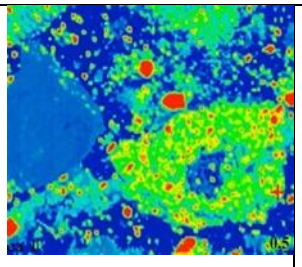
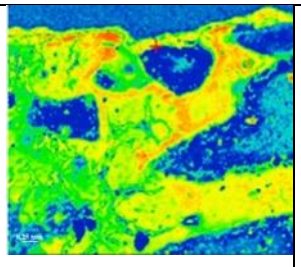
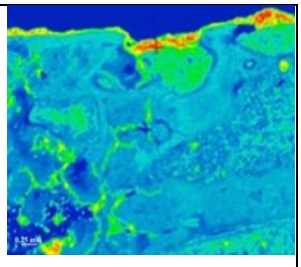
			
Si=O at 995 cm^{-1} "Amorphous silicate" in Ceramic – 22% of image surface area, roughly 50% of aggregate content.	Si=O at 1200 cm^{-1} - Quartz "natural temper in clay for making ceramic" 1% of image, 3% of ceramic aggregate area.	-OH at 3400 cm^{-1} "bound water, likely from C(A)SH and gypsum" 5% of image, 10% of binder area.	$-SO_4$ at 1004 cm^{-1} "likely gypsum" 1% of image, 2.5% of binder area, therefore roughly 25% of the -OH in the previous image could be bound to gypsum.

Figure 7.19 Surface Area Percentage determinations by FTIR-imaging for some common mortar contents.

Examples of this are shown in Figure 7.19 above. The -OH hydroxyl band can be used to obtain information about the content of portlandite, gypsum or C(A)SH or even ettringite within a mortar. Differentiating between different hydrated compounds would require the creation and analysis of maps that overlap both -OH and (for example) $-SO_4$ band found around 1004 cm^-, in manner similar as was done for C(A)SH in Figure 7.6 above. Generating reproducible results that were statically relevant, FTIR-mapping-based image analysis was performed on polished thin sections of all the experimental mortars created in the laboratory, as well as a selection of ancient mortar samples. At least 2 regions were mapped and analyzed for each, with the average results shown in Table 7.20 below. They show a clear trend in terms of the amount of reaction products found for each mortar type, with the volcanic pozzolan - lime mortar exhibiting more reaction product whether it is newly made or ancient. These data are later shown in Chapter 8 to measure the comparative efficacy of this technique with more traditional destructive ones.

Mortar Type	Reaction products as % of mortar	Reaction products as % of binder
Experimental Mortar		
(Volcanic) Pozzolana-Lime Mortar, Lab	12.5%	45.0%
Ceramic-Lime Mortar, Lab	6.0%	12.5%
Archeological Mortar		
Pozzalana-Lime, Ancient	8.0%	20.0%
Ceramic-Lime, Ancient	5.0%	13.0%

Table 7.20: Pozzolanic Reaction Products detected in both Experimental and Archeological Mortar per image analysis; Averaged by type

7.7 Summary

These results of this chapter show that entirely image-based methods on polished petrographic thin sections can be used to extract the maximum amount of information possible without destroying the sample preparation, referred to as the protocol. This protocol was applied to both archeological samples and two sets of control samples to test the efficacy of these methods. The results from this chapter show that the experimental and archeological mortars essentially represent before and after cases, that is, the experimental mortar was a good analogue for the archeological mortar in its original state.

Chapter 8 will give examples of combining the results of physical, thermal, and chemical testing of the mortars (Chapter 6) with those shown in this chapter. Thus, can the efficacy of this novel image-based protocol relative to the established physical, thermal, and chemical methods be established

8.0 Conclusions and Outlook

Much of this work was dedicated to displaying the vast amount of information that can be obtained from a polished (uncovered) petrographic thin section, by applying a comprehensive, image-based protocol. The Venn diagram shown in Figure 8.1 below illustrates three groups of information that mortar researchers look to acquire that were performed in this work. On the right side are types of information that is traditionally gained through the analysis of thin sections, in which case the value of the thin section is not in dispute. The left side displays types of information that can generally only be gained through physical or chemical testing. The middle overlap area shows analytical goals that are used to infer a correlation with the physical performance of a mortar without the direct observation of that physical parameter, e.g., correlating higher aggregate reactivity (regardless of detection method) with a higher mortar strength, even when the strength cannot be directly tested. One of the main goals of this work was to show that many of these correlations could be made from information that can be found on the polished thin section itself, without the need to compare results from a wide variety of (often destructive) techniques.

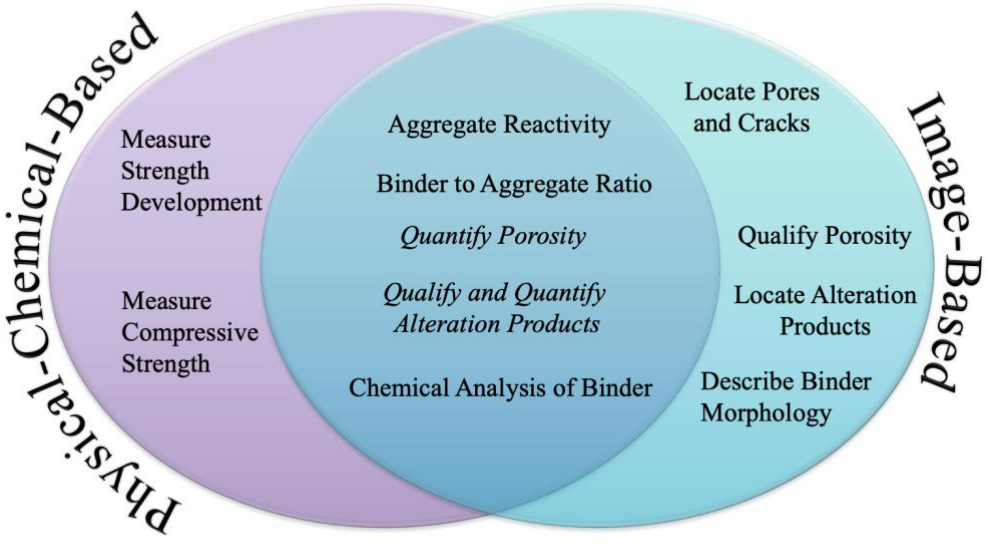


Figure 8.1: Venn diagram illustrating the methods used during this work, with central items being ones that can be directly related. *Note: Italicized items can be done by both physical-chemical and Image-Based methods but were not performed (see 8.2.1 and 8.2.2).*

When evaluating a novel technique, it is necessary to have a set of control specimens; Chapters 3 and 6 detailed the process of creating and testing experimental mortars to be analyzed by means of the image-based protocol (Chapter 7) in parallel with the historical material. In the following sections, not only is the comprehensive image-based protocol compared with physical and chemical laboratory techniques, but also it is performed on both historical and experimental mortar samples, a double-control. Sections 8.1.1 to 8.1.3 show comparisons between the results obtained by both physical-chemical laboratory testing and the image-based protocol by means of statistical analysis for both experimental and historical mortar. The comparisons illustrate that these new uses for imaging help to overcome one of the perceived drawbacks of imaging methods: that they are generally not considered tools by which quantitative analysis can be made on a cementitious system. In the past, destructive means such as chemical or thermal dissolution, or powder X-ray diffraction have been used to perform quantitative analysis on historical mortars. However, the results below serve to further the author's contention that *the strong results shown by the comprehensive image-based analytical protocol, as applied to historical mortars with the experimental ones serving as a control, eliminate the need, at least in part, for most of the "traditional" techniques, especially those that rely on destruction of the sample.*

8.1 Correlative Analysis of Image-Based Protocol

The following three sections are examples, that use correlative, statistical analysis between image-based techniques and established laboratory procedures, which are used to highlight the efficacy of the protocol. The first two show direct comparisons between techniques, that is, the results of the image-based protocol are directly compared to laboratory results that were used to describe the same feature of a mortar. While the image-based results should be considered volumetric (as discussed in 5.6 above) and the laboratory-based results are gravimetric, in the case of the binder of ancient mortar, the average density of the solids (carbonate binder and highly porous ceramic or volcanic aggregate) are roughly equivalent, allowing for direct comparison. This is partially because the types of mortar described herein are made with highly porous, lightweight aggregate with a bulk density close to that of the binder. Even in future experiments where this might not be the case, great differences in bulk density between the binder and aggregate would not affect the types of analysis shown in Sections 8.1.2 and 8.1.3.

Section 8.1.1 compares the results of image-based assessment of the binder-to-aggregate ratio with those determined by chemical dissolution. Second 8.1.2 compares the results of three methods of determination of binder hydraulicity (how reactive the pozzolan was); comparisons are made between image-based, chemical dissolution and thermal decomposition techniques. The third section demonstrates the correlation between binder hydraulicity, as determined by the three methods described above, with the measured compressive strength of the experimental mortar types.

While a wide variety of mortar characteristics *should* be compared in the same manner as the following sections demonstrate, in the course of this work for only the three cases presented below (binder to aggregate ratio, percentage of cement hydrates in the binder, and the correlation of detected cement hydrates by method with the compressive strength of the mortar) were enough data was acquired from both experimental and historical mortar, of both pozzolanic types, to make statistically significant comparisons. These data mostly speak to two of the questions that are most interesting to researchers and restorers, strength and hydraulicity, and thus was specifically targeted for every mortar type.

8.1.1 Direct Comparison of Binder to Aggregate Ratio Determination Methods

The creation of pseudo-color images based on petrographic photomicrographs, in order to determine the binder-to-aggregate ratio (b:a) of a mortar, is a method that has been employed increasingly since image-editing software has become widely available (about 15 years). The ratio is determined by pixel-counting the pseudo-colored areas of each mortar constituent. This has been employed in several publications cited herein, some of which the author was also a contributor [1, 9, 33, 128]. As it has become a standard practice (of this author) to perform this technique on historical mortars being analyzed, a large amount of data has been created, and thus for comparison, this technique was applied to the experimental control samples as well. Afterwards a portion of the same mortar was dissolved chemically by the technique

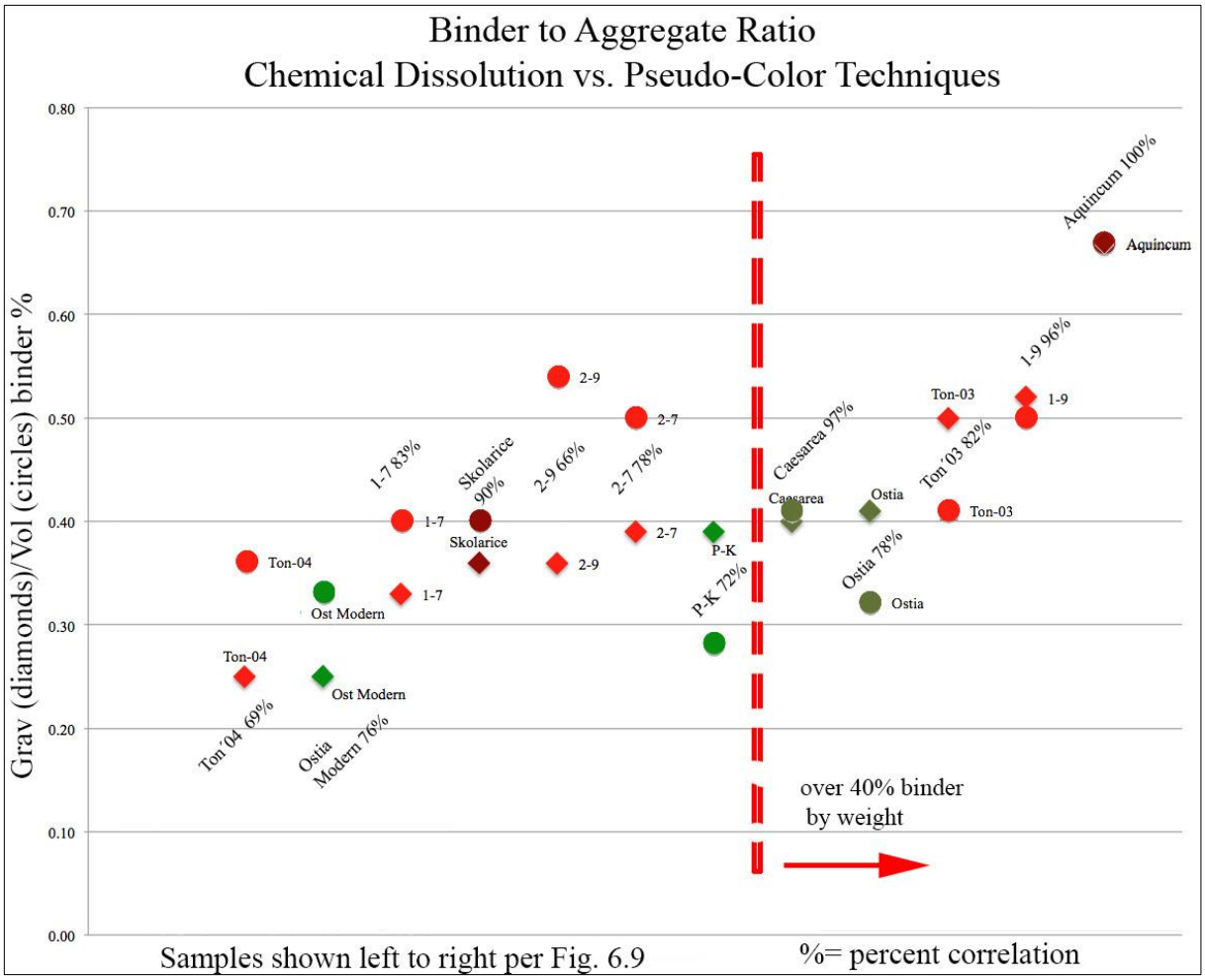


Figure 8.2: Chart showing the correlation between the chemical dissolution and pseudo-color editing techniques for determining binder to aggregate ratio, with degree of correlation for a few examples shown.
Circles: Pseudo-color results, Diamonds: Dissolution Results; Red: Ceramic, Green Pozzolana. Dark shades represent archeological mortar. Samples to the right of the dashed line were more than 40% binder by weight.

outlined by RILEM (TC 167-COM). The comparative results are shown in Figure 8.2 above and the tables in 8.3 below. The figure (8.2) shows the same information as previously shown in Figure 6.9, in which the gravimetric b:a (diamonds) for various mortars is expressed as a percentage from least to greatest, from left to right. Shown directly above or below are the results from pseudo-color image analysis of the same mortar type (circles), showing the volumetric b:a. The distance between the two markers shows how closely correlated[28] the two (absolute) values are, which is quantified as a percentage in the tables in Table 8.3 below that interpret the data in the chart three different ways.

[28] Percent correlation was derived by dividing the smaller value (gravimetric or volumetric result) by the larger one, e.g., both values were 67% in the case of Aquincum, so it had a correlation value of 100%, while 2-9 was 35% by gravimetric analysis and 55% by image-analysis (volumetric), so 66% correlation.

Percent Correlation Comparison Tables										
by pozzolan type				*Archaeological vs. Experimental*				*by weight percentage binder*			
Ceramic		**Volcanic**		**Archaeological**		**Experimental**		**binder < 40% mortar wt.**		**binder > 40% mortar wt.**	
Aquincum	100%	Caesarea	97%	Aquincum	100%	Clay 1 950°	96%	Školarice	90%	Aquincum	100%
Clay 1 950°	96%	Ostia, Ancient	78%	Caesarea	97%	Clay 1 750°	83%	Clay 1 750°	83%	Caesarea	97%
Školarice	90%	Ostia, Modern	76%	Školarice	90%	Ton-03	82%	Clay 2 750°	78%	Clay 1 950°	96%
Clay 1 750°	83%	P-K	72%	Ostia, Ancient	78%	Clay 2 750°	78%	Ostia, Modern	76%	Ton-03	82%
Ton-03	82%			Ostia, Modern*	76%	P-K	72%	P-K	72%	Ostia, Ancient	78%
Clay 2 750°	78%					Ton-04	69%	Ton-04	69%		
Ton-04	69%					Clay 2 950°	67%	Clay 2 950°	67%		
Clay 2 950°	67%										
Avg.	**83%**	**Avg.**	**81%**	**Avg.**	**88%**	**Avg.**	**78%**	**Avg.**	**76%**	**Avg.**	**91%**
StdDev.	**11%**	**StdDev.**	**10%**	**StdDev.**	**11%**	**StdDev.**	**10%**	**StdDev.**	**7%**	**StdDev.**	**10%**

Table 8.3: Grouping Tables of showing the correlation between the chemical dissolution and pseudo-color editing techniques for determining binder to aggregate ratio for experimental and archeological mortars. **The modern Ostia samples were from 1930s and 1960s restorations, hence are considered separately from the experimental mortars.*

There does not immediately appear to be a clear pattern in the degree of correlation (for example that the methods show a closer correlation depending on mortar type or provenance), which may only be reflective of the diversity of mortar types and the various densities of both binder and aggregate types affecting the gravimetric value. However, grouping these data according to different criteria as shown in Figure 8.3 above reveals several patterns. The left comparison table shows the averaged results of the ceramic pozzolan mortar compared to the volcanic pozzolan mortar, regardless of age or origin. While the correlation between techniques is shown to be less than optimal, the similarity in average correlation (81% for ceramic and 83% for pozzolanic) shows that the methods are reproduceable. The middle table compares the archeological to the experimental samples, showing that the techniques have the greatest correlation when examining archeological mortar. This is quite a positive result, as the goal of any of these analytical techniques is ultimately the understanding of historical mortar, the experimental mortar being a tool to further the understanding of the historical. The right table illustrates the fact that the more binder rich a sample is, the closer the correlation between the two methods. The average correlation of the samples that shows higher than 40% binder content (to the right of the dashed line in Figure 8.2) by the dissolution method is 91%, meaning that on average, for those sample types, the gravimetric binder percentage value was within 91% of the volumetric one determined by image analysis.

Thus, while the technique shows great potential, it can also benefit from additional data from further applications of the image-based techniques, since for each sample the image-based techniques were applied to a single thin section, while the dissolution technique could be

repeatedly made with additional portions of the same sample. As the image-based technique appears effective, accumulating more data additional applications (on future samples) should provide further testaments to its value.

8.1.2 Direct Comparison of Methods for Determining Mortar Binder Hydraulicity

The defining characteristic of pozzolanic mortar is its hydraulicity, that is, its ability to form cement hydrates and therefore a strong, durable binding material. In this work a method similar to using pixel-counting to determine the binder to aggregate ratio explained above and detailed in Section 5.6, photomicrographs were used to determine the surface area of the binder of a mortar that exhibited hydraulic phases (C(A)SH) detected by FTIR imaging. The results of this process were given in Section 7.6. The aim of the laboratory procedures detailed in Sections 6.3 and 6.4 was likewise to determine the level of hydraulicity (hydraulicity index) of the same mortars by chemical and thermal dissolution methods, respectively. Table 8.4 below gives the results of these 3 methods for determining the hydraulicity index for several samples studied in this work. These data are then correlated with each other, as shown in Figure 8.5 and Table 8.6, and discussed below.

Type	by Image Analysis	by RILEM	by TGA-DSC
Experimental			
Ton-3	6%	12%	24%
1-7	7%	9%	14%
1-7	8%	13%	14%
2-7	13%	12%	13%
2-9	17%	22%	6%
Ton-6	17%	13%	29%
Ton-4	19%	26%	42%
P-K	45%	25%	17%
Archaeological			
Školarice	5%	13%	16%
Ostia	7%	27%	28%
Aquincum	7%	20%	74%
Caesarea	10%	31%	13%

Table 8.4: Comparative Values of the Index of Hydraulicity for the Experimental and Archeological mortars; hydraulic portion of the binder as a percentage of the whole binder. Average Values by Type are used in the charts below. *Note: While the RILEM values are averages of 5 repetitions for archeological mortar and 10 for experimental, the TGA values are only 2, and the image analysis, is, by nature a single value representing the entire thin section's surface area, thus averages and standard deviations are not included.*



Figure 8.5: Scatter Plots for the determination of C(A)SH content in a mortar's binder. Clockwise from Top Left: As a weight percentage as determined by chemical dissolution; as a volume percentage as determined by image analysis; as a weight percentage as determined by thermogravimetric analysis, standard method; as a weight percentage as determined by thermogravimetric analysis, total binder method (used for Table 8.6 below).

Mortar Type	% correlation Chemical: Image	% correlation Thermal: Image	% correlation Thermal: Chemical
Arch., Pozzolana-Lime	89%	49%	55%
Archeological, Ceramic-Lime	84%	78%	95%
Experimental, Ceramic-Lime	83%	83%	70%
Exper., Pozzolana-Lime	56%	37%	67%

Table 8.6: Correlation Percentages by mortar type for the methods used to determine their binder hydraulicity. Method of determining as above.

The scatter plots shown in Figure 8.5 give average values of the determined binder percentage of C(A)SH by the three methods used in this work, averaged by mortar type. The

bottom two charts display the results of the thermogravimetric analysis by both the traditional method of interpretation and the novel one discussed in Section 7.6; once the data is averaged for mortar type, rather than for individual sample, it can be seen that these methods are in fact roughly equivalent. It is this latter value that is used for the correlation table shown above, which compares the methods to one another. These percentages quantify how equivalent the methods are (shown visually in the figure as how "close" they would be if the images were overlapped).

There are two clear trends revealed by comparing these techniques. First, that there is great difficulty in achieving consistent results for pozzolana-lime mortars relative to ceramic-lime mortars regardless of technique used (correlation values from 37%-89%). This is caused by the discrepancy between the amount of C(A)SH detected by image-based methods being much higher for the experimental pozzolana-lime mortar than the archeological, while the reverse is true when determined by the other two methods. It is possible that the in the experimental pozzolana-lime mortars, FTIR measurements are recording a large amount of hydroxyl that is mistakenly included in C(A)SH (while in fact contributable to calcium hydroxide). The thermal and chemical methods, on the other hand, report a superficially high level of C(A)SH in the historical samples which may be an erroneous inclusion of degradation products or additional soluble silica, respectively, as evidence of C(A)SH. This could be further refined by additional research specifically on degradation products (see Section 8.2.2 below).

Second, the correlation between thermal- and image- methods is not any lower that between that between thermal and chemical, that is to say, the novel technique is not any less consistent than the more time-tested ones. In fact, the highest correlation can be found in the comparison between the chemical dissolution results (which additionally have the largest amount of test results to average) and the image-based results, again the with exception of the experimental pozzolana-lime value. The best overall results are unsurprisingly between the two most common analytical techniques (chemical and thermogravimetric) with the material most widely studied, ancient ceramic-lime mortar.

Despite the inconsistencies described above, all results still point to the overall finding that pozzolana is more reactive and thus creates more C(A)SH and forms a stronger mortar. This is further analyzed in the next section. Although beyond the scope of this work, a large database with results from all methods described here would be greatly beneficial to determining the statistical accuracy of each method, as well as a useful tool when describing the results from any sample that is analyzed.

8.1.3 Correlating Mortar Binder Hydraulicity with Compressive Strength

In the case of the experimental mortars produced in the laboratory (as well as 3 of those produced in the field), the information previously discussed could be compared to compressive strength data gathered previously in this work, which was discussed in Section 6.2. For these mortar types, a statistically significant number of samples could be subjected to the standardized compressive strength test *and* all three types of determination of binder C(A)SH content (thermal, chemical and image-based on petrographic thin section), and therefore correlative analysis could be performed. The results in Figure 8.7 below, show the correlation between the measured compressive strength of a mortar type and the amount of the binder determined to contain hydraulic compounds; this is repeated for… binder hydraulicity detection method. Figure 8.7 shows as a baseline the measured compressive strength in mega-Pascals (MPa), adjusted by multiplying by 0.1 so that the results fit on a chart where the other data is a percentage expressed decimally. The pozzolana-lime mortar produced in the laboratory is clearly much stronger. The three remaining lines represent percentage of C(A)SH detected in the binder of each mortar type by each analytical process. While it was expected that these lines overlap, the data they display is nonetheless telling. The results from the thermogravimetric analysis show a very poor correlation with the increasing measured strength per sample type, although when averaged into a best-fit line (as is shown in Figure 8.8 below) the general trend of increasing strength with increased hydraulicity is shown. When correlating increasing strength from sample to sample, the image-based method results (blue line) most closely follow their corresponding compressive strength values (black line), including the outlying pozzolana-lime mortar, i.e., the shape of this line is most similar.

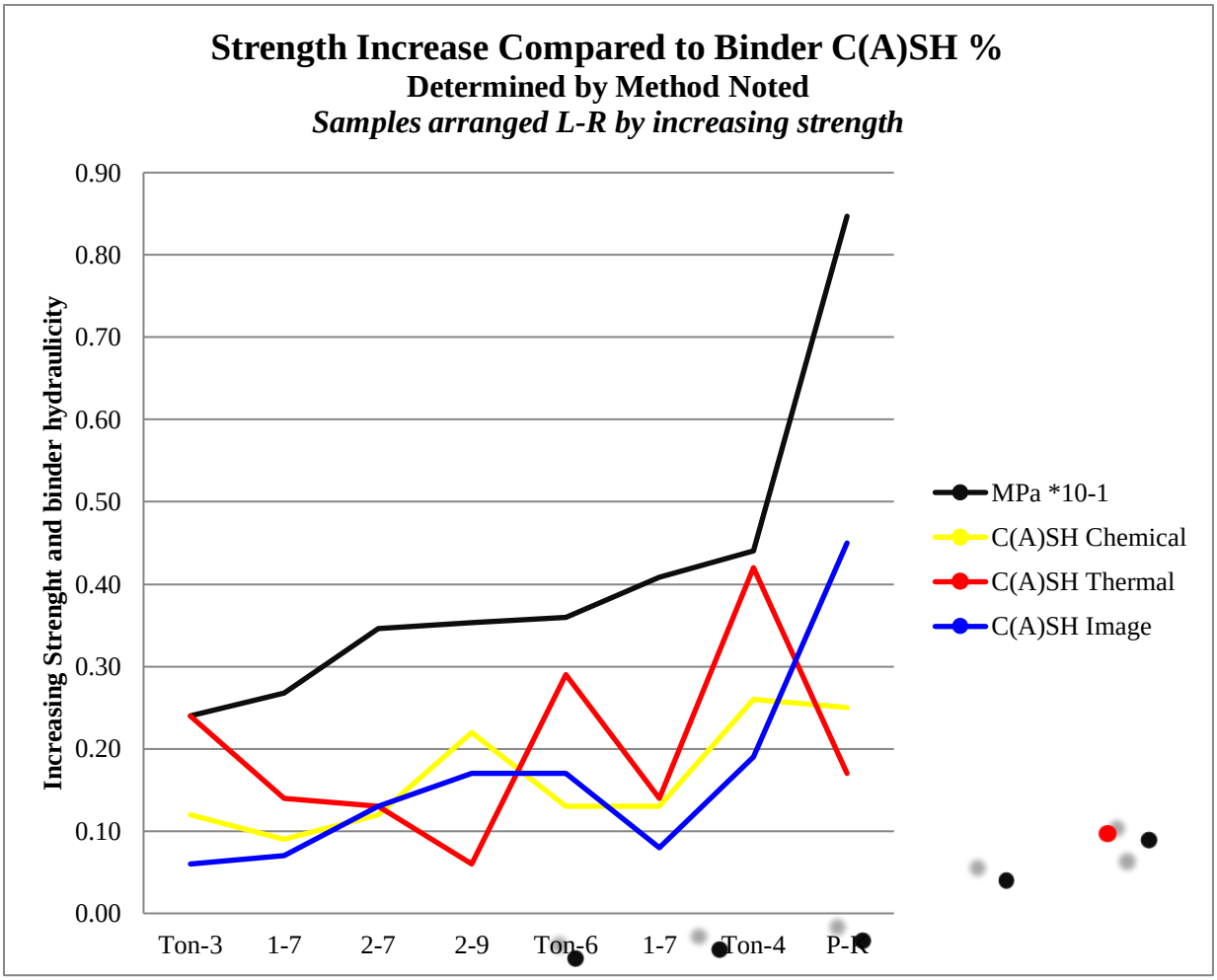


Figure 8.7: Comparison between methods of binder hydraulicity detection as compared to tested mortar compressive strength. Experimental samples are listed from left to right in order of increasing compressive strength in MPa, expressed here at the value x 10^{-1} in for scaling purposes.

A further refinement of the data shown in Figure 8.7 above can be found in Figure 8.8 below. In this chart, the strength values in MPa have been multiplied by the detected C(A)SH binder percentage (for example 25% binder C(A)SH x 4 MPa would give a value of 1) to give a strength per hydraulicity index value. This has the effect of normalizing the C(A)SH binder percentage values and the results can been seen to form tighter clusters per sample. The pozzolana-lime mortar remains an outlier with both correspondingly high C(A)SH (by all methods) and strength. In fact, it is this final value that most affects the overall slope of the green trend-line (image-based analysis). This is not misleading; the much higher C(A)SH content should result in much higher strength. This aside, it can be seen for the wide variety of ceramic-lime mortars produced, once the data has been further refined, there is a rough equivalency in methods. Although this is comparing the strength of the whole mortar, while the detection methods focus on the binder only, generally the aggregates can be omitted since they

are of near-equal strength and the binder to aggregate ratio was kept the same for the experimental mortar series. Based on these analysis, this model can be considered predictive, in that higher detected C(A)SH (by any method) can be associated with higher strengths, as all trendlines are increasing from left to right, following the increasing strength.

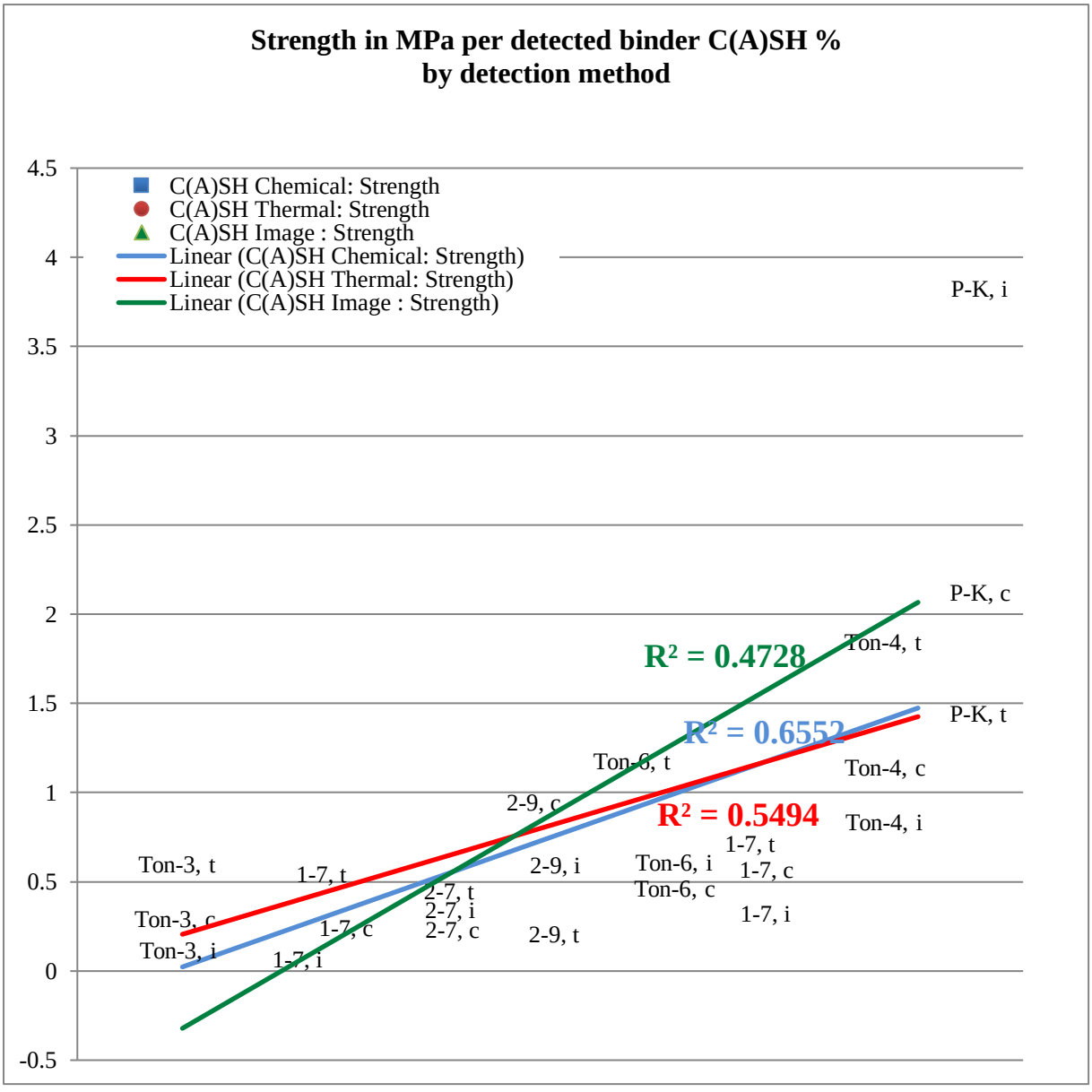


Figure 8.8: Mortar Strength Adjusted by detected binder C(A)SH % per sample. Strength in MPa multiplied by binder C(A)SH percentage. Listed left to right by increasing measured mortar strength. Image-Based (FTIR) analysis (green) shows a clearly trend in the correlation between increasing C(A)SH and increasing strength compared to Thermal (red) and Chemical (blue) methods.

It can be hypothesized that for a sample that is too small for standardized strength testing, the larger amount of binder C(A)SH that can be detected the stronger that mortar is likely to be (or have been historically). The charts presented in this section demonstrate that achieving this

information by image-based analysis on polished petrographic thin sections is as good, if not better, than methods that rely on thermal or chemical dissolution of the sample. Future work could focus exclusively on this topic, by comparing results from these 3 types of C(A)SH detection methods with the strength results from historical samples on which micro-scale strength testing can be performed (see [101]).

8.2 Outlook

As with any scientific effort, the work described herein can serve as a launching point for a wide variety of potential future paths of investigation. Because of limitations in time, money or both, there comes a point when there are diminishing returns on increased effort. If a solution can be found with 2 or 3 methods, it is perhaps unnecessary to corroborate with additional testing. This aside, three avenues of further exploration of the topics in this work are proposed. They are listed in order of increasing complexity, ranging from a relatively simple laboratory procedure involving porosimetry (Section 8.2.1), the application of the image-based protocol to studying degradation phenomena (Section 8.2.2), and an efficiency study that could put a value in terms of comparative time and effort on a method by method basis for achieving similar results to this work.

8.2.1 Direct Comparison of Methods for Determining Mortar Porosity

When studying the porosity of a mortar, it would be possible to make a direct comparison between the (macro-) porosity as determined by pseudo-color image analysis of photomicrographs of mortar thin sections and the application of mercury intrusion porosimetry (MIP) on a piece of the same mortar sample from which the thin sections was made. Since pseudo-color imaging relies on the user being able to "hand select" porosity from the photomicrograph, it is likely that only the only the macro-porosity could be directly compared, since the very fine binder porosity is both difficult to resolve by microscopy and difficult to select by image editing software. Nonetheless, there is no reason that the large pores and cracks routinely selected by image analysis could not be compared to large-diameter porosity determined by MIP. This would have produced results that could be correlated with those found those found in Section 7.5.

This was not pursued in the course of this work for the practical reason that that for the archeological samples, there was often not enough material to perform MIP in addition to all of the other testing performed. Thus, there would have been insufficient results to compare the methods' application between experimental and archeological samples. What is more, the use of mercury for this procedure makes it so it cannot be reused. Additionally, there would have been significant difficulty with the samples made of volcanic pozzolana, as the aggregate itself contains porosity similar in size to the macro-porosity of the binder. While this is clearly visible in photomicrographs, it would require a second round of MIP on the pozzolana itself. This would both require more material and the ability to completely remove the pozzolana from a historical mortar for separate analysis without destroying its structure, which would be quite time-consuming.

8.2.2 Application of Protocol to Quantification of Alteration Products

Binder alteration products are an area of great interest when it comes to the study of historical mortars, both to understand a mortar's behavior and to allow conservators/restorers to make crucial decisions regarding the care of a piece of built heritage. This work has demonstrated the use of a comprehensive image-based protocol to locate and identify binder alteration products (Sections 7.4). Going a step further with this would be the volumetric quantification of these compounds in a manner like the application shown in Sections 7.5 and 7.6. Then these volumetric data of alteration products could be compared to the gravimetric data acquired by chemical and thermal dissolution, such as was done previously in this chapter.

Although data collected during this work would allow for this type of analysis for a handful of the archeological samples discussed herein, a systematic study would require re-analysis. If this were to be attempted, the method would be best if proved effective by the systematic comparison of archeological/ historical material and both new and artificially aged experimental material. In this manner, the alteration products often seen by PLM and SEM, such as gypsum, ettringite, a variety of silica and magnesium-based gels and re-precipitated carbonate polymorphs (vaterite and aragonite) could be located and quantified by EDX and FTIR mapping, the results of which can be compared with chemical and thermal dissolution techniques.

8.2.3 Value Assessment: Towards a Simplification of Historical Mortar Analysis

The assertion that this image-based protocol can be used as a replacement for (and not corroboration of results gained through sample destruction) has both a practical and philosophical basis. The philosophy and practical aspects are intertwined and are largely dependent on the efficient use of time and resources to achieve a goal, in this case to assess a material that is considered to have historical value. As time and resources are finite, this is often particularly true in the case of conservation sciences. It can be observed through a cursory inspection of the literature cited that the procedures for mortar analysis involves correlative analysis of a wide variety of techniques, most likely all that are readily available to the authors and lay in their specific area of expertise. This work attempts to streamline the process by extracting the maximum amount of information from a single, re-usable sample (the thin section) that is analyzed by a single researcher.

Herein lies the philosophical aspect of this type of analysis. A huge percentage of the knowledge that can be gained from the initial examination of a polished mortar thin section by optical microscopy, with additional analysis serving to corroborate or make more specific these findings. The application of each new method of analysis exponentially increases the amount of time and resources used, with inversely proportional additional results, either in terms of increased corroboration or new information gained. This must also be balanced by the value of the information gained, be it practical (such as using it to inform a conservation treatment) or educational (such as helping with interpretation of a site). During this work these sorts of practicalities were not considered; indeed, they would have required the documentation of the time and money spent on each phase of the research. Doing this would be perhaps the most valuable additional follow-up to this work that could be done, a value assessment that rigorously compared time and resources spent versus information gained. This sort of "audit" should be planned for any future study form the beginning. The underlying assertion of this conclusions section is that once this comprehensive, image-based protocol is corroborated by established, traditional laboratory techniques, it stands alone and only using the protocol for analysis on the future would result in a considerable savings of time, effort and financial (and perhaps environmental) resources. Confirming this assertion would be the most valuable future path of research that could stem from this work.

9.0 References

[1] Weber J, Baragona, A (2021/2017) *Microscopy brings it to light:Roman mortar technology studied by polarizing microscopy and SEM* in Cavalieri M. & Tomassini P. (eds.), La peinture murale antique : méthodes et apports d'une approche technique, Bordeaux (Pictor collection)

[2] Zimmermann N, Ladstätter S (2010)*Wandmalerei in Ephesos von hellenistischer bis in byzantinische Zeit*. Phoibos Verlag.

[3] Weber J, Prochaska W, Zimmermann N (2009)*Microscopic techniques to study Roman renders and mural paintings from various sites*. Materials Characterization, 60(7), p. 586-593.

[4] Jackson MD, Moon J, Gotti E, Taylor R, Chae SR, Kunz M, Emwas AH, Meral C, Levitz P, Wenk HR, Monteiro PJM (2013) *Material and Elastic Properties of Al-Tobermorite in Ancient Roman Seawater Concrete.*J. Am. Ceram. Soc. 96 pp. 2598–2606

[5] Jackson MD, Mulcahy SR, Chen H, Li Y, Li Q, Cappelletti P, Wenk HR (2017) *Phillipsite and Al-tobermorite mineral cements produced through low-temperature water-rock reactions in Roman marine concrete*American Mineralogist 102 pp. 1435–1450

[6] Baronio G, Binda, L (1997) *Study of the pozzolanicity of some bricks and clays.*Construction and Building Materials 11-1 pp.41-46

[7] Moropoulou A,Maravelaki-Kalaitzaki PN, Borboudakis E, Bakolas A, Michailidis P, Chronopoulos M (1998) *Historic mortars technologies in Crete and guidelines for compatible restoration mortars*. Compatible Materials for the Protection of European Cultural Heritage, Technical Chamber of Greece, Athens, 55 pp. 55–72.

[8] Gotti E, Oleason JP, Bottalico L, Brandon C, Cucitore R, Hohlfelder RL (2007) *A Comparison of the Chemical Engineering Characteristics Of Ancient Roman Hydraulic Concrete With A Modern Reproduction Of Vitruvian Hydraulic Concrete.*Archaeometry 100 pp. 1-15 University of Oxford

[9] Weber J, Baragona A, Pintér F, Gosselin C (2014)*Hydraulicity In Ancient Mortars: Its Origin And Alteration Phenomena Under The Microscope* Proceedings 15th Euroseminar on Microscopy Applied to Building Materials 16-19 June 2014, Delft, The Netherlands

[10] Cowper A (1927) *Lime and Lime Mortars.* The Building Research Station by HM Stationery Office, London ISBN 1873394292, 9781873394298

[11] Thuesen I, Gwozdz R (1982) *Lime plaster in Neolithic Hama, Syria.A preliminary report*. PaléorientAnnée 8-2pp. 99-103

[12] Barnett WK, Hoopes JW (1995) *The Emergence of Pottery: Technology and Innovation in Ancient Society.* Smithsonian Institution Press

[13] Tubb JN (1998) *Canaanites*. University of Oklahoma Press, Norman ISBN 080613108X, 9780806131085

[14] Evans ST (2008) *Ancient Mexico & Central America: Archaeology and Culture History* 2nd Edition Thames & Hudson, London 978-0500287149, 0500287147

[15] Maravelaki-Kalaitzaki P, Bakolas A, Moropoulou A (2003) *Physico-chemical study of Cretan ancient mortars* Cement and Concrete Research 33 pp. 651-661

[16] Vitruvius MP*The Ten Books on Architecture* trans. Morgan MH (1914) Harvard University Press; retrieved 2014 via Project Gutenburg

[17] Plinius CS*The Natural History* trans. Riley HT (1860) Taylor and Francis Pub.; retrieved 2019 via Project Gutenburg

[18] Mehta PK (1987) *Natural pozzolans: Supplementary cementing materials for concrete*. CANMET Special Publication, 86, 1–3
[19] Heiken G, Wohletz K (1985) *Volcanic Ash*. University of California Press;, pp. 246ISBN: 9780520052413
[20] Massazza F (2001)*Pozzolana and pozzolanic cements.*Lea's Chemistry of Cement and Concrete. Butterworth-Heinemann: 471–636.ISBN 9780080535418
[21] Snellings R, Mertens G, Elsen J (2012) *Supplementary cementitious materials*, Reviews in Mineralogy and Geochemistry. 74: 211–278
[22] Murat M, Driouche M (1988) *Chemical reactivity of thermally activated clay minerals*, Cem. Concr. Res. 18 221–228.
[23] Ilić BR, Mitrović AA, Miličić LR (2010) *Thermal Treatment Of Kaolin Clay*, Hem. Ind. 64 (4) pp. 351–356
[24] Taylor HFW (1964) The Chemistry of Cements. Vol.1, Academic Press, LondonISBN 7361446
[25]Taylor HFW (1968) *The Calcium Silicate Hydrate* in Proceedings of the Fifth International Symposium on the Chemistry of Cement, Vol. 2. pp. 1–26 Cement Association of Japan, Tokyo, Japan
[26] Davidovits J (2011) *Geopolymer Chemistry and Applications*, 3rd Ed. Institut Géopolymère, Saint-Quentin, France ISBN 9782951482050
[27] Taylor HFW (1992)*The Chemistry of Cement.*Academic Press, London ISBN012683900
[28]Cong XD, Kirkpatrick RJ (1996) *29Si MAS NMR Study of the Structure of Calcium Silicate Hydrate*Adv.Cem.Bas. Mater.,3, pp. 144–56
[29] Taylor HFW (1993) *Nanostructure of C-S-H: Current Status*, Adv. Cem. Bas. Mater.1, 38–46
[30]Yu P, Kirkpatrick RJ, Poe B, McMillan PF, Cong XD (1999) *Structure of calcium silicate hydrate (C-S-H): near, mid and far-infrared spectroscopy*. J Am Ceram Soc.82:742-748
[31]Iwaida T, Nagasaki S, Tanaka S, Yaita T, Tachimori S (2002) *Structure alteration of C-S-H (calcium silicate hydrated phases) caused by sorption of caesium*, Radiochim. Acta 90, 677–681
[32] Rosen JE (2014) *Composition and morphology of C-A-S-H in pastes of alite and cement blended with supplementary cementitious materials* PhD. Dissertation École Polytechnique Federale de Lausanne
[33] Weber J, Baragona AJ, Pintér F, Gosselin C (2015) *Hydraulicity in Ancient Mortars: Its Origin and Alteration Phenomena Under the Microscope* 15th Euroseminar on Microscopy Applied to Building Materials 16-19 June 2014, Delft, The Netherlands
[34] Winter TN (1979) *Roman Concrete: The Ascent, Summit, And Decline Of An Art in* Transactions of the Nebraska Academy of Sciences—Volume VII
[35] Heather LH, Hobbs L (1986*) Roman Concrete and the Roman Architectural Revolution* Ceramics and Civilization Volume 3: High Technology Ceramics: Past, Present, Future, W.D. Kingery, ed. American Ceramics Society
[36] Adam J (1994) *Roman Building: Materials and Techniques* Routledge, London ISBN 0415208661
[37] Smeaton J (1793) *A Narrative of the Building and a Description of the Construction of the Edystone Lighthouse with Stone* Book II Chapter IV (pp.122 in particular), G. Nicol Printers, London; retrieved via Project Gutenburg

[37A] Vicat LJ (1818) *Recherches expérimentales sur les chaux de construction, les bétons et les mortiers ordinaires* pp.39 Printed by L'Ecole Technique, Paris retrieved via Google Books
[37B] Weber J, Mayr N, Bayer K, Hughes D, Kozłowski R, Stillhammerova M, Ullrich D, Vyskocilova R (2007) *Roman cement mortars in Europe's architectural heritage of the 19th century*. Journal of the American Society for Testing Materials International, Vol, 4 No 8
[38] Moore D. (1995) *The Roman pantheon: the triumph of concrete* University of Guam Station Publishers OCLC 43120778
[39] Harring B (2002) The Secrets of Roman Concrete Constructor September 2002, retrieved 2019 romanconcrete.com
*[40] Courland R (2011) Concrete Planet: the strange and fascinating story of the world's most common man-made material. Amherst, N.Y.: Prometheus Books. ISBN 9*781616144814, 1616144815
[41] Idorn GM (1997) Concrete Progress: from the Antiquity to the Third Millennium. Telford Publishers, London ISBN 9780727726315, 0727726315
[42] Stamatakis MG, Fragoulis D, Kartanou D (2013) *The production of cementitious compounds using calcareous diatomite raw materials and possible industrial uses* Proceedings of the 3rd Historic Mortars Conference, 11-14 September 2013, Glasgow, Scotland
[43] Celik K,Jackson M, Akhul CM, Adbul-Hamid E, Mancio M, Mehta PK, Monteiro PJM (2014) *High-volume natural volcanic pozzolan and limestone powder as partial replacements for Portland cement in self-compacting and sustainable concrete*. Cement and Concrete Composites, 45, pp. 136–147
[44] Cai G, Noguchi T, Degée H, Zhao J (2016) *Volcano-related materials in concretes: a comprehensive review*. Environmental Science andPollution Research, 23, pp. 7220–724
[45] Kostuch JA, Walters GV, Jones TR (1993) *High performance concrete incorporating metakaolin — a review*. Concrete 2000. University of Dundee, pp. 1799–1811
[46] Bager GS, Hansen E, Wood M, Neary T, Beech, D Jaquier D (2001) *Production and use of calcined natural pozzolans in concrete*. Cement, Concrete and Aggregates 23-2, pp. 73–80
[47] Chakchouk A, Samet B, Mnif T (2006) *Study on the potential use of Tunisian clays as pozzolanic material* Applied Clay Science 33 pp. 79–88
[48] Vejmelková E, Pavlíková M, Keppert M, Keršner *Z, Rovnaníková P, Ondráč*ek M, Sedlmajer M, Černy R (2010) *High performance concrete with Czech metakaolin: Experimental analysis of strength, toughness and durability characteristics* Construction and Building Materials 24 pp. 1404–1411
[49] Davidovits J (1999) *Geopolymer '99 Proceedings*, pp. 283-295 Institut Géopolymère, Saint-Quentin, France
[50] Lothenbach B, Scrivener KL, Hooton D (2011) *Supplementary cementitious materials*. Cement and Concrete Research 41 pp. 217–229
[51] Celik K, Meral C, Gursel AP, Horvath A, Monteiro PJM (2015) *Mechanical properties, durability, and life-cycle assessment of self-consolidating concrete mixtures made with blended Portland cements containing fly ash and limestone powder.*Cem.Concr.Compos. 56 pp. 59–72
[52] Shafigh P, Nomeli MA, Alengaram UJ, Mahmud HB, Jumaat Z (2016) *Engineering properties of lightweight aggregate concrete containing limestone powder and high volume fly ash*. J. Clean. Prod. 135 pp. 148–157

[53] Alnahhal MF, Alengaram UJ, Jumaat MZ, Alqedra MA, Mo KH, Sumesh M(2017) *Evaluation of Industrial By-Products as Sustainable Pozzolanic Materials in Recycled Aggregate Concrete* Sustainability 2017, 9, 767
[54] Trotignon L, Devallois V, Peycelon H, Tiffreau C, Bourbon X (2007) *Predicting the Long Term Durability of Concrete Engineered Barriers in a Geological Repository for Radioactive Waste*. Phys. Chem. Earth, Parts A/B/ C, 32 1–7 pp. 259–74
[55] Theodorou M, Ioannou I, Philokyprou M (2013) *New evidence of early use of artificial pozzolanic material in mortars.* Journal ofArchaeological Science 40 pp. 3263-3269
[56] Papayianni I, Stafanidou M, Pachta V (2013) *Analysis and characterization of Hellenistic plasters*. Proceedings of the 3rd Historic Mortars Conference, 11-14 September 2013, Glasgow, Scotland
[57] Drdácky M, Fratini F, Frankeová D, Slížková Z (2013) *The Roman mortars used in the construction of the Ponte di Augusto (Narni, Italy) – A comprehensive assessment.* Construction and Building Materials 38 pp. 1117–1128
[58] Miriello D, Barca D, Bloise A, Ciarallo A, Crisci G, De Rose T, Gattuso C, Gazineo F, La Russa M (2010) *Characterisation of archaeological mortars from Pompeii (Campania, Italy) and identification of construction phases by compositional data analysis.* Journal of Archaeological Science 37 pp. 2207-2223
[58A] Carran D, Hughes J. Leslie, A, Kennedy CJ (2010) *Lime lump development and textural alteration during the production of mortar* 2nd Conference on Historic Mortars HMC 2010 and RILEM TC 203-RHM final workshop (Peer-reviewed conference paper/ chapter of book) ed. Válek J, Groot C, Hughes JJ
[59] Sánchez-Moral S, Luque L, Cañaveras JC, Soler V, Garcia-Guinea J, Aparicio A (2005) *Lime pozzolana mortars in Roman catacombs: composition, structures and restoration* Cement and Concrete Research 35 pp. 1555–1565
[60] Degryse P, Elsen J, Waelkens M (2002) *Study of ancient mortars from Sagalassos (Turkey) in view of their conservation.* Cement and Concrete Research 32 pp. 1457–1463
[61] Özkaya ÖA, Böke H (2009) *Properties of Roman bricks and mortars used in Serapis temple in the city of Pergamon.*Materials Characterization 60 pp. 995–1000
[62] Brandon C, Hohlfelder RL, Oleason JP (2008) *The concrete construction of the Roman harbours of Baiae and Portus Iulius, Italy: The ROMACONS 2006 field season.* International Journal of Nautical Archaeology 37(2) pp. 374 – 379
[63] Kramar S, Zalar V, Urosevic M, Körner W, Mauko A, Mirtič B, Lux J, Mladenović *A* (2011) *Mineralogical and microstructural studies of mortars from the bath complex of the Roman villa rustica near Mošnje (Slovenia).* Materials Characterization 62 pp.1042–1057
[64] Velosa AL, Coroado J, Veiga MR, Rocha F (2007) *Characterisation of roman mortars from Conímbriga with respect to their repair.* Materials Characterization 58 pp.1208–1216
[65] Binici H, Arocena J, Kapur S, Aksogan O, Kaplan H (2010) *Investigation of the physico-chemical and microscopic properties of Ottoman mortars from Erzurum (Turkey).* Construction and Building Materials 24 pp. 1995–2002
[66] Siddal R (2013) *Medieval Mortars and the Gothic Revival: The Cosmati Pavement at Westminster Abbey*. Proceedings of the 3rd Historic Mortars Conference, 11-14 September 2013, Glasgow, Scotland
[67] Biscontin G, Birelli MP, Zendri E (2002) *Characterization of binders employed in the manufacture of Venetian historical mortars.* Journal of Cultural Heritage 3 pp. 31–37

[68] Moropoulou A, Bakolas, A, Bisbikou K (2000) *Investigation of the technology of historic mortars.*Journal of Cultural Heritage 1 pp. 45–58
[69] Bertolini L, Carsana M, Gastaldi M, Lollini F, Redaelli E (2013*) Binder characterisation of mortars used at different ages in the San Lorenzo church in Milan.*Materials Characterization 80 pp.9–20
[70] Kyropoulou D, Dotsika E, Raco B, Andrikou D, Dadaki S, Iliadis EI (2013) *The transition from Hellenistic to Roman and Byzantine mortars in Greece*. Proceedings of the 3rd Historic Mortars Conference, 11-14 September 2013, Glasgow, Scotland
[71] Pavía S, Caro S (2008) *An investigation of Roman mortar technology through the petrographic analysis of archaeological material.* Construction and Building Materials 22 pp. 1807–1811
[72] Mertens G, Elsen J, Brulet R, Brutasaert A, Deckers M (2008) *Quantitative composition of ancient mortars from the Notre Dame Cathedral in Tournai (Belgium)*. Materials Characterization 60 pp. 580–585
[73] Robador, M.D. (2010) *Hydraulic structures of the Roman Mithraeum house in Augusta emerita, Spain*. Journal of Archaeological Science 37 2426-2432
[74] Stanislao C, Rispoli C, Vola G, Cappelletti P, Morra V, de Gennaro M (2011) *Contribution to the knowledge of ancient Roman seawater concretes: Phlegrean pozzolan adopted in the construction of the harbour at Soli-Pompeiopolis (Mersin, Turkey).*Periodico di Mineralogia 80-3 (Spec. Issue) pp. 471-488
[75] Lindqvist JE, Johansson S (2013) *The development of binders and mortars in Sweden.* Proceedings of the 3rd Historic Mortars Conference, 11-14 September 2013, Glasgow, Scotland
[76] Moropoulou A, Tsiourva T, Bisbikou K, Biscontin G, Bakolas A, Zendri E (1996) *Hot lime technology imparting high strength to historic mortars*. Construction and Building Materials10-2 pp. 151-159
[77] Jackson M, Chae SR, Mulcahy SR, Meral C, Taylor R, Li P, Emwas AH, Moon J, Yoon S, Vola G, Wenk HR, MOntiero PJM (2013) *Unlocking the secrets of Al-tobermorite in Roman seawater concrete.*American Mineralogist 98 p. 1669–1687
[78] Borges C, Silva AS, Veiga R (2014) *Durability of ancient lime mortars in humid environment*. Construction and Building Materials 66 pp. 606–620
[79] Moropoulou A, Cakmak AS, Biscontin G, Bakolas A, Zendri E (2002) *Advanced Byzantine cement based composites resisting earthquake stresses: the crushed brick-lime mortars of Justinian's Hagia Sophia*. Construction and Building Materials 16 pp. 543–552
[80] Papayianni I, Stefanidou M (2007) *Durability aspects of ancient mortars of the archeological site of Olynthos.* Journal of Cultural Heritage 8 pp. 193-196
[81] Böke H, Akkurt S, İpekoğlu, B, Uğurlu, E (2006) *Characteristics of brick used as of brick used as aggregate in historic brick-lime mortars and plasters*. Cement and Concrete Research 36 pp. 1115–1122
[82] Teutonico JM, McCraig I, Burns C, Ashurst J (1993) *The Smeaton Project: Factors Affecting the Properties of Lime-Based Mortars*APT Bulletin 25-3/4 pp. 32–49
[83] Teutonico JM (2000) *A comparative study of hydraulic lime-based mortars*, in: Bartos P, Groot C, Hughes JJ (Eds.), International RILEM Workshop on Historic Mortars: Characteristics and Tests, RILEM Publications, Cachan Cedex, France pp. 339–349
[84] Heide M (2001) *Brennprodukte von Tonen als Puzzolane für hydraulisch erhärtende Mörtel: früher und heute* Dissertation, University of Siegen, Germany

[85] Azerêdo A, Struble L, Carneiro AMP (2013*) Lime-Metakaolin Mortars Produced From Kaolin Wastes: Hardened and Microstructural Properties.* Proceedings of the 3rd Historic Mortars Conference, 11-14 September 2013, Glasgow, Scotland
[86] *Č*erný R, Kunca A, Tydlitát, V, Drchalová J, Rovnanikova P (2006) *Effect of pozzolanic admixtures on mechanical, thermal and hygric properties of lime plasters.* Construction and Building Materials 20 pp. 849–857
[87] Cardoso D, Gameiro A, Santos-Silva A, Faria P, Viedra R, Veiga R, Velosa A (2013*) Influence of curing conditions in air lime-metakaolin blended mortars – A mineralogical and mechanical study.* Proceedings of the 3rd Historic Mortars Conference, 11-14 September 2013, Glasgow, Scotland
[88] Slavid I, Thomson ML, Wathne J, Weiss NR (2013*) Development and evaluation of a lime-metakaolin grout.* Proceedings of the 3rd Historic Mortars Conference, 11-14 September 2013, Glasgow, Scotland
[89] Borsoi G, Pasccoal P, Pinto JP, Veiga R, Faria P, Santos-Silva A (2013*) Chromatic reintegration of historical mortars with lime-based pozzolanic consolidant products.* Proceedings of the 3rd Historic Mortars Conference, 11-14 September 2013, Glasgow, Scotland
[90] Matias G, Faria P, Torres I (2013*) Viability of ceramic residues in lime-based mortars.*Proceedings of the 3rd Historic Mortars Conference, 11-14 September 2013, Glasgow, Scotland
[91] Maravelaki-Kalaitzaki P, Bakolas A, Karatasios I, Kilikoglou V (2005) *Hydraulic lime mortars for the restoration of historic masonry in Crete.* Cement and Concrete Research 35 pp. 1577-1586
[92] Moropoulou A, Bakolas A, Moundoulas P, Aggelakopoulou E, Anagnostopoulou S (2005) *Strength development and lime reaction in mortars for repairing historic masonries*. Cement & Concrete Composites 27 pp. 289–294
[93] Fragata A, Veiga MR, Velosa AL (2013*) "Ventilated render" system: a replacement render for historic construction.* Proceedings of the 3rd Historic Mortars Conference, 11-14 September 2013, Glasgow, Scotland
[94] Stefanidou M, Papayianni I (2007) *Analysis of the old mortars and proposals for the conservation of the archeological site of Logos-Edessa.* Conference Proceedings: Structural Studies, Repairs and Maintenance of Heritage Architecture pp. 261-265
[95] Moropoulou A, Bakolas A, Bisbikou (1995) Characterization of ancient, byzantine and later historic mortars by thermal and X-ray diffraction techniques. Thermochimica Acta 269/270 pp. 779-795
[96] Bakolas A, Biscontin G, Moropoulou A, Zendri E (1998) Characterization of structural byzantine mortars by thermogravimetric analysis. Thermochimica Acta 321 pp. 151-160
[97] Paama L, Pitkänen I, Rönkkömäki H, Perämäki P (1998) Thermal and infrared spectroscopic characterization of historical mortars. Thermochimica Acta 320 pp. 127-133
[98] Genestar C, Pons C, Más A (2006) Analytical characterisation of ancient mortars from the archaeological Roman city of Pollentia (Balearic Islands, Spain). Analytica Chimica Acta 557 pp. 373–379
[99] Middendorf B, Hughes JJ, Callebaut K, Baronio G, Papayianni I (2005) Investigative methods for the characterisation of historic mortars- Part 2: Chemical characterization. Materials and Structures 39 p. 771-780

[100] Hauková P, Frankeová D, Slížková Z (2013) Characterisation of historic mortars for conservation diagnosis. Proceedings of the 3rd Historic Mortars Conference, 11-14 September 2013, Glasgow, Scotland
[101] Drdácky M (2011) Non-Standard Testing Of Mechanical Characteristics Of Historic Mortars. International Journal of Architectural Heritage, 5 pp. 383–394
[102] Panzera TH, Coat FP, Christoforo AL, Borges PHR, Bowen CR (2011) Ultrasonic Pulse Velocity Evaluation of Cementitious Materials in Advances in Composite Materials - Analysis of Natural and Man-Made Materials, Chapter 17 Ed. P. Tesinová, Pub. InTech, Croatia
[103] Kurugöl S (2012) Correlation of Ultrasound Pulse Velocity with Pozzolanic Activity and Mechanical Properties in Lime-Calcined Clay Mortars.Gazi University Journal of Science Journal 25-1 pp. 219-233 (2012)
[104] Plassard C, Lesniewska E, Pochard I, Nonat A (2007) Intrinsic elastic properties of Calcium Silicate Hydrates by nanoindentation. Conference Proceedings: 12th International Congress on the Chemistry of Cement, Montreal, Canada
[105] Nežerka V, N*ě*meček J, Slížková Z, Tesárek P (2015) Investigation of crushed brick-matrix interface in lime-based ancient mortar by microscopy and nanoindentation. Cement & Concrete Composites 55 pp. 122–128
[106] Silva J, de Brito J, Veiga R (2009) Incorporation of fine ceramics in mortars. Construction and Building Materials 23 pp. 556–564
[107] Sala E (2010) Caratterizzazione Meccanica di Malte a Base di Calce e Pozzolana Naturale. In Arkos, Scienza e Restauro 25
[108] Farci A, Floris D, Meloni P (2005) Water permeability vs. porosity in samples of Roman mortars. Journal of Cultural Heritage 6 pp. 55–59
[109] Papayianni I, Stefanidou M (2006) Strength–porosity relationships in lime–pozzolan mortars. Construction and Building Materials 20 pp. 700–705
[110] Moropoulou A, Bakolas A, Aggelakopoulou E (2004) Evaluation of pozzolanic activity of natural and artificial pozzolans by thermal analysis. Thermochimica Acta 420 pp. 135–140
[111] Müller CJ, (2005)Pozzolanic activity of natural clay minerals with respect to environmental geotechnic. Dissertation, Swiss Federal Institute Of Technology Zurich
[112] Cabrerea J, Rojas MF (2001) Mechanism of hydration of the metakaolin-lime-water system. Cement and Concrete Research 31 pp. 177-182
[113] Agarwal SK (2006) Pozzolanic activity of various siliceous materials. Cement and Concrete Research 36 pp. 1735–1739
[114] Tashima MM, Soriano L, Monzó J, Borrachero MV, Akasaki JL, Payá J (2014) New method to assess the pozzolanic reactivity of mineral admixtures by means of pH and electrical conductivity measurements in lime: pozzolan suspensions. Materiales de Construcción64-31 pp. 1-12
[115] From Metakoalin.info: Metakaolin – measuring the total quantity of fixed Calcium Hydroxide (Chapelle test modified) Referring to the French norm NF P 18-513, Annexe A, retrieved 2016
[116] Válek J, Matas T, Machová D, Petráňová V, Frankeová D, Zeman A (2013*) Assessment of properties of lump lime produced in a 'traditional' flare kiln.* Proceedings of the 3rd Historic Mortars Conference, 11-14 September 2013, Glasgow, Scotland

[117] Balksten K, Persson C, Eriksson J (2013*) Lime burning tradition in field kilns – a case study of the Jämtland tradition in Sweden.* Proceedings of the 3rd Historic Mortars Conference, 11-14 September 2013, Glasgow, Scotland
[118] Demelenne M, Van Parys L, Scaillet JC, Hayen R (2013*) Experiment craft lime kilns in the Walloon Region (Belgium) in order to understand the lime properties.* Proceedings of the 3rd Historic Mortars Conference, 11-14 September 2013, Glasgow, Scotland
[119] Pittalunga D (2013*) Restoration of "Fornace Bianchi" lime production plant in Cogoleto (Italy)* Proceedings of the 3rd Historic Mortars Conference, 11-14 September 2013, Glasgow, Scotland
[119A] Brandon, CJ (2008). *Roman structures in the sea: Sebastos, the Herodian harbor of Caesarea.* Memoirs of the American Academy in Rome, Supplementary Volumes, 6, 245-254.
[120] Copsey N, Gourley B (2013*) Hot-Mixed Lime Mortars.* Proceedings of the 3rd Historic Mortars Conference, 11-14 September 2013, Glasgow, Scotland
[121] Hughes JJ, Leslie AB, Callebaut K (2001) *The Petrography of lime inclusions in lime base mortars.* Annales Geologiques des pays Helleniques, Ed. Spec. 39 pp. 359-364
[122] Elsen J, Van Balen K, Mertens G (2010*) Hydraulicity in Historic Lime Mortars: a Review.* Proceedings of the 2nd Historic Mortars Conference, 22-24 September 2010, Prague, Czech Republic
[123] Binda, L, Baronio G, Tedeschi C (1999) *Experimental Study on the Mechanical Role of Thick Mortar Joints in Reproduced Byzantine Masonry* Conference Proceedings, International RILEM Workshop on Historic Mortars, 12th-14th of May 1999, Paisley Scotland
[123A] - Margalha G, Veiga MDR, Silva AS, de Brito J [2011] *Traditional methods of mortar preparation: The hot lime mix method.* Cement and Concrete Composites 33(8): 796-804
[124] Miriello D, Baraca D, Bloise A, Ciarallo A, Crisci GM, De Rose T, Gattuso C, Gazineo F, La Russa MF (2011) *Characterisation of archaeological mortars and plasters from Kyme (Turkey).* Journal of Archaeological Science 38 pp. 794-804
[125] Karatasios I, Alexiou K, Müller NS, Day P, Kilikoglou V (2014) *The second life of ceramics: a new home in a lime environment.* in M Martinón-Torres (Ed.), Craft and science: International perspectives on archaeological ceramics. Doha, Qata pp. 271-279
[126] Bröckerbaum S, Funke F, Zier C (2013*) Experimental Replication of a Roman lime plaster floor.* Proceedings of the 3rd Historic Mortars Conference, 11-14 September 2013, Glasgow, Scotland
[127] Baronio G, Binda L, Lombardini N (1996) *The role of brick pebbles and dust in conglomerates based on hydrated lime and crushed bricks.*Construction and Building Materials 11-1 pp. 33-40
[128] Baragona A, Weber J, Anghelone M (2019) A map is worth a thousand pictures: Using FTIR-imaging to analyze petrographic thinsections of historical and experimental mortar. Proceedings of the 5th Historic Mortars Conference, 19-22 June 2019 Pamplona, Spain
[129] Elsen J (2006).*Microscopy of historic mortars — a review*. Cement and Concrete Research, 36-8 pp. 1416-1424
[130] Pavía S, Caro S (2008) *An investigation of Roman mortar technology through the petrographic analysis of archaeological material*. Construction and Building Materials 22 pp. 1807–1811

[131] Borges C, Santos Silva A, Veiga R (2011) *Natural Consolidation Of Ancient Historic Buildings Mortars Submitted To Humid And Marine Environment: A Microscopic Study*13th Euroseminar on Microscopy Applied to Building Materials 14-18 June 2011, Ljubljana, Slovenia
[132] Blaeuer C, Kueng A (2007) *Examples of microscopic analysis of historic mortars by means of polarising light microscopy of dispersions and thin sections*. Materials Characterization 58 pp. 1199–1207
[133] *Š*tukovnik P, Marin*š*ek M, Bosiljkov VB (2013) *Observations of reactions between dolomite aggregate grains and lime-based binder in lime mortars.*Proceedings of the 3rd Historic Mortars Conference, 11-14 September 2013, Glasgow, Scotland
[134] Guerra-García P, Sanz-Arauz D, Heras C (2014) *Historic Mortars Micro-stratigraphy.* First Step in Restoration Process. Proceedings from 1st International Congress on research in Construction and Architectural Technologies. Universidad Politécnica de Madrid. ETSAM. Madrid, 11-13 Junio de 2014
[135] Peterson K, Gress D, Van Dam T, Sutter L (2006) *Crystallized alkali-silica gel in concrete from the late 1890s*. Cement and Concrete Research 36 pp. 1523–1532
[136] Katayam T (2011) *So-Called Alkali-Carbonate Reaction - Petrographic Details Of Field Concretes In Ontario.*13th Euroseminar on Microscopy Applied to Building Materials 14-18 June 2011, Ljubljana, Slovenia
[137] Stástná A, *Šachlová Š, Pertold Z,* Přikryl R(2015) *Factors affecting alkali-reactivity of quartz-rich metamorphic rocks: Qualitative vs. quantitative microscopy,* Engineering Geology 187 pp. 1–9
[138] Goines ES (2004) *Standard Practice for Determining the Components of Historic Cementitious Materials.*Retrieved online from: US Department of the Interior National Park Service National Center for Preservation Technology and Training Publication No. 2002-20
[139] Tuncoku SS, Caner-Saltik EN (2006) *Opal-A rich additives used in ancient lime mortars*. Cement and Concrete Research 36 pp. 1886–1893
[140] Moropoulou A, Cakmak AS, Biscontin G, Bakolas A, Zendri E (2002) *Advanced Byzantine cement based composites resisting earthquake stresses: the crushed brick lime mortars of Justinian's Hagia Sophia*. Construction and Building Materials 16 pp. 543–552
[141] Riccardi MP, Lezzerini M, Caró F, Franzini M, Messiga B (2007) *Microtextural and microchemical studies of hydraulic ancient mortars: Two analytical approaches tounderstand pre-industrial technology processes*. Journal of Cultural Heritage 8 pp.350-360
[142] Mertens G (2009) *Characterisation of historical mortars and mineralogical study of the physico-chemical reactions on the pozzolan-lime binder interface.*Dissertation, Katholieke Universiteit Leuven
[143] Böke H, Akkurt S (2003) *Ettringite formation in historic bath brick–lime plasters*. Cement and Concrete Research 33 pp. 1457–1464
[144] Weber J, Köberle T, Pintér F (2013*) Methods of microscopy to identify and characterise hydraulic binders in historic mortars – a methodological approach.*Proceedings of the 3rd Historic Mortars Conference, 11-14 September 2013, Glasgow, Scotland
[145] Gardiner DJ, Graves PR (ed.) (1989) Practical Raman spectroscopy. Springer-Verlag, *New York City* ISBN 978-3-642-74040-4
[146] Fries M, Steele A (2011) *Raman Spectroscopy and Confocal Raman Imaging in Mineralogy and Petrography.* 28 pages, Published online by NASA JPL, Pasadena, California

[147] Castriota M, Cosco V, Barone T, De Santo P, Carafa P, Cazzanelli E (2008) *Micro-Raman characterizations of Pompei's mortars*. J. Raman Spectrosc. 39: 295–301
[148] Martínez-Ramírez S, Fernández-Carrasco L (2011)*Raman Spectroscopy: Application To Cementitious Systems*Construction and Building: Design, Materials, and Techniques pp. 233-244
[149] Dariz P, Schmid T (2017) *Ferriginous phases in 19th century lime and cement mortars: A Raman microspectroscopic study.* Mater Charact 129:9-17
[150] Schmid T, Dariz P (2016) *Chemical imaging of historical mortars by Raman microscopy.* Const Build Mater 114:506-516
[151] Nyquist A, Kagel R (1971) *Infrared Spectra of Organic Compounds*. Academic Press, London LCCCN: 76-180797
[152] Ghosh SN, Handoo SK (1980) *Infrared and Raman Spectral Studies in Cement and Concrete (Review)*Cem. Concr.Res.,10, 771–82 (1980).
[153] Hughes TL, Methven CM, Jones TGJ, Pelham SE, Fletcher P, Hall C (1995) *Determining cement composition by Fourier Transform Infrared Spectroscopy.*Adv Cem Based Mater2:91-104
[154] Yu P, Kirkpatrick RJ, Poe B, McMillan PF, Cong X (1999) *Structure of calcium silicate hydrate (C-S-H): near, mid and far-infrared spectroscopy.*J Am Ceram Soc82:742-748
[155] Farcas F, Touzé P (2001) *La spectrométrie infrarouge à transformée de Fourier (IRTF) Une méthode intéressante pour la caractérisation des ciments.* Bulletin des laboratoires des ponts et chaussées - 230:77-88
[156] Hidalgo Lopez A, García Calco JL, García Olmo J, Petit M, Alonso MC (2008) *Microstructural evolution of calcium aluminate cements hydration with silica fume and fly ash additions by SEM, and mid and near-infrared spectroscopy.* J Am Ceram Soc91:1258-1265
[157] Horgnies M, Chen JJ, Bouillon C (2013) *Overview about the use of Fourier Transform Infrared spectroscopy to study cementitious materials*.Mater Charact VI:251-262
[157A] Diekamp A, Stalder R, Konzett J , Mirwald PW *Lime mortar with natural hydraulic components - characterization of reaction rims with FTIR-imaging in ATR-mode*
2nd Conference on Historic Mortars - HMC 2010 and RILEM TC 203-RHM final workshop
[158] Diekamp A (2014) *Bindesmitteluntersuchungen an historischen Putzen und Mörteln aus Tirol und Südtirol.*Dissertation University of Innsbruck
[159] Palanivel R, Velraj G (2007) *FTIR and FT-Raman spectroscopic studies of fired clay artifacts recently excavated in Tamilnadu, India.* Indian Journal of Pure & Applied Physics 45 pp. 501-508
[160] Swinford, A. (ed.) (1960) *Experimental Studies of Illite, A Discussion of the Water Content of Vermiculite and Rapid Dissolution of Allophane and Kaolinite-Halloysite after Dehydration in Clays and Clay Minerals*1st EditionProceedings of the Seventh National Conference on Clays and Clay Minerals Pergamon Press, London
[161] Anthony D, Garn P (1974) *Kinetics of Kaolinite Dehydroxylation* Journal of American ceramic society 57:3 pp. 132-135
[162] Gábor M, Wajand J, Pöppl L, Szabó ZG (1977) *Steps in Low Temperature Dehydroxylation of Clay*. In: Wood J., Lindqvist O., Helgesson C., Vannerberg NG. (eds) Reactivity of Solids. Springer, Boston, MA
[163] Kakali G, Perraki T, Tsivilis S, Badogiannis E (2001) *Thermal treatment of kaolin: the effect of mineralogy on the pozzolanic activity*, Appl. Clay Sci. 20 pp. 73–80.

[164] Shvarzman A, Kovler K, Grader GS, Shter GE (2003) *The effect of dehydroxylation/ amorphization degree on pozzolanic activity of kaolinite*, Cem. Concr. Res. 33 405–416
[165] ASTM C136 / C136M - 14 *Standard Test Method for Sieve Analysis of Fine and Coarse Aggregates* retrieved from ASTM International Online 2018 from astm.org
[166] (ASTM C511) *Standard Specification for Mixing Rooms, Moist Cabinets, Moist Rooms, and Water Storage Tanks Used in the Testing of Hydraulic Cements and Concretes*retrieved from ASTM International Online 2015 from astm.org
[167]ASTM C597-83 *Standard Test Methods for Compressive Strength of Chemical-Resistant Mortars, Grouts, Monolithic Surfacings, and Polymer Concretes*retrieved from ASTM International Online 2015 from astm.org
[168] ASTM C 109/ C109M equivalent to EN 998 *Standard test method for compressive strength of hydraulic cement mortars (using 2-in. Or 50-mm cube specimens)* retrieved from astm international online 2015 from astm.org
[169] Middendorf B, Hughes JJ, Callebaut K, Baronio G, Papayianni I (2005) pp. 167-COM :*Characterisation of old mortars with respect to their repair Materials and Structures* 38 pp.771-780
[170] Coats AW, Redfern JP (1963) *Thermogravimetric Analysis: a review* pp 906-933 Battersea College of Technology, London, retrieved from scribd.com August 2019
[171] Barin I, Knacke O, Kubaschewski O (1973) *Thermochemical properties of inorganic substances – A supplement* Springer-Verlag GmbH Berlin ISBN 978-3-662-02293-1
*[172] Griffiths P, de Hasseth JA, Winefordner JD (eds.) (2007).Fourier Transform Infrared Spectrometry (2nd ed.).Wiley-Blackwell. Hoboken, N.J.*ISBN: 978-0-471-19404-0
[173] Derrick MR, Stulik D, Landry JM (2000) *Infrared Spectroscopy in Conservation Science, Scientific Tools for Conservation* Getty Publications, Los Angeles ISBN 0892364696 9780892364695
[174] Quarcioni VA Chotoli F, Cincotto MA (2015)*Indirect and direct Chapelle's methods for the determination of lime consumption in pozzolanic materials*. Ibracon Structures and Materials Journal 8:1 pp.1-7
[175] Brunello V, Corti C, Sansonetti A, Tedeschi C, Rampazzi L (2019) *Non-invasive FTIR study of mortar model samples: comparison among innovative and traditional techniques* Eur. Phys. J Plus134:270
[176] Qing Y, Zenall Z, Li S, Rongshen C(2006). *A comparative Study on the pozzolanic activity between nano-SiO2 and silica fume.*Journal of Wuhan University of Technology-Materials Science Edition 21, 153-157
[177] Pintér F, Weber J, Bajnóczi B, Tóth M (2011): *Brick-Lime Mortars and Plasters of a Sixteenth Century Ottoman Bath from Budapest, Hungary*. Turbanti-Memmi, I. (Ed.): Proceedings of the 37th International Symposium on Archaeometry, 12th-16th May 2008, Siena, Italy. Springer Berlin Heidelberg, 293-298.
[178] Goto S, Suenaga K, Kado T, FukuharaM. (1995): *Calcium Silicate Carbonation Products* Journal of the American Ceramic Society, 78, 2867–2872
[179] Flett JS (1911) "*Petrology*". In Chisholm, Hugh (ed.). Encyclopedia Britannica.21 (11th ed.).Cambridge University Press.pp. 323–333.
[180] W. D. Nesse WD (1991).Introduction to Optical Mineralogy, 2nd ed. xii pp. 253-255 New York, Oxford: Oxford University Press. ISBN 0195060245

[181] Goldstein J, Newbury DE, Echlin P, Joy DC, Fiori C, Lifshin E (1981)*Scanning Electron Microscopy and X-Ray Microanalysis: A Text for Biologists, Materials Scientists, and Geologists*New York, Springer 978-1-4613-3273-2
[182] Hughes DC, Sugden DB (1999) *The use of brick dust as a pozzolanic additive to hydraulic lime mortars*. Proceedings of the International RILEM workshop on historic mortars: Characteristics and Tests University of Paisely, Scotland, May 1999 pp. 351-359
[183] Alvarez JI, Martin A, Garcia-Casado PJ, Navarro I, Zornoza A (1999)*Methodology and validation of a hot hydrochloric acid attack for the characterization of ancient mortars.*Cem.Concr. Res. 29 pp. 1061-1065
[184] Secco M, Dilaria S, Addis A, Bonetto J, Artioli G, Salvadori M (2018) *The Evolution of Vitruvian recipes over 500 years of floor making techniques: the case studies of the* Domus Delle Bestie Ferite *and the* Domus di Tito Macro *(Aquileia, Italy).* Archeometry 60, 2 pp. 185-206